Decoding Complex Structures in Medical Physics, Plasma Physics and Astrophysics

Christoph Räth

München 2017

Decoding Complex Structures in Medical Physics, Plasma Physics and Astrophysics

Habilitation an der Fakultät für Physik

Ludwig–Maximilians–Universität München

eingereicht von
Christoph Räth
geboren in München

München, 2017

Für Katrin, Korbinian und Benedict

Ich bitte die Leserinnen und Leser
nur um jenen Vorschuss an Sympathie,
ohne den es kein Verstehen gibt.
(J. Ratzinger)

Contents

1 Complexity and complexity measures **1**
- 1.1 Complex systems . . . 1
- 1.2 Complexity measures . . . 3
  - 1.2.1 Complexity measures in phase space or embedding space . . . 6
  - 1.2.2 Morphological measures . . . 10
  - 1.2.3 Complexity measures based on the Fourier phase information . . . 12

2 Surrogates **15**
- 2.1 The need for surrogates . . . 15
- 2.2 Generating surrogates . . . 17
- 2.3 Variation on a theme: assessing higher order statistics using surrogates . . . 21

3 Inner bone as a complex adaptive system **23**
- 3.1 Bone remodeling . . . 23
- 3.2 Malfunction of bone remodeling: osteoporosis . . . 25
- 3.3 Quantifying bone structures . . . 27

4 Phenomena of self-organization in complex plasmas **31**
- 4.1 (Complex) Plasmas . . . 31
- 4.2 Fluid demixing . . . 37
- 4.3 Lane formation . . . 38
- 4.4 String formation in electrorheological plasmas . . . 39

5 Complex patterns in astrophysics **43**
- 5.1 Sources of information in astrophysics . . . 43
- 5.2 Time series analysis of GBHs and AGNs . . . 46
- 5.3 Probing isotropy and statistics of the CMB . . . 52

6 Synthesizing complex structures **65**

7 Summary and outlook **67**

Bibliography **97**

Acknowledgements **99**

Original Publications **101**

Chapter 1

Complexity and complexity measures

1.1 Complex systems

It is one of the basic findings of nonlinear dynamics that a plethora of observable and seemingly simple, often also deterministic systems give already rise to "complex" behavior. The three-body problem [259], the double pendulum [316, 197] the Lorenz [202] and Rössler [284] system represent classical examples of nonlinear deterministic systems, whose dynamics is unpredictable, very sensitive on the choice of initial conditions and whose trajectories form nontrivial, "aesthetically appealing" [321] structures in the phase space representation. In other words, already these deterministic systems with a low number of degrees of freedom show many features typical for "complex systems". But what makes a system "complex" and distinguishable from systems, which one would not hesitate to call "simple"? This question is not yet answered comprehensively, but a few essential criteria for complexity can be enumerated:

From a physical point of view complex behavior typically (but not always) arises in situations far from thermal equilibrium. One usually does not speak of a complex system if its behavior is described by the laws of linear thermodynamics. The entire framework of equilibrium thermodynamics may even become inapplicable in such situations.

Complex systems are usually open systems, which exchange energy and/or matter and information with their environment. Driven damped oscillatory systems like Duffing's oscillator [77] and the special case discussed by Ueda [349] are prototypical early examples for low-dimensional open complex systems.

Many complex systems can be decomposed into components (elements, units, particles) that may function as individuals, generating some form of local behavior, activity or dynamics. Self-sustained oscillators like clocks, electronic circuits or oscillatory chemical reactions represent examples of such components that may be parts of a complex system.

In order to make this happen, the components must interact in some way, which leads to the integration or binding of these components across space and time into an organized whole. Interactions often modulate the individual actions of the components, thus altering their local functionality by relaying global context. This is exactly what e.g. happens when

N weakly coupled oscillators with varying eigenfrequencies synchronize and thus form a complex system [245].

The interactions of the components among each other give then rise to phenomena that cannot be trivially reduced to properties of the components alone. Rather, these system states emerge as a result of structured interactions and are properties of the system as a whole. In many cases, even a detailed and complete examination of the individual components will fail to predict the range of emergent processes that these components are capable of if allowed to interact as part of a system. These emergent properties are manifested by the creation of self-organized states, where order and coherence are the result of a bottom-up process. The Rayleigh-Bénard convection patterns [17, 278] are the classical example for emergent structures and one of the most carefully examined example of self-organizing nonlinear systems. This experiment also shows prototypically how the system behavior depends on external control parameters (Rayleigh number and temperature gradient in the case of Rayleigh-Bénard convection) and how a system undergoes phase transitions leading to emergent large-scale structures when the control parameters are varied. Well-defined order parameters play a key role for a quantitative description of the phase transition in those emergent systems.

Complex systems further often exhibit an intertwining of regularities and seemingly erratic behavior. There is thus a coexistence of order and disorder. Both perfectly ordered structures and completely random ones are not considered to be complex. The intuitively most complex structures are those, where both aspects, regularity (i.e. determinism) and randomness are present at the same time [115].

It is often a necessary prerequisite for a system to exhibit complex behavior that the dynamics of the components of a complex system and/or their interactions are nonlinear. The mere evidence for weak nonlinearities in a system may be indicative of an more complex underlying dynamics.

Notwithstanding the lack of a formal definition, the study of complex systems has seen tremendous growth and the new concepts emerging from these studies are now influencing disciplines ranging from astronomy to physics, biology, medicine and finance [9].
A large number of new developments for better understanding complex systems stem from the fields of nonlinear dynamics, stochastic geometry and – more recently – the science of networks. In this work we will present further developments of techniques for the quantitative characterization of complex structures as well as applications of them to a number of interdisciplinary research themes. The applications range from the study of emergent phenomena in complex plasmas, which are a many particle system with unique properties, to the quantitative characterization of the inner bone, which is a prototypical example for a self-organizing biological system and satellite measurements of astrophysical data, where a refined analysis is crucial to derive most of the information content of the highly expensive and thus precious data that are often hardly reproducible.

1.2 Complexity measures

As a consequence of the lack of a formal definition for complexity there are a number of complexity measures quantifying some of the aspects of complexity listed above. Subsequent to the algorithmic complexity [178, 40, 41] a large number of further measures has been proposed over the decades including e.g. the spectrum of generalized Rényi dimensions, generalized entropies, Kullback information, mutual information, effective measure complexity, fluctuation complexity and ϵ-complexity and all sorts of network measures. Classical overviews can be found in [116, 354, 329, 4]. Although some complexity measures have attracted more attention than others, there are no rigorous criteria for selecting a "correct" definition for complexity and reject the rest. It even appears that for a proper characterization of complexity the fundamental principle of universality has to be complemented by an unavoidable context dependence or contextuality. It was found out that only when considering the context dependence, which can be done by employing second order statistical measures ("meta-statistics") the so-defined complexity measures are more than essentially a measure for randomness and assign the highest values to structures that lie somewhere between perfect order and randomness [10, 264]. Notwithstanding the still open issues concerning the formal definition of complexity, many complexity measures have successfully been applied in various problems. For obtaining a better overview of the multitude of measures for complexity they have been categorized into structural and dynamical measures [354], deterministic and statistical measures [65] or monotonous and convex measures with respect to randomness [115].
Another very obvious distinction of measures quantifying complex structures can be made between linear and nonlinear measures. While the linear measures are only sensitive to the linear correlations in the data, the nonlinear measures are able to also quantify the nonlinearities or higher order correlations in them. Linear measures comprise the autocorrelation function for time series or the two-point correlation function for spatial data, respectively. On the other hand, there is a battery of nonlinear measures like e.g. the Lyapunov exponent, nonlinear prediction error, spectrum of Rényi-dimensions, Minkowski functionals that are all sensitive to nonlinearities in data sets. Most of these measures are, however, sensitive to changes in both the linear and nonlinear information content of data sets. It is thus in general necessary to figure out by e.g. using surrogates (see chapter 2) to which extent the variations in the nonlinear measure can be attributed to an increase or decrease of nonlinearities in the data.
A clear distinction between linear and nonlinear information content of a data set and thus between linear and nonlinear complexity measure can be made, if the data set is represented in the Fourier space. As this reasoning is essential for many aspects of this thesis, it is outlined in more details. Consider the d-dimensional function $g(\vec{x}), \vec{x} = (x_0, x_1, \ldots, x_{d-1})$, which is discretely sampled at the points $x_0 = 0, 1, \ldots, N-1$, $x_1 = 0, 1, \ldots, N-1$, ..., $x_{d-1} = 0, 1, \ldots, N-1$. Then the discrete Fourier transform $G(\vec{k})$ of $g(\vec{x})$ is given by

$$G(\vec{k}) = FT(g(\vec{x})) = \frac{1}{N^d} \sum_{x_0=0}^{N-1} \sum_{x_1=0}^{N-1} \ldots \sum_{x_{d-1}=0}^{N-1} g(\vec{x}) e^{-i2\pi \vec{k}\vec{x}/N} \; . \tag{1.1}$$

Figure 1.1: Upper row: portraits of C. F. Gauss (left) and J. B. Fourier (right). Lower row: resulting images when combining the Fourier amplitudes of Gauss' portrait with the Fourier phases of Fourier's portrait (left) and vice versa (right).

$G(\vec{k})$ is a complex number and can thus be represented by $G(\vec{k}) = |G(\vec{k})|e^{i\phi(\vec{k})}$ with $|G(\vec{k})|$ being the Fourier amplitudes or modulus and $\phi(\vec{k}) = Im(G(\vec{k}))/Re(G(\vec{k}))$ being the Fourier phase for the mode $\vec{k}$. The square of the modulus $|G(\vec{k})|$ is called the power spectrum of $g(\vec{x})$. In 1914 A. Einstein was the first to note in a largely underrated paper [83] a relationship between the autocorrelation of a time series and the modulus of its Fourier, or more precisely, its cosinus transformation. N. Wiener and A. Khintchine then proved in the thirties of the last century the mathematical one-to-one relation between the autocorrelation function and the power spectrum, which led to the famous Wiener-Khintchine-theorem [361, 166]. This theorem states that the Fourier transformation of the autocorrelation function is the power spectrum. Thus one has to conclude that all linear correlations among the data are fully characterized by the modulus $|G(\vec{k})|$. As the Fourier transformation is bijective, one has to infer that *any* nonlinearity is – solely and completely – coded in the Fourier phases $\phi(k)$ and correlations among them.

The constitutive character of the nonlinear information content as coded in the Fourier phases for complex structures is visualized in fig. 1.1. There we show the portraits of C. F. Gauss and J. B. Fourier and the resulting images, when the Fourier amplitudes of one image are combined with the phases of the other image. It becomes immediately obvious

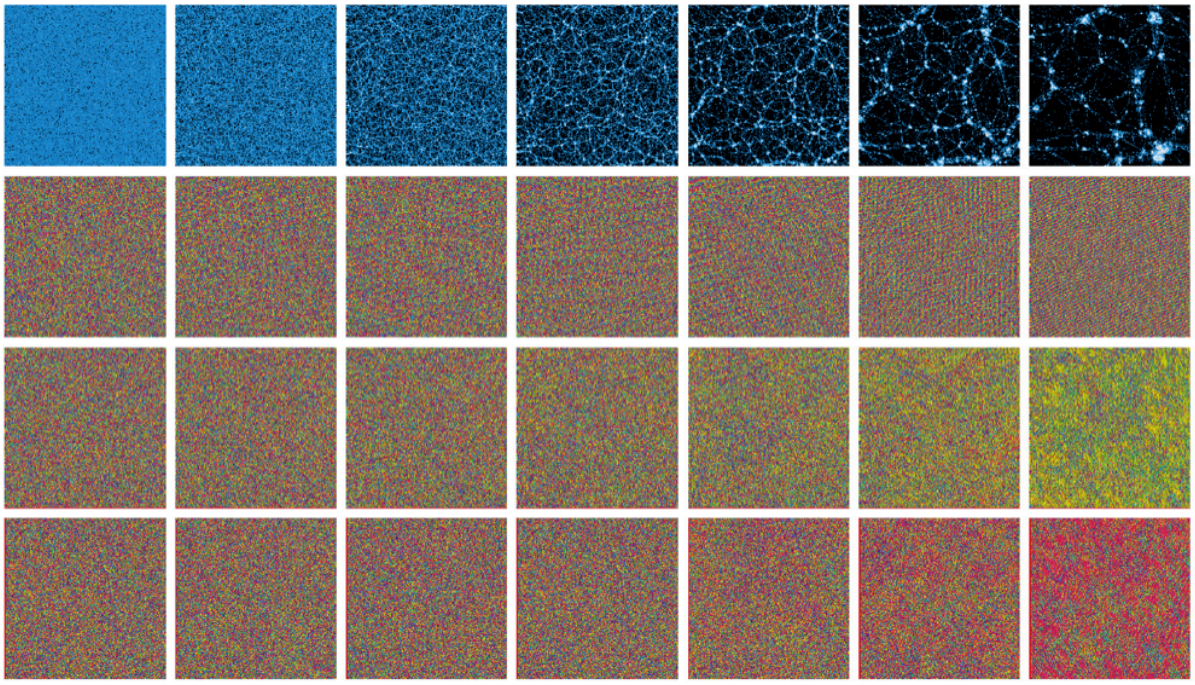

Figure 1.2: The upper row shows a sequence of snapshots from a two-dimensional N-body simulation starting with Gaussian initial conditions. The second column (from above) shows the corresponding color-coded Fourier phases, and the third and fourth columns show phase gradients in the x-direction and y-direction, respectively. Dominant hues in the phase gradients clearly indicate the presence of phase correlations at late times (Source: [56]).

that the portraits remain recognizable, if the phase information is preserved. The Fourier amplitudes do only code a negligible amount of information of the complex image structure. The fact that we can recognize image structures when the nonlinear information is preserved implies that human texture recognition must rely on nonlinear data processing steps. In fact, experiments revealed that already the first signal processing steps in human vision are nonlinear as will be briefly outlined in chapter 2.
A second example, which highlights the importance of nonlinearities and thus of the the Fourier phases on complex structures in a physical context is shown in fig. 1.2. The nonlinear structure formation governed by a comparatively simple gravitational interaction with a $1/r$ interaction potential in the Universe is simulated and the phase response to the nonlinear growth of the emerging large-scale structure is visualized. It is clearly visible that the phases become more and more correlated at late times - yet *"the relation between nonlinear growth and phase correlations is still a mystery."*[1] In this work nonlinear complexity measures are employed and further developed in order to shed more light on underlying (bio-)physical processes. Throughout this thesis we focus on the use of three

[1] Quote from A. Szalay.

classes of nonlinear complexity measures, namely measures in phase or embedding space, morphological measures and Fourier phase statistics.

1.2.1 Complexity measures in phase space or embedding space

The investigation of the properties of the phase space and embedding space representation of dynamical systems offers a complimentary approach to study the behavior of dynamical systems besides the Fourier analysis of the data. The concept of phase space was already developed in the realm of statistical physics by Boltzmann, Poincaré and Gibbs in the late 19th century. But it happened only with the increased interest in complex systems in the last four to five decades that sophisticated analyses of the phase portraits of dynamical systems attracted a lot of attention - not least motivated by the great successes one could achieve in understanding nonlinear systems that even early led to concepts for controlling them [237].

Phase space and embedding space

The phase space of a dynamical system is a space in which all possible states of a system are represented, with each possible state of the system corresponding to one unique point in the phase space. For (mechanical) N-body systems, the phase space usually consists of all possible values of position and momentum variables, i.e. it has $6N$ dimensions. For a system that can be modeled mathematically, the phase space is known from the equations of motion. For experimental and naturally occurring chaotic dynamical systems, the phase space and a mathematical description of the system are often unknown. Attractor reconstruction methods have been developed as a means to reconstruct the phase space and develop new predictive models. Central for this fundamental new concepts of time series analysis were Whitney's and Takens's embedding theorem [360],[335] (for a review see [296]). The Whitney embedding theorem holds that a generic map from an n-manifold to $2n+1$ dimensional Euclidean space is an embedding, i.e. the image of the n-manifold is completely unfolded in the larger space. In particular, no two points in the n-dimensional manifold map to the same point in the $(2n+1)$-dimensional space. As $2n+1$ independent signals measured from a system can be considered as a map from the set of states to 2n+1 dimensional space, Whitney's theorem implies that each state can be identified uniquely by a vector of $2n+1$ measurements, thereby reconstructing the phase space. Takens then showed that the goal of reconstructing the phase space can be reached much easier, namely by measuring only a single quantity. It was proven that instead of $2n+1$ generic quantities $x_0, x_1, \ldots, x_{2n}$, the time-delayed versions $\vec{x_i}(t) = (x_i(t)), x_i(t-\tau), y(t-2\tau), \ldots, y(t-2n\tau))$ of one generic signal x_i (τ: delay time) suffice to embed the n-dimensional manifold. This means that the series of vectors $\vec{x_i}(t_1), \vec{x_i}(t_2), \ldots, \vec{x_i}(t_M)$ is diffeomorphically equivalent to the attractor of the original dynamical system in the limit of infinitely long time series ($M \to \infty$). In real experimental situations one obviously observes a system only for a finite time. Thus one has to check carefully, whether the number of reconstructed phase space vectors is large enough to get an approximation which is good enough for the diffeo-

morphical equivalence to be true at least approximately. Also the embedding dimension and delay time have to be chosen appropriately to efficiently reconstruct the phase portrait of the dynamical system for a limited amount of data. The method of false neighbors [165] offers a framework for unknown data to estimate whether the trajectory has been fully unfolded. The first zero crossing of the autocorrelation function and the first minimum of the mutual information [95] give criteria for an appropriate choice of the delay time τ. Packard and co-workers were the first to demonstrate [238] the feasibility to reconstruct the phase space pictures from the observation of a single coordinate of a dynamical system. Applications of embedding time series data have then been extensive, because methods for the determination of e.g. attractor dimensions, Lyapunov exponents and nonlinear filtering and prediction became applicable to the investigation of the dynamics of complex, higher-dimensional systems, for which one or just a few parameters are accessible by measurement.
One can then even use the idea of embedding beyond dynamical systems theory and embed quite diverse (static) data sets like e.g. image data for further analyses. Two-dimensional (three-dimensional) gray-valued image data are represented in a three-dimensional (four-dimensional) artificial embedding space with the additional dimension (beside the space information) being spanned by the intensity values. Similarly, two-dimensional color images can be represented as five-dimensional point distributions, where the five dimensions are spawned by the two space coordinates and the three color channels (e.g. RGB). In this sense also the two-dimensional temperature maps of the cosmic microwave background radiation, which can be regarded as an intensity image on the unit sphere, are represented as a three-dimensional point distribution by coding the temperature fluctuations as a jitter around the unit sphere (see chapter 5). Although there is no longer a direct link between measures quantifying the point set and system properties, if the embedding is performed by ad-hoc prescriptions, a structural characterization with nonlinear measures remains possible. It turns out that these methods of image processing yield highly sensitive texture measures, which outperform conventional techniques like e.g. wavelets. This is outlined in the chapters 2 and 5 of this thesis.

Estimating scaling properties

In order to assess the (fractal) dimension(s) of the structures such as strange attractors formed by the trajectory of the dynamical system in phase space or embedding space, one makes by some means or other use of estimating the scaling properties of a point set. It has been shown [121, 136] that there is an infinite number of different generalized dimensions that characterize an attractor and its (multi)fractal properties. The most widely used dimension is the correlation dimension D_2 [113, 114], which measures the scaling of the correlation sum

$$C(r) = \frac{2}{N(N-1)} \sum_{i,j;i<j}^{N} \theta(r - \|\vec{x}_i - \vec{x}_j\|) \tag{1.2}$$

(r: size of the neighborhood around each point, N: number of points, θ: Heaviside function) as a function of r, i.e. $C(r) \sim r^{D_2}$ then. D_2 can then be estimated by calculating the logarithmic derivative of $C(r)$ as a function of r,

$$D_2 = \frac{d\log(C(r))}{d\log(r)} \ . \tag{1.3}$$

Rather than looking at the scaling properties of the attractor as a whole one can turn the attention to a local analysis of the scaling properties of a point set by calculating the pointwise dimension D_p, which is also often called scaling indices. To this end one counts only the density of neighboring points $\rho_i(r)$ for each point $\vec{x}_i$,

$$\rho(\vec{x}_i, r) = \frac{1}{(N-1)} \sum_{j=0; j\neq i}^{N} \theta(r - \|\vec{x}_i - \vec{x}_j\|) \tag{1.4}$$

and measures again its scaling with respect to r, i.e. $\rho(\vec{x}_i, r) \sim r^{D_p}(\vec{x}_i, r)$. The pointwise dimension is then assessed in the same manner as the correlation dimension,

$$D_p(\vec{x}_i, r) = \frac{d\log(\rho(\vec{x}_i, r))}{d\log(r)} \ . \tag{1.5}$$

Since the Heaviside-function is non-differentiable, one cannot determine the pointwise dimension $D_p(\vec{x}_i, r)$ at one specific scale r, because the differential quotient for $\log(\rho(\vec{x}_i, r))$ does not exist. To estimate the exponent $D_p(\vec{x}_i, r)$ one rather has to rely on the difference quotient $D_p(\vec{x}_i, \Delta r) \approx \log(\rho(\vec{x}_i, r_2))/\rho(\vec{x}_i, r_1)))/\log(r_2/r_1)$, which only allows to assess the scaling of $\rho(\vec{x}_i, r)$ in a $r-$interval $\Delta r = [r_1; r_2]$. A continuous assessment of the scaling of $\rho_i(r)$ becomes possible, if one replaces the Heaviside function by a differentiable weighting function. In this way one obtains weighted scaling indices $\alpha(\vec{x}_i, r)$ measured at any scale r [265] The general formalism for calculating $\alpha(\vec{x}_i, r)$ reads as follows:
For each point the local weighted cumulative point distribution ρ is calculated. In general form this can be written as

$$\rho(\vec{x}_i, r) = \sum_{j=1}^{N} s_r(d(\vec{x}_i, \vec{x}_j)) \ , \tag{1.6}$$

where $s_r(\bullet)$ denotes a kernel function depending on the scale parameter r and $d(\bullet)$ a distance measure.
The weighted scaling indices $\alpha(\vec{x}_i, r)$ are obtained by calculating the logarithmic derivative of $\rho(\vec{x}_i, r)$ with respect to r,

$$\alpha(\vec{x}_i, r) = \frac{\partial \log \rho(\vec{x}_i, r)}{\partial \log r} = \frac{r}{\rho}\frac{\partial}{\partial r}\rho(\vec{x}_i, r) \ . \tag{1.7}$$

In principle, any differentiable kernel function and any distance measure can be used for calculating α. In the following we use the euclidean norm as distance measure and a set

of Gaussian shaping functions. So the expression for ρ simplifies to

$$\rho(\vec{x}_i, r) = \sum_{j=1}^{N} e^{-(\frac{d_{ij}}{r})^q} \, , d_{ij} = \|\vec{x}_i - \vec{x}_j\| \, . \tag{1.8}$$

The exponent q controls the weighting of the points according to their distance to the point for which $\alpha(\vec{x}_i, r)$ is calculated. The higher q is the more steplike becomes the weighting function resembling more and more the Heaviside-function, which is used for the calculation of the unweighted scaling indices. If $q = 2$ is chosen, the kernel function becomes the well-known Gaussian exponential function, which is widely used for linear filtering of time series and image data. Using a Gaussian shaping function thus allows to contrast the results for local scaling properties with those obtained by linear filtering with filters with the same shape. Throughout all studies in this thesis we calculate the scaling indices α only for the case of $q = 2$. Inserting the expression eqn. 1.8 in the definition for the weighted scaling indices in eqn. 1.7 yields the following analytical expression for α:

$$\alpha(\vec{x}_i, r) = \frac{\sum_{j=1}^{N} q(\frac{d_{ij}}{r})^q e^{-(\frac{d_{ij}}{r})^q}}{\sum_{j=1}^{N} e^{-(\frac{d_{ij}}{r})^q}} \, . \tag{1.9}$$

The scaling indices for the point set form the probability distribution

$$P(\alpha)d\alpha = Prob(\alpha \in [\alpha, \alpha + d\alpha[) \, . \tag{1.10}$$

The $P(\alpha)$-representation of a point set can be regarded as a nonlinear structural decomposition of the data where the points are differentiated according to the local dimensionality of the structure elements to which they belong to. A more refined dimensional analysis, which takes into account the directionality of structures under study, becomes possible by calculating a set of anisotropic weighted scaling indices. The implementation is straightforward in the framework of weighted scaling indices. One only has to use a generalized quadratic distance measure $\| \bullet \|_{\mathbf{A}}$, where $\mathbf{A}$ is a metric tensor, instead of the isotropic Euclidean norm. In the general case $\mathbf{A}$ ($\mathbf{A} = \mathbf{R}^{\mathbf{T}} \cdot \mathbf{M} \cdot \mathbf{R}$) is a product of a rotation matrix $\mathbf{R}$ and a diagonal matrix $\mathbf{M}$ containing the eigenvalues, which control the weighting along the principal axes, i.e. the amount of anisotropy. In *Paper VII.* and *Paper IV.* in this thesis a detailed description of the formalism for calculating weighted anisotropic scaling indices for two- and three-dimensional data sets is given.

Nonlinear prediction error (NPLE)

The mere fact that chaotic time series can be predicted on short time scales at all [73] came as a stunner, as one of the defining properties of chaotic systems is the high sensitivity of the dynamics of the system to changes in the initial conditions and to small fluctuations. But since chaotic systems are still deterministic and show some order, the phase portrait of the trajectories of chaotic systems reflects the order by forming non-random structures

like strange attractors. Also the temporal development of the trajectories on the attractor follows rules. One of them is that trajectories being close to each other move similar in time. Following this basic idea the definition of the nonlinear prediction error (NLPE) ψ is given by the comparison of the predicted behavior of the embedded time series based on the local neighbors with the real trajectory of the system

$$\begin{aligned} \psi &= \psi(d, \tau, T, N) \\ &= \frac{1}{(M - T - (d-1)\tau)} \sqrt{\sum_{n=(d-1)\tau}^{M-1-T} [\vec{g}_{t+T} - F(\vec{g}_t)]^2} \,, \end{aligned} \tag{1.11}$$

where F is a locally constant predictor, M is the length of the time series, and T is the lead time. The predictor F is calculated by averaging over future values of the $N = d + 1$ nearest neighbors in the delay coordinate representation. The choice of N is motivated by the fact that the smallest simplex, which can contain a d-dimensional point, is given by a simplex formed by $d + 1$ vertices (= next neighbors) [332]. It has beed shown [304] that the NLPE is a robust measure for detecting weak nonlinearities in chaotic time series with superimposed noise yielding the overall best performance, when compared with e.g the correlation dimension, three-point correlation function or time reversibility. Therefore, the nonlinear prediction error (NLPE) became a very common statistics to test for weak nonlinearities in time series - especially when the number of time steps for which measurements are available, is limited. Very recent studies even showed that the NLPE also outperforms measures based on recurrence networks [72] and symbolic networks [333] for detecting week nonlinearities in additive superpositions of a linear autoregressive process with the data from the Lorenz system as well as in observational AGN-data [193, 195].

1.2.2 Morphological measures

Another approach for quantifying the information content of complex patterns besides calculating the scaling properties of them is to analyze the morphology of the objects. A full morphological specification of spatial patterns requires topological as well as geometrical descriptors to characterize not only the connectivity but also the content and shape of figures.

The quantification of the one or the other geometrical or topological aspect of spatial patterns has already been introduced in the 1970s and 1980s in image processing [286, 314] and astrophysics, where e.g. the genus of density contours in smoothed three-dimensional density distributions of galaxies was calculated [112], [357] or the number of hot and cold spots in two-dimensional Gaussian and non-Gaussian random fields were counted [54] and then also the Euler-Poincaré characteristic was estimated for these random fields [55]. All these morphological characterizations can be subsumed by the family of measures being called Minkowski functionals (MF), whose origin can be traced back to early work by Minkowski in 1903 [220]. The mathematical formalism was then further developed [119] [295] [2],[327] now also including the valuation of Minkowski tensors (MT) [307], which are

explicitly sensitive to anisotropic aspects of morphology. MFs are defined as follows. Let K be a convex body with a smooth boundary contour ∂K embedded in a d-dim Euclidean space. Then the $d+1$ Minkowski functionals are given by

$$W_0(K) = \int_K d^d r \tag{1.12}$$

$$W_\nu(K) = \int_{\partial K} G_\nu(r) d^{d-1} r \tag{1.13}$$

with $1 \leq \nu \leq d$ and $G_\nu(r)$ being elementary polynomials of the local principal curvatures. Minkowski functionals are motion invariant, additive and continuous. Hadwiger's theorem [119] in the field of integral-geometry further states that the MFs are complete. This is meant in the following sense: Let K^d denote the family of all compact convex subsets of the Euclidean space R^d . Let further L be a linear space. Then a function $\phi : K^d \to L$ is called valuation if $\phi(K_1 \cup K_2) + \phi(K_1 \cap K_2) = \phi(K_1) + \phi(K_2)$ for any $K_1, K_2 \in K^d$ such that $K_1 \cup K_2 \in K^d$. If $\phi : K^d \to L$ is now a continuous, translation- and $SO(d)$-invariant valuation, then ϕ is given by

$$\phi(K) = \sum_{j=0}^{d} c_j W_j(K) \; , \tag{1.14}$$

where $W_j(K)$ is thej^{th} Minkowski valuation and the c_j's are fixed and uniquely defined coefficients. In other words, eqn. 1.14 states that every morphological measure is a linear combination of Minkowski valuations.
The most important property of the Minkowski functionals in the context of this work is the following one: It can be shown [212] that the Minkowski functionals can be expressed as a sum of all n-point correlation functions. Thus the MFs contain information about the higher order correlations making them a natural family of measures for testing for non-Gaussianities and nonlinearities in spatial data.
In two dimensions the three Minkowski functionals have a straightforward interpretation. They are the area A, the perimeter U and the Euler characteristic χ of an excursion set. The Euler characteristic is a topological quantity and measures the number of connected regions minus the number of the holes in this region. The excursion set is obtained by taking all points (i.e. pixels in the discretized case), which exceed a certain threshold ν. This can be obtained by thresholding an intensity or temperature map with respect to ν [298]. Another possibility to define an excursion set of a point distributions is to use the so-called Boolean grain model [212]. In this case one constructs virtual d-dimensional spheres of different size around each point. The space inside the spheres is defined to belong to the excursion set. As the radius of the spheres increases the spheres start to intersect and form partly disconnected bodies with complex morphologies containing holes, tunnels etc. If the spheres become very large, however, the whole point set degenerates into one single filled convex body. The interpretation of the Minkowski functionals in three dimensions is similar to the one in two dimensions. The four quantities are the volume V, the surface

S , the mean breadth B and the Euler characteristic χ of the excursion set. In three dimensions the Euler characteristic is defined as the number of regions plus the number of holes minus the number of tunnels, i.e. regions which pierce the excursion set.
Due to the additivity of the MFs it turns out that there are rather simple prescriptions for calculating the MFs for discretized two- and three-dimensional data [217]. One only has to count the total number of the squares n_s, edges n_e and vertices n_v (cubes n_c, faces n_f, edges n_e and vertices n_v in three dimensions) of the elementary cells making up the excursion set. The Minkowski functionals are then given by the expressions

$$A = n_s, \quad U = -4n_s + 2n_e, \quad \chi = n_s - n_e + n_v \tag{1.15}$$

for the case of two dimensions and by

$$V = n_c, \quad S = -6n_c + 2n_f, \quad 2B = 3n_c - 2n_f + n_e, \quad \chi = -n_c + n_f - n_e + n_v \tag{1.16}$$

for three-dimensional point sets.

1.2.3 Complexity measures based on the Fourier phase information

Eckmann and Ruelle [79] wrote as early as in 1985 in their seminal review on chaos and strange attractors that *"...the analysis of the chaotic motions themselves does not benefit much from the power spectra, because (being the squares of absolute values) they lose phase information, which is essential for the understanding of what happens on a strange attractor"* and thereby acknowledge the importance of the Fourier phase information for understanding complex systems. However, most of the research thereafter was dedicated to the quantification of motion of the system and the (strange) attractors in the higher-dimensional phase space or embedding space. There are so far only a few examples, where the phase information is directly analyzed and attributed to system properties. Coles and Chiang demonstrated (fig. 1.2) [56], how the nonlinear growth of the cosmic structures obviously induces phase correlations. They further introduced (global) phase entropies [46] to characterize the nonlinear growth of the large-scale structure in the Universe and to establish links between the spatial patterns and the physical processes driving galaxy clustering growth.
Another phase statistics put forward by these authors are so-called phase maps [47, 48, 49], which represent an easy, yet versatile way to find nonlinearities and to visualize their presence. Therefore, phase maps are frequently used throughout this thesis as a way to detect and assess nonlinearities in Fourier space. A phase map is defined as a two-dimensional set of points $G = \{\phi_k, \phi_{k+\Delta}\}$, where ϕ_k denotes the phase of the kth Fourier mode and Δ is a mode delay. The mere eye-inspection of the the two-dimensional point distribution G can already give clear indications of the presence of nonlinearities. If the phases were taken from a random, uniform and uncorrelated distribution, the phase maps G would be a random two-dimensional distribution of points in the interval $[-\pi, \pi]$. Any significant deviation from this random distribution often already seen with the naked eye points towards

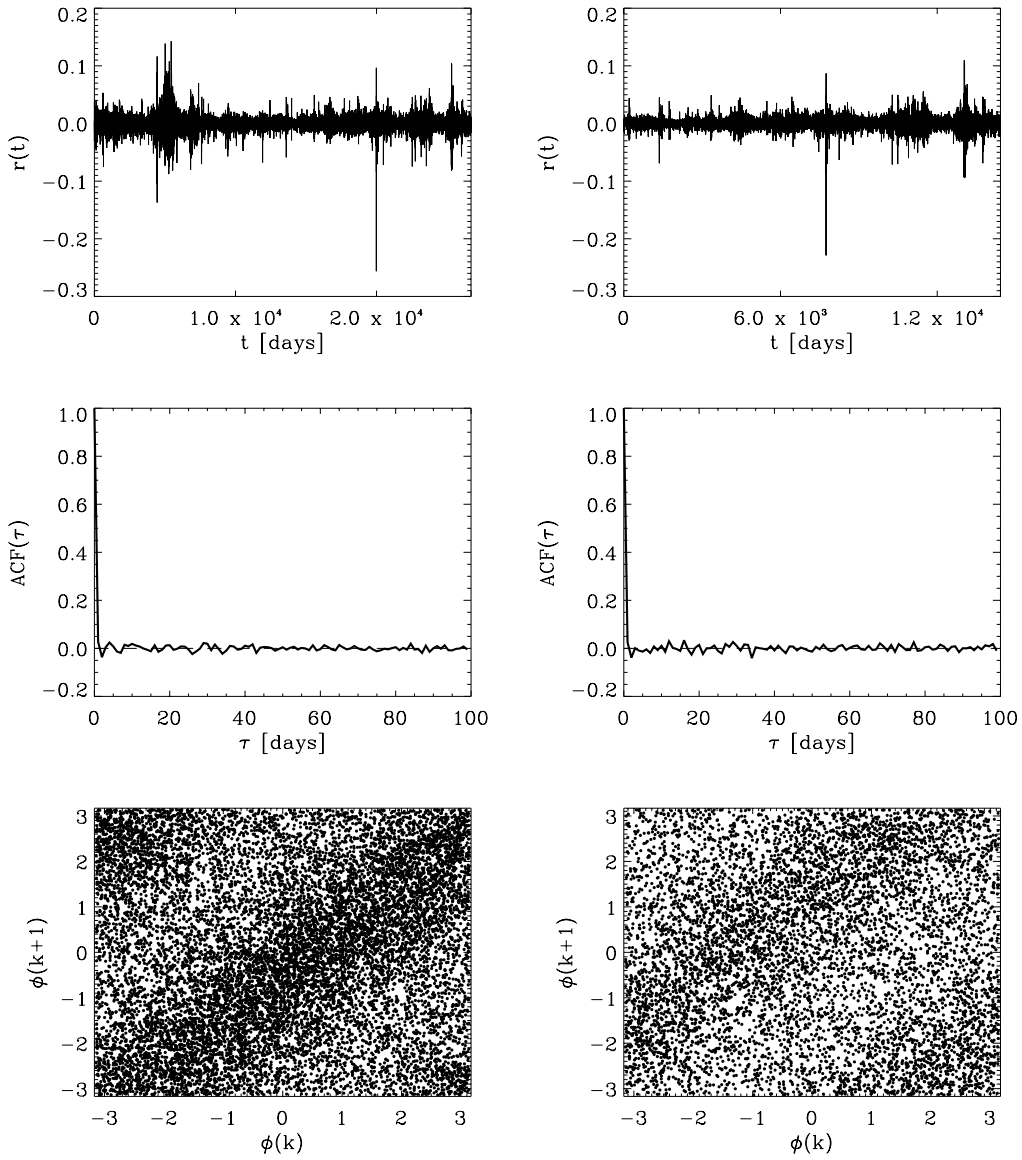

Figure 1.3: Upper row: Day-to-day returns $r(t)$ derived from several thousand consecutive trading days for the Dow Jones (left) and S & P (right) index. Middle row: Respective autocorrelation functions. Lower Row: Respective phase maps with a mode-lag of $\Delta = 1$.

the presence of nonlinearities in the data. The features in the non-uniform distribution of G can already point towards the kind of correlations among the phases.
As an example we show one phase map of the day-to-day returns $r(t)$ derived from several thousand consecutive trading days for two very broad stock market indices, namely the Dow Jones and Standard & Poor's (S & P) index. In fig. 1.3 we also show the autocorrelation function of the two time series. The immediate insight one can gain from the autocorrelation function on the one hand and the phase map on the other hand is that the two time series have no linear correlations while the deviations from randomness in the phase maps clearly indicate the presence of nonlinearities. The somewhat strange and rare behavior that *only* nonlinear correlations are detected in the data is often observed in financial time series and makes them highly attractive candidates for developing, applying and testing new methods of nonlinear time series analysis - also and especially from an academic and/or scientific point of view. A closer investigation of the detected features in the phase maps reveals that the linear correlations can be attributed to the bursts in the time series, which are characteristic for an intermittent signal. This will be described in more details in chapter 6.
Another way to quantify the information content of the phases is to apply Kuiper's test (KT) [184] to a distribution of phases or phase differences. The KT is a variant of the standard Kolmogorov-Smirnov test, which has yet the advantages to be as sensitive in the tails as at the median and to be invariant under cyclic transformations. This invariance makes the Kuiper's test invaluable for testing the fit of and the differences between circular probability distributions og e.g. Fourier phases. The standard Kolmogorov-Smirnov statistic is taken as the maximum deviation of the cumulative probability distribution being compared. For a circular function, however, one needs to take into account the maximum deviation both above and below the cumulative probability being compared. Kuiper's test is thus based on the sum of the maximal positive and negative deviation from the cumulative probability function tested against. Applying Kuiper's test to the distribution of Fourier phases and phase differences of the maps of the cosmic microwave background (CMB) yielded significant signatures for deviations from randomness [57, 50, 222] representing an example for unexpected anomalies in the CMB (for more details see chapter 5). Kuiper's test represents one example for a more sophisticated analysis of the Fourier phases. Currently we are working on the development of phase walk statistics [302], which are defined in close analogy to random walk measures, to assess the deviations from randomness for the Fourier phases. First results obtained for leptokurtic time series are very encouraging.

Chapter 2

Surrogates

2.1 The need for surrogates

A specification of Immanuel Kant's first (of his four) famous question "What can we know?" formulates exactly one of the first questions to be addressed in the analysis of complex systems, namely: "What can be inferred about an underlying dynamical process in practical situations where all that is available are data?" The final aim is of course to develop a suitable model that explains the system behavior by some basic laws and thus describes it quantitatively and is able to predict the system behavior to some extent. Yet, there are a lot of cases where the number of free parameters of the system and their linear and nonlinear interactions are far too large so that a closed model is at least hard to find if not impossible. Still, also in those cases the identification of different states of the system may given valuable insights and yield a valuable classification between e.g. healthy and ill patients. Major progress in data-drive analyses would also be achieved, if one is also able to make predictions of extreme events in complex systems like e.g. stroke, heart attack, epileptic seizure or stock market crash only on the basis of the data and their evolving characteristics. Although some partly impressive progress in forecasting systems has been made [111], long term predictions of complex system are still far from being reliable as can be seen in the daily weather forecast. For both the purely descriptive data analysis and the model building the first question to be addressed is whether the data set has nonlinearities in it or not. If there are no nonlinearities the knowledge of the autocorrelation or power spectrum is sufficient to describe the regularities in the data and to make predictions. Linear equations describe the underlying physical process properly and can often easily be built by e.g. autoregressive-moving-average (ARMA) models [28]. If nonlinear correlations can unambiguously be identified in the data, the model equations have to have also nonlinear terms and forecasting becomes at least difficult or is simply impossible. In general, the situation becomes complex - not least because the mere detection of nonlinearities does not constrain the nonlinear terms in the model equations.
As briefly outlined in the previous section there is a plethora of nonlinear statistics with which complex structures can be assessed in a quantitative manner. Many of them are,

however, not very reliable when applied to often short and noisy experimental data sets, so that simple autocorrelations in the data can lead to a false detection of nonlinearities. Further, if a nonlinear statistics yields values that deviate from those expected for the pure linear case, it is not clear how significant this deviation is and whether it already assigns the presence of nonlinearities. These problems can – to a great extent – be overcome by applying the method of surrogates [339] (for a review see [306]). This approach is formulated in the language of statistical hypothesis testing and need two ingredients, namely a null hypothesis and a discriminating statistics. The null hypothesis is formulated in such a manner that it should turn out to be inadequate for describing the data. The discriminating statistics is a number which quantifies some aspects of the data set. If the number is different for the observed data than would be expected under the null hypothesis, then the null hypothesis can be rejected. The significance with which the discriminating statistics deviates from the expected value under the null hypothesis is directly determined by generating a set of surrogate data, which have some properties of the original time series ("the null hypothesis") in common while all other properties are subject to randomization. If the computed discrimination statistics for the original data is significantly different from the values obtained for the set of surrogates, one can infer that the null hypothesis has to be rejected. The method of surrogates also represents a resampling technique like jackknife and bootstrapping, which were earlier developed for determining the error and bias of discriminating statistics [81]. There are, however, important differences. While jackknife and bootstrapping see an observation as a sample of data points where some elements are left out or counted more than once, the surrogate data sets are realizations of randomized versions of the whole sample, where no data are left out. What matters in the latter case are the *global* properties of the data sample that are preserved or randomized.

It is interesting to notice that the ideas of the method of surrogates were already developed and applied in the field of image processing some years before Theiler's seminal paper on timer series analysis was published. As it was already shown in fig. 1.1 the information in an image which is important for a human observer to recognize the faces in the images is contained in the Fourier phases. One can thus immediately infer that human image perception image has to contain nonlinear data processing steps. It was Bela Julesz and his co-workers who was the first to develop the theory of human visual perception of textures (see [160, 161] and references therein). It was found that human texture detection and texture discrimination is based on a few local conspicuous features, called textons. To obtain the result that not global differences but rather local ones directly contribute to the discrimination of textures the use of surrogates turned out to be crucial. Specifically, the construction of iso-second-order texture pairs that are effortlessly discriminable by humans (see fig. 2.1) lead to the conclusion that human texture recognition is based on textons. Formalizing the concept of textons in machine vision leads to the introduction of local nonlinear filtering techniques using Gabor filters, wavelets, scaling indices etc. for texture detection and texture discrimination as it was first outlined in the pioneering work of A. Jain and F. Farrokhnia [154].

This examples show that the application of the method of surrogates is not restricted to time series analysis. The general idea can be applied – mutatis mutandis – to any n-

Figure 2.1: Two examples of iso-second-order texture pairs, which are preattentively discriminable by humans. The left texture pair is discriminated due to the local conspicuous feature, i.e., texton, of "quasicollinearity", the right pair is discriminable due to the texton of "corner" (Source:[161]).

dimensional data set, which considerably enlarges the fields of application of the method of surrogates. Surrogate-assisted analyses of two- and three-dimensional scientific image data are one of the general themes of this work as will be outlined in the next chapters.

2.2 Generating surrogates

Most commonly used surrogates in time series analysis and image processing are those where the linear properties of the data set and/or the probability density (PDF) in real space are preserved, while all other properties are subject to randomization. Preserving the linear properties means that the autocorrelation function in real space or – according to the (Einstein-)Wiener-Khintchine-theorem – the power spectrum in Fourier space is to be preserved. Two classes of algorithms for generating surrogates have been developed. They are methods based on the Fourier transformation (FT surrogates) [339, 303] and simulated annealing [215, 173]. An obvious way to generate surrogates with the same linear properties is to replace the Fourier phases of the original data by a set of uncorrelated and uniformly distributed ones and to perform an inverse Fourier transformation with the set of random phases. These so called FT (Fourier-transformed) surrogates exactly reproduce the linear properties of the original time series. All other properties, including the PDF of course, are lost.
Amplitude adjusted Fourier-transformed surrogates [339] are intended to reproduce both the linear features and the PDF of the original data. The algorithmic steps are the following ones. The data are first rank-ordered remapped onto a Gaussian distribution. For the

remapped data FT surrogates are generated by phase randomization. Finally, the data in real space are rank-ordered remapped back onto the original PDF. The so-obtained surrogates exactly reproduce the original PDF but only approximately reproduce the linear properties, since the last remapping step obviously influences the power spectrum.
Schreiber and Schmitz showed that AAFT surrogates generally whiten the power spectrum [303], which can lead to a false indication of nonlinearities in linear time series. They introduced the iterated amplitude adjusted Fourier-transformed (IAAFT) surrogates, which preserve both the power spectrum and the PDF very well. The iterative algorithm consists of the following steps: First, one stores the PDF and the power spectrum of the original time series and shuffles the data. The iteration consists of two steps. First, the data are Fourier-transformed and the power spectrum is replaced by the stored one. Then an inverse Fourier transformation with the desired power spectrum is performed and the data in real space are rank-ordered remapped onto the stored PDF. The iteration is repeated for a defined number of times or until no further change occurs. It is worth noting that in this algorithm the randomness of the phases is nowhere explicitly imposed.
Another approach for generating surrogates relies on the optimization of constraints by simulated annealing (SA) [305]. Specifically the constraints $C_i(data) = 0$ are specified in terms of a cost function $E(data)$ which has a global minimum when the constraints are fulfilled. Second, the cost function E(data) has to be minimized among all permutations of the data by simulated annealing. In this context the cost function is interpreted as an energy in a thermodynamic system. At a finite temperature T, system configurations are visited with a probability according to a Boltzmann distribution $e^{-E/T}$ of the canonical ensemble. This can be achieved by accepting changes of the configuration with a probability $p = 1$ if the energy decreases ($\Delta E < 0$), and $p = e^{\Delta E/T}$ if the energy increases ($\Delta E \geq 0$). During the iteration the temperature is decreased which corresponds to an annealing of the system to the ground state of minimal energy. In the specific case where one wants to reproduce the linear properties of a time series the cost function E to be minimized is the difference between the autocorrelation function $A(\tau)$ of a permutation of the data and the original ones, $E = \left(\sum_{\tau=0}^{N-1} |A^{perm}(\tau) - A^{orig}(\tau)|^q\right)^{1/q}$.
The different permutations of the time series are obtained by starting with a random shuffle of the data and then interchanging pairs of values. With this approach, one ensures that the PDF of the time series is exactly preserved. The linear correlations are also well reconstructed as E approaches zero. The simulated annealing approach is much more CPU intensive than FT-based methods for generating surrogates. But it has the big advantage that it is more flexible. One can generate surrogates for time series with gaps [300], where FT methods used in the standard way cannot be applied, because the basis functions are no longer orthonormal and thus a simple phase shuffling cannot be applied. (In principle, one can still apply FT-based methods with phase shuffling, if one performs first a transformation into a new set of basis functions, which is orthonormal in the data space with gaps. The mathematical procedure is, however, rather elaborate and the methodology has so far only worked out for a few numerically solvable cases of (CMB-)data being represented on the unit sphere [288, 290]. Using simulated annealing also allows to generate surrogates,

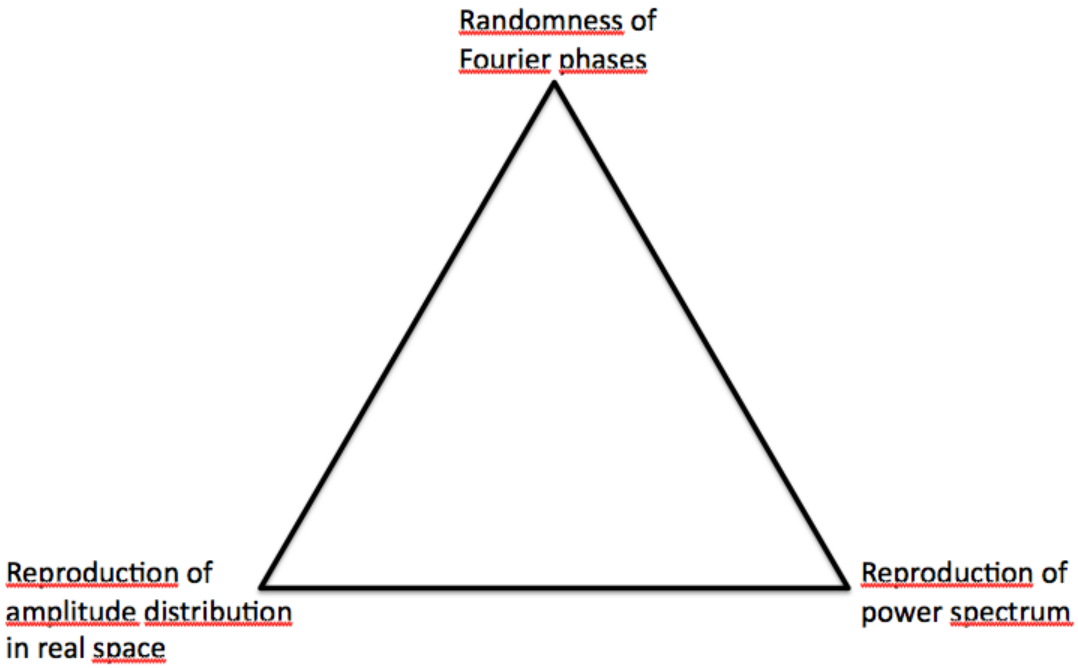

Figure 2.2: Triangle of constraints for surrogate generating algorithms.

in which other constraints than the autocorrelation function are preserved. This allows e.g. for a comparison of different higher order statistics by generating surrogates with e.g. the same Minkowski functionals that are assessed with scaling indices [267]. In chapter 5 an analysis of light curves of an active galactic nucleus (AGN) with SA-surrogates will be presented.
Methods for generating surrogates should aim for an as accurate as possible reproduction of the power spectrum and the amplitude distribution in real space while preserving the randomness of the Fourier phases. These three constraints can be visualized as a triangle of surrogate constraints and are shown in Fig. 2.2. As outlined above, the (I)AAFT algorithms put much emphasis on very accurately reproducing the power spectrum and the amplitude distribution. Less attention is paid to preserving the randomness of the phases after remapping or during iteration. In

Paper I. [275]: Revisiting algorithms for generating surrogate time series, Phys. Rev. Lett. ***106****, 155001 (2012)*

the FT-, AAFT- and IAAFT-algorithm for generating surrogate time series are reassessed with a yet unprecedented level of scrutiny by studying both Fourier phase statistics and the nonlinear prediction error. Using an XMM observation of the narrow-line Seyfert 1 galaxy Mrk 766 as well as the Dow Jones day-to-day returns as examples, it is demonstrated that the (I)AAFT algorithms for generating surrogates often fail to generate truly linear time series. Rather, they often create surrogate realizations with Fourier phase correlations

leading to non-detections of nonlinearities. It is argued that reliable surrogates can only be generated, if one tests separately for static and dynamic nonlinearities. In the light of our new findings it may be necessary that previous results obtained with surrogates have to be critically reassessed.

More applications of Fourier phase manipulations are found in image processing. On the one hand, the randomization of phase information has become a standard technique for optical image encryption [280]. In x-ray crystallography, on the other hand, the phase problem, i.e. the reconstruction of the phase information has to be solved for the determination of two- and three-dimensional structures of e.g. biomolecules like DNA or drug receptor from diffraction data, which only yield the power spectrum of the probes. Jerome Karle along with Herbert Hauptmann [162, 163] (for a review see [130]) and later on Wayne Hendrickson [135] developed the mathematics upon which single wavelength anomalous dispersion (SAD) and multi-wavelength anomalous dispersion (MAD) techniques are based. Both approaches allow to infer the phase information. SAD is based on diffraction measurements of the original sample and of one in which multiple isomorphous replacement (MIR) of constituents preferably with heavy atoms has been performed. MAD takes advantage of the fact that resonance between beams of x-ray waves and electronic transitions from bound atomic orbitals leads to anomalous, wavelength-dependent scattering.

Phases can also be retrieved by image post processing methods alone, if an object, that is to be reconstructed, fulfills some - rather general - constraints (see e.g. [99, 93, 94, 218, 90, 285]). It has been demonstrated that it is already sufficient to demand that e.g. the object intensities are positive. An additional constraint that may be enforced is that the diameter of the reconstructed image may not exceed the known diameter of the object. Modifications of the iterative, so-called Gerchberg-Saxton algorithm solve the phase retrieval problem. In its easiest form the iteration comprises the following steps: At the k'th iteration, $g_k(x)$, an estimate of the object, is Fourier transformed; the Fourier transform is made to conform to the known modulus and the result is inverse-Fourier transformed, giving the image $g'_k(x)$. Then the iteration is completed by forming a new estimate of the object that conforms to the object-domain constraints, i.e. $g_{k+1}(x) = g'_k(x)$ if $g'_k(x)$ fulfills the constraints and $g_{k+1}(x) = 0$ otherwise. Fig. 2.3 shows a block diagram of the Gerchberg-Saxton algorithm for phase retrieval. One finds striking similarities between the IAAFT surrogate generation algorithm and the Gerchberg-Saxton phase retrieval algorithm. Both methods are essentially based on the same iteration scheme. Having revealed the similarities between the Gerchberg-Saxton and IAAFT algorithm it is no longer a surprise that the IAAFT method is prone to induce phase correlations in surrogate time series as it is essentially a phase retrieval algorithm.

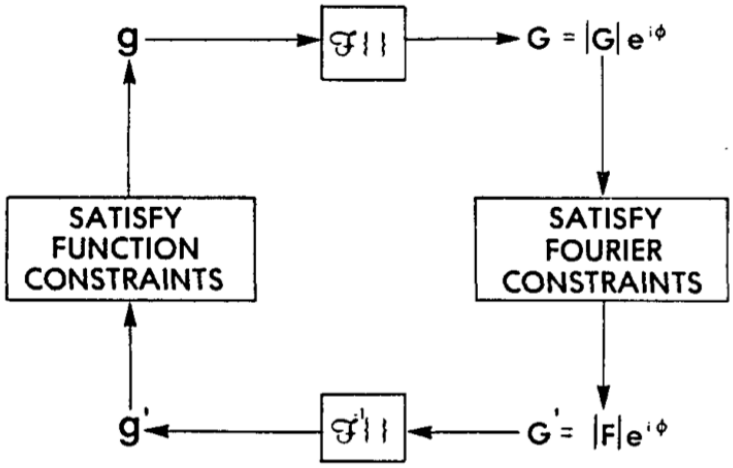

Figure 2.3: Block diagram of the Gerchberg-Saxton algorithm for phase retrieval. (Source: [94])

2.3 Variation on a theme: assessing higher order statistics using surrogates

The method of surrogate data providing a rigorous statistical test for the null hypothesis that the data have been generated by a linear stochastic process or that a random field is Gaussian, can also be used to assess the performance of a number of measures being sensitive to higher order correlations. Measures of nonlinearity in a time series were compared numerically with the result that the rating of the different measures varied from example to example. The nonlinear prediction error yielded, however, a good overall performance and is therefore a preferable measure [304]. We recently demonstrated [195] that this result remains even valid, when newly developed network-based measures for nonlinearities are considered. In the paper

Paper II. [271]: Comparing the sensitivity of wavelets, Minkowski functionals and scaling indices to higher order correlations in MR images of the trabecular bone using surrogates, Proc. of SPIE ***7259****, 72590D (2009)*

we extend the idea of testing different higher order statistics by means of surrogate data to the two-dimensional case. We propose and apply a general statistical framework, with which one can systematically assess the sensitivity of texture measures to higher order correlations (HOCs) and to select the suited ones in a given context. Here, we were interested in quantifying the information content of the complex inner trabecular bone structure as visualized with high resolution magnetic resonance imaging techniques. To this end, surrogate images are generated, in which the linear properties are preserved, while all higher order correlations are *gradually* wiped out. This is achieved by an iterative pairwise exchange of the Fourier phase. We compare three commonly used classes of texture measures,

namely spherical Mexican hat wavelets (SMHW), Minkowski functionals (MF) and scaling indices (SIM). While the SMHW yield only very poor sensitivity to HOCs in these cases, the MF and SIM could detect the HOCs very well with high significance. Thus the latter two are to be preferred in this context. It is worth mentioning that higher order correlations are no longer detected by none of the measures when only approximately 50% of the phases are randomized. Higher order correlations thus become rather quickly immeasurable when the phase information is manipulated.
In a subsequent study we compared the three classes of texture measures with respect to their sensitivity to scale-dependent higher order correlations and found very similar results [273]. The bad performance of the SMHW obviously explains why we did not obtain convincing discrimination results between healthy and osteoporotic bones in previous studies, where we used wavelets as structure measure. In all our subsequent studies on bone stability SMHW were not considered any more.

Chapter 3

Inner bone as a complex adaptive system

3.1 Bone remodeling

In the 19th century the German physician Julius Wolff investigated for decades the inner structure, the growth and the changes of bones. These long-term studies ended in his main work entitled "Das Gesetz der Transformation der Knochen" [363], in which he formulated the general principles, which govern the bone formation and bone transformation processes during lifetime. These general rules became famous as Wolff's law of bone remodeling. It states that bone in a healthy person or animal will adapt to the loads under which it is placed. If loading on a particular bone increases, the bone will remodel itself over time to become stronger to resist that sort of loading. The internal architecture of the inner bone, the so-called trabecular network, undergoes adaptive changes. The inverse is true as well: if the loading on a bone decreases, the bone will become less dense and weaker due to the lack of the stimulus required for continued remodeling. It was obviously J. Wolff's ingenuity, that led to a correct prediction of all basic mechanisms of bone remodeling by only interpreting the morphology of a large number of bone probes and without having any knowledge about the physiological processes on the cell-level and molecular level. The essentials of bone remodeling can nowadays be summarized as follows [368, 293, 260]:

Bone remodeling relies on the correct function of two principal cells of the bone tissue: the osteoclasts [337], multinucleated cells that destroy the bone matrix, and the osteoblasts [76], having osteogenic functions. The osteocytes [23], another important cell type arising from the osteoblasts, are also involved in the remodeling process as they have a mechanosensorial function. A correct balance between bone resorption and osteogenic functions is mandatory to maintain a constant bone mass. Bone remodeling is accomplished according to the following phases (see fig. 3.1). In the initiation phase, mechanical loading and microdamage are sensed by osteocytes, which stimulate the recruitment of osteoclast precursor cells. Osteoclastogenesis is stimulated by the expression of RANKL (Receptor Activator of Nuclear κB Ligand), macrophage colony-stimulating factor (M-

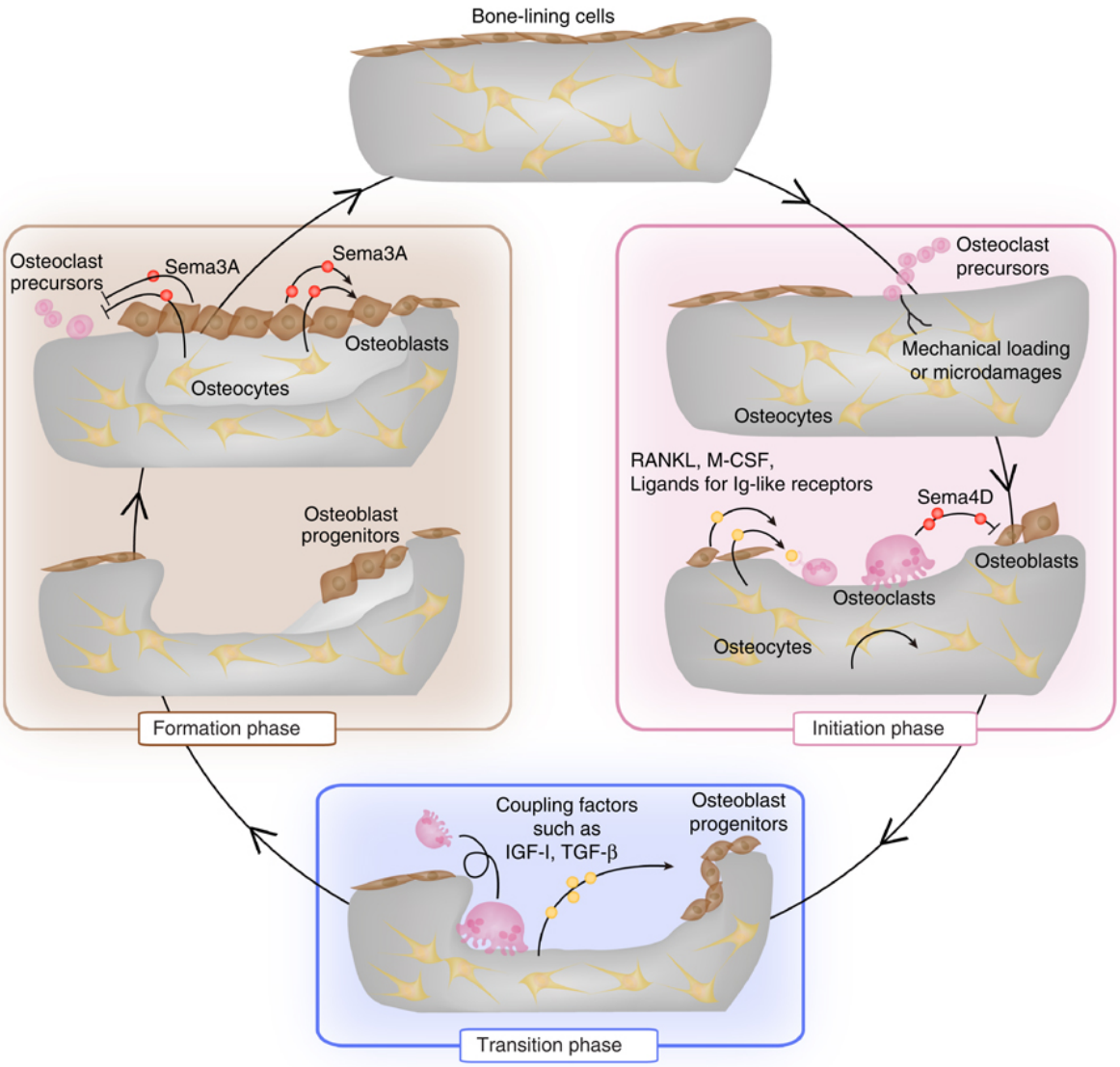

Figure 3.1: The bone remodeling cycle (Source:[234]). For a detailed description see text.

CSF) and ligands for immunoglobulin-like receptors, which are produced by osteoblast lineage cells including osteocytes. The osteoclast precursor cells have RANK receptors on their surface to which RANKL binds and transforms the osteoclast precursor cells to osteoclasts. The bone resorption now starts. To modulate the effect of the RANKL protein the osteoblasts secretes also another protein, the osteoprotegerin (OPG). OPG binds RANKL and thus prevents RANKL from binding to RANK. Therefore, OPG controls the intensity and length of osteoclastformation and thus bone resorption. Osteoclasts inhibit, on the other hand, bone formation during bone resorption through the expression of Semaphorin 4D. In the transition phase, classical coupling factors, including IGF-I and TGF-β1, stimulate the migration of osteoprogenitors to the resorbed sites and promote differentiation into osteoblasts. In the bone formation phase, osteoblasts replenish the resorbed area with new bone. Semaphorin 3A, which is produced by osteoblast lineage cells, inhibits the genesis of osteoclasts and simultaneously promotes bone formation in this phase. Although the major coupling factors especially between osteoblasts and osteoclasts controlling the delicate balance of the interactions of bone cells so as to maintain bone homeostasis have been elucidated, ongoing research still reveals new communication paths among bone cells. They give rise to an increasingly complex description of the bone remodeling process.
But already the assumption that the coupling factors between osteoblasts and osteoclasts are (purely) mechanical and governed by strain perturbations - be they generated externally by different load conditions or internally by resorption cavities - allows to model the bone remodeling process in a realistic manner. For instance, these model calculations can explain the emergence and maintenance of trabecular architecture as an optimal mechanical structure, as well as its adaptation to alternative external loads (see e.g. [141, 294, 268, 155, 347, 348]). The bone remodeling processes are described by nonlinear rate equations, which model the effect of osteoblasts and osteoclasts on the local change of relative bone density. Furthermore, the effect of external mechanical forces on the structural adaptation in trabecular bone is included in the model equations [141]. The rate equations are solved numerically by finite element analysis (FEA) [294] or by cellular automata [268]. From a complex systems perspective, the bone remodeling process and its simulation represents yet another remarkable example of a natural system being described by comparably few and simple but discontinuous and nonlinear (partial) differential equations whose solutions lead to very complex spatiotemporal patterns.

3.2 Malfunction of bone remodeling: osteoporosis

A malfunction of the bone remodeling process leads to an imbalance in skeletal turnover. The delicate balance between bone resorption and bone formation becomes distorted, such that perturbations in either process can result in reduced bone mass, altered bone architecture and a greater propensity for fracture. The most important disease, that arises when bone resorption exceeds bone formation, is osteoporosis. By far the most common form of this disease is primary or idiopathic osteoporosis, which affects people in the second half of their lives. Although the mechanisms in female and males are probably similar, the

disease starts earlier in women, as estrogens in women decrease earlier than androgens in men. There are several other factors that contribute to the negative net effect like decrease reduced physical activity, insufficient vitamin D and calcium intake, lower endogenous production of vitamin D due to e.g. reduced UV exposure or reduced renal function secondary to diabetes. Secondary osteoporosis is an accompanying illness following other endocrine, metabolic or oncological diseases or is a results of side-effect of long-term drug intake.
Osteoporosis became a common disease endemic in (aging) Western societies and manifests itself as back pain and fractures without significant trauma occurring at multiple skeletal sites, most often at the spine, hip, or wrist. Osteoporotic fractures cause significant morbidity and increased mortality, which is mainly induced by secondary diseases of immobile (elder) patients. According to the world health organization (WHO) osteoporosis belongs to the ten most important chronic diseases worldwide and the burden of is expected to rise in the future with the aging of our societies. One estimates that by 2025 the number of incident osteoporosis attributable fractures (OAF) will surpass three million causing 25 billion Dollar direct medical costs only in the United States [36]. Similar studies forecast for Germany a rise of OAFs from 115.248 in 2010 to 273.794 in 2050. Total undiscounted incident OAF costs will increase from around one billion Euros in 2010 to 6.1 billion Euros in 2050. Discounted (3%) cumulated costs from 2010 to 2050 will amount to 88.5 billion Euros (168.5 undiscounted), with 76% being direct and 24% indirect costs [21].
Having elucidated the complex regulatory network of bone remodeling it became clear that osteoporosis is not just an unchangeable effect of aging but rather a disease that can be treated:
The most commonly prescribed drugs used to treat osteoporosis are bisphosphonates like alendronate or risendronate. They inhibit the digestion of bone by encouraging osteoclasts to undergo apoptosis, i.e. cell death, thereby slowing bone loss. Clinical studies showed that alendronate increases the bone mass in the spine, hip, and total body and reduces the incidence of vertebral fractures, the progression of vertebral deformities, and height loss in postmenopausal women with osteoporosis [199]. Risendronate decreased the cumulative incidence of new vertebral fractures. Bone mineral density increased significantly compared with placebo at the lumbar spine, femoral neck, femoral trochanter, and midshaft of the radius [127].
Selective estrogen receptor modulators (SERMs) are a class of non-hormonal drugs that act on the estrogen receptor (ER). A characteristic that distinguishes these substances from pure ER agonists and antagonists is that their action is different in various tissues, thereby granting the possibility to selectively inhibit or stimulate estrogen-like action in various tissues. The SERM raloxifen is estrogenic in bone and thus impedes the action of the osteoclast. It could be shown that in postmenopausal women with osteoporosis, raloxifene increases bone mineral density in the spine and femoral neck and reduces risk of vertebral fracture [88].
The parathyroid hormone (PTH) - although classically considered to be a bone catabolic agent - can stimulate cortical and trabecular bone growth by increasing the activity of osteoblasts when delivered intermittently at low doses. Large clinical studies showed that PTH leads to increase of vertebral, femoral, and total-body bone mineral density and to a

decrease of vertebral and nonvertebral fractures [231].
Denosumab is a new class of osteoporosis treatment called a human monoclonal antibody that inhibits osteoclast formation by imitating the effects of OPG on RANKL. It was shown that denosumab given subcutaneously (only) twice yearly for 36 months was associated with a reduction in the risk of vertebral, nonvertebral, and hip fractures in women with osteoporosis [67].
Both the diagnosis of osteoporosis and the monitoring of a chosen therapy requires a best possible quantification of the complex bone structures before and during therapy.

3.3 Quantifying bone structures

Osteoporosis is nowadays defined as a skeletal disorder characterized by compromised bone strength predisposing to an increased risk of fracture. To clarify this definition the following statements were added: Bone strength reflects the integration of two main features: bone density and bone quality. Bone density is expressed as grams of mineral per area or volume. Bone quality refers to architecture, turnover, damage accumulation (e.g. microfractures) and mineralization. The measurement of the bone mineral density (BMD) became the first diagnostic parameter for the diagnosis of osteoporosis. Measuring the BMD with dual energy X-ray absorptiometry (DEXA) and dual energy quantitative computed tomography (DEQCT) is now a well established and widespread technique for assessing the bone strength. A number of studies, however, have quickly indicated (see e.g. [351, 355]) that BMD alone has limitations in determining the strength of cancellous bone. The other important component responsible for bone strength is the trabecular architecture, which is not yet assessed as a standard procedure. Techniques that assess the trabecular structure were later developed than those focusing on BMD. Structural analyses of the inner could only be performed with the availability of imaging modalities with spatial resolution in the range of the size of the trabecular network. Advances in tomographic imaging techniques, such as computed tomography (CT), micro CT (μCT) and high-resolution magnetic resonance imaging (HR-MRI) have significantly improved the spatial resolution being now of the order of the trabeculae in bone. The conventional procedure to examine structural properties of cancellous bone is to use the (two-dimensional) histomorphometric measures as they were used in histological investigations of 2D sections of bone biopsies. The primary indices are bone fraction (BV/TV), trabecular separation (Tb.Sp), trabecular thickness (Tb.Th) and trabecular number (Tb.N) [242]. As histomorphometric analyses are performed at a much higher spatial resolution than that obtained in clinical CT or MR images, the structure parameters are defined as apparent values (app.BV/TV, app.Tb.Sp, app.Tb.Th, and app.Tb.N). With the advent of 3D imaging techniques, also three-dimensional extensions of the histomorphometric parameters were introduced [137].
The first aim of our studies in bone research was to investigate to which extent the quantitative characterization of the trabecular bone structure can be improved, if the complex bone network is described by more sophisticated, nonlinear estimators. We used scaling indices, which seemed to be particularly well suited to quantify the transition from plate-

like to rod-like structures during osteoporosis and Minkowski-functionals, which capture the topological changes of the trabecular network. Among the many in vivo and in vitro studies we conducted (see also e.g. [330]) we present below three exemplary papers, where the advantages of the newly introduced structure measures become obvious and where new insights on processes governing bone remodeling are gained.
The aim of

Paper III. [227]: The 3D-Based Scaling Index Algorithm - A New Structure Measure to Analyze Trabecular Bone Architecture in High-Resolution MR Images In Vivo, Osteoporosis International, ***17****,1483-1493 (2006)*

is twofold. Firstly, it is demonstrated that it is feasible to perform high resolution imaging of the trabecular bone with clinical MR scanners, which are available at most institutions and can be used in vivo. Secondly, it is shown that with more complex structural complexity measures, which are based on an assessment of the local scaling properties of point sets, a better discrimination between patients with and without osteoporosis is made possible. We therefore performed a clinical study with patients (forty postmenopausal women) with osteoporotic spine fractures and healthy controls. Three-dimensional high resolution tomographic magnetic resonance images of the distal radius were acquired. The bone mineral density was determined by QCT examinations. The standard two-dimensional (2D) bone histomorphometric parameters and the 3D-based (isotropic) scaling indices were calculated after segmentation from the high resolution magnetic resonance data (HRMR) from the distal radius. Receiver operating characteristic (ROC) analyses for determining the diagnostic performance in differentiating both groups revealed that the discrimination between the two classes became significantly better as compared to BMD and the histomorphometric measures, when scaling indices were used as structure measure. This 3D characterization of the trabecular microarchitecture may thus provide a new approach to better assess the strength of human cancellous bone using HR-MR image data.
The two further in vitro studies are based on a rather unique data sample of bone probes, which were acquired by medical institutions in Munich, where bone research is actively performed, namely the Institute of Anatomy of the Ludwig-Maximilians-University and the Department of Radiology of the Technical University. It consists in total of several hundred cylindrical bone probes with a diameter of 8 mm taken from different skeletal sites and represents the largest currently available sample of bone probes, which has been imaged with μCT with a isotropic spatial resolution of 26 μm and mechanically tested afterwards. These data thus allow to apply complex three-dimensional texture measures and subsequently test their performance by correlating them with the the strength of the bone as measured by the maximum compressive strength (MCS).
In the paper

Paper IV. [270]: Strength through structure: visualization and local assessment of the trabecular bone structure, New Journal of Physics, ***10****, 125010 (2008)*

it is demonstrated how the use of nonlinear, structural complexity measures for the analysis of the three-dimensional image data leads to additional diagnostic parameters, which

go beyond the mere bone mineral density, for quantifying the bone strength. A special emphasis is put on the investigation and exploitation of features of (vertical) anisotropy in the trabecular network as they are induced by quite well-defined loading conditions in vertebral bone probes, which were solely used in this study. When analyzing a subsample consisting only of weak bones, a local structural analysis using Minkowski functionals and anisotropic scaling indices leads to even better correlations with MCS as compared to BV/TV, which corroborates the hypothesis that the bone structure (and not only its mineral mass) constitutes an important component of bone stability. It also becomes obvious that the alignment of structural components, which is identified by anisotropic texture measures, also plays an important role for the bone stiffness and flexural rigidity.
The purpose of the second study using now the full sample of in vitro μCT probes was to investigate the relations between bone volume fraction and microstructure at different skeletal sites. How does the microstructure change with the bone volume fraction? And what are the similarities and differences in the mass-structure relations of the trabecular bone taken from different locations, where the loading conditions are very different? In the paper

Paper V. [276]: Scaling relations between trabecular bone volume fraction and microstructure at different skeletal sites, Bone ***57****, 377-383 (2013)*

we used in total 349 bone probes from different skeletal sites of 154 human donors in vitro: 87 from the distal radius, 59 (69) from the thoracic (lumbar) spine, 51 from the femoral neck, and 83 from the greater trochanter. BV/TV and trabecular microstructure parameters (TbN, TbTh, TbSp, scaling indices, and Minkowski Functionals) were computed for all bone probes. By plotting BV/TV versus the respective microstructure parameter in a double-logarithmic way, we could immediately identify scaling relations between trabecular bone volume fraction and microstructure, which are characterized by the regression coefficient β as the slope of a linear fit to the data. The 95% confidence intervals of β overlapped for almost all microstructure parameters at the different skeletal sites. The scaling relations were independent of vertebral fracture status and similar for subjects aged 60-69, 70-79, and >79 years. Therefore, the bone volume fraction-microstructure scaling relations of the bone probes taken from different sites showed surprisingly small variations. The relations showed rather a universal character and thus obviously do not depend so much on the exposure of the bone to external mechanical forces. Thus, a naive interpretation of Wolff's law may not be valid. Following Wolff's reasoning, one would expect that the bone structures exhibit systematic differences for bone probes taken from different sites, because the inner bone structure should show signs of different adaptation to external forces acting on the bone. Such universal scaling relations may, on the other hand, allow for the development of additional diagnostic tools to assess the bone quality during disease (e.g. osteoporosis) and drug treatment. It may be sufficient to measure microstructural properties in bones of the arm (most preferable the distal radius) and then deduce the structural properties of e.g. the femur, where the severe osteoporotic fractures occur. It is much easier to obtain high resolution images of the forearm than of the (upper) thigh. For MR imaging the fat and muscle tissue around the femur poses problems. For CT modalities one has to take

into account the exposure to radiation which limits the choice of CT sequences and thus the spatial resolution.
So far, we were not involved in larger longitudinal clinical studies, in which disease- or drug-induced changes of the trabecular bone structure during therapy are investigated. Given the high sensitivity to small structural changes of the scaling indices (see also sects. 4.3 and 4.4 in this thesis), it is very likely that the higher order statistics, which we introduced to assess the structure of the inner bone, will only show its full potential, if they are applied for quantifying temporal variations at a very early stage. Therefore, we are planning to participate in future long-term bedrest studies, which are conducted on a regular basis at the institute of aerospace medicine of the German aerospace center (DLR), in order to gain first experiences in analyzing data from longitudinal studies.
Recent developments of new x-ray imaging modalities, namely dark field imaging [358, 244, 340], allow – at least in principle – to map structures and their orientation, which are as small as the wavelength of the used light-source. For the case of the inner bone this means that both trabecular and subtrabecular structures may become visualizable. Although a lot of details of this phase-contrast imaging are still to be understood to achieve the theoretical possible spatial resolution, first applications for bone structure imaging [297, 82] yielded promising results that may even be improved, if dark field imaging is followed by multidimensional, nonlinear image analysis.

Chapter 4

Phenomena of self-organization in complex plasmas

4.1 (Complex) Plasmas

A *plasma* [189] – also known as the fourth state of matter – is a multi-particle system consisting of ions, electrons and neutral atoms coupled together. Plasmas exist widely in nature. In fact, over 99% of the visible matter in the universe is in the plasma state [14]. For example, the intergalactic medium, the interstellar medium, and the solar wind are all mainly diffuse plasma. The matter in the interior of stars such as our sun is in the state of a dense plasma. Furthermore, the whole baryonic matter content of the early Universe, when it was hot and dense, was in the plasma state. Thus, the development and the nature of the primordial matter density fluctuations as measured with the cosmic microwave background (CMB) radiation is to be understood by the concept of first propagating and then frozen sound waves in a plasma (see section 5.3).
In geophysics plasmas occur naturally in the ionosphere, where mainly the higher energetic radiation (ultraviolet, X-ray, etc.) from the sun ionizes the gas atoms in the atmosphere. Due to the low density at higher altitudes the recombination rate is low and the plasma state is retained. The existence of an atmospheric layer reflecting radio signals, i.e. an ionosphere, was proven by E. Appleton in 1924 [8] (Nobel Prize 1947) using the frequency modulation method. Obviously, the refractive properties of the ionosphere for high frequency radio signals play the key role for long range communication using radio signals.
Plasmas have found numerous applications in engineering. Energy production by means of nuclear fusion is only possible by taming the hydrogen plasma inside the tokamak [12] or stellarator [359] in order to achieve the desired densities and temperatures for igniting the fusion of H-atoms.
Plasma accelerators [158] may path the way to new classes of particle accelerators. While conventional accelerators use RF waves to accelerate charged particles, plasma accelerators use plasma-oscillation waves excited by lasers or by driver beams of charged-particles [336]. The accelerating gradients and focusing strengths that have been demonstrated in plasma

experiments were orders of magnitude greater than those achieved thus far by rf accelerators. The greater the accelerating gradient the shorter would be the accelerator required to reach a given energy. The impressive plasma-acceleration results already demonstrated so far (see e.g. [204, 98, 91]) raise hopes that this revolutionary technology may miniaturize future accelerators in the same way that semiconductor processors miniaturized electronics.

More recently, it also turned out that the use of plasmas may have great potentials in the fields of medicine and hygiene, when cold (i.e. less than 40°C) atmospheric plasma (CAP) sources have been developed [191]. This innovative medium initiates reactions in the surrounding air, which lead to the production of a reactive mix composed of electrons, ions, neutrals, exited atoms and molecules, reactive species and UV light. The interactions of the reactive mix with biological tissues can be used for e.g. antifungal treatment and probably most importantly for sterilization - especially in cases, where multi-resistant bacteria pose severe problems to conventional chemical-based sterilization methods [181]. Yet, both the composition and concentrations of the produced species in the CAP and the exact mode of action of the CAP for respective tasks is still not known in detail and thus requires further research for better targeted applications.

A *complex plasma* being the basis of all studies within this section can be defined as plasma with an additional charged component of microparticles [317]. Formerly, the so-called dusty plasmas were thought to be mainly of relevance in space physics, because in most space environments such as interplanetary space, comets, or planetary rings dust particles are exposed to plasma and UV radiation and, consequently, start carrying electrostatic charges. The dynamics of the small charged dust particles is governed not only by gravity, drag and radiation pressure but also by electric and magnetic fields. Further, their presence can in turn influence the plasma properties by e.g. altering the wave modes and triggering new instabilities. Considering the multitude of forces acting on the particles and the feedback their presence has on the plasma conditions it is no surprise that the dynamics of small charged dust particles can be complex, leading to levitation, rapid transport, energization and ejection, capture, and even to the formation of new planetary rings [139, 140].

Early interest in dusty plasmas under laboratory conditions was first triggered in applied physics. In semiconductor manufacturing plasmas are used extensively for materials etching, deposition and surface treatment, where plasma contaminations are a crucial concern in the manufacturing of microelectronic devices. It was found that particles can grow in the plasmas of commercial rf etching reactors, remain electrically suspended there and then can fall to a surface and contaminate it [313, 27]. In the course of time the view also changed when it was realized that dust in plasmas is not only an unwelcome process killer contaminants but also often a desired element that can dramatically affect and improve the basic properties of plasma-made surface structures [353].

Similarly, it was found early that in high temperature plasma in experimental fusion devices impurities such as oxygen, carbon and metal atoms are introduced from and finally redeposited at the first wall surrounding the plasma [16, 164]. Film studies also revealed that bright moving macroscopic particles can be observed in many tokamaks [110], which occasionally result in the termination of the discharges. However, only in recent years the

role of dust particles in fusion plasmas which may be fast moving has fully been recognized [226, 188].
Dusty plasmas became interesting as a possible model systems of crystalline structures to study phase transitions when Ikezi [145] suggested in 1986 that small particles in a plasma can form a Coulomb lattice [80, 189]. Generally, a Coulomb lattice is formed, when the ratio Γ between the Coulomb energy and the kinetic energy of a charged particle system exceeds a critical value $\Gamma_c \approx 170$. In one component plasmas (OCP), where the electrical charge of a particle q equals the charge of an electron e the solidification condition $\Gamma > \Gamma_c$ requires a high-density and low temperature system, so it is difficult to realize it experimentally. However, small, micron-sized particles can accommodate $10^3 - 10^4$ electron charges and thus Γ can be made larger than Γ_c at particle temperatures of the order of 300 K. In 1994, a series of experimental realizations of two-dimensional plasma crystals were reported [343, 51, 131]. The microparticles were confined in a monolayer in a radio frequency (rf) discharge and self-organized in a triangular lattice with hexagonal symmetry. Since then, the study of complex plasma has come to a new era. It was immediately realized that complex plasmas are an ideal model system for studying all sorts of dynamical processes of self organization and structure formation at the most elementary individual particle level (see e.g. the following reviews: [92, 225, 318, 24]. Among the properties that make the system of strongly coupled plasmas unique are the following ones:

- The microparticles, i.e. the principal component, are individually observable. Note that unlike to e.g. a typical class of turbulence experiments [186, 365] the charged particles are not just tracer particles, but the sources of the interaction potential and of the structure forming elements of the complex system.

- The characteristic length scales, e.g. the interaction or coupling length and mean particle separation are a few 100s of μm so that complex plasmas are optically thin up to a few 10s of cm in size. Therefore a complete three-dimensional diagnostic becomes possible.

- The characteristic dynamical time scales associated with microparticles, e.g. the inverse Einstein frequency are in the range of tens of milliseconds, allowing studies of fully resolved individual particle dynamics. Investigations of such dynamical phenomena in complex plasmas can thus provide important insights into major generic processes governing the behavior of other strongly coupled particle systems.

- The rate of momentum or energy exchange between microparticles can substantially exceed the damping rate due to neutral gas friction. Thus, the dynamics of individual particles is virtually undamped, providing a direct analogy to regular liquids and solids in terms of the internal atomistic dynamics.

- Complex plasmas consisting of four components (electrons, ions, neutral atoms, and charged microparticles) with each of them being tunable to some extent turn out to be very versatile allowing research of a vast range of structural and temporal self-organization processes.

- Finally, complex plasmas can be manipulated in many different ways by e.g using electrostatic and/or magnetic forces, thermal gradients, light pressure, etc. Thus it becomes possible to systematically study the (often nonlinear) response of complex systems on external forces and fields and to identify generic structure formation properties.

The melting of a flat three-dimensional plasma crystal consisting of a few lattice planes was naturally among the first phase transition phenomena which was studied on the single particle level using complex plasmas [344]. A large number of much more detailed experiments on the generation, melting and (re-)crystallization of plasma crystals were performed in the following years (see e.g. [224, 370, 292, 224, 169, 170]), where it was often crucial to perform the experiments under microgravity conditions, since the gravitational force on the microparticles has – though being low – considerable effects on the formation and size of three-dimensional plasma crystals. The solid-liquid phase transitions are often quantified by the well-established bond order parameters [323, 324], which characterize the local order in crystals. It is worth mentioning that it was already shown [176, 159] that anisotropic scaling indices, as they are used in a number of applications in this thesis, are also equally well suited to distinguish different lattice types, most notably fcc from hcp. Very recently we could even demonstrate that scaling indices often show superior results as compared to the bond order parameters [128, 129]. Detailed, systematic and comparative studies of the performance of different local order parameters in the context of solid-liquid phase transitions belong to ongoing and future research activities.
Two-dimensional plasma crystals can be generated and studied in laboratory experiments on the ground. The investigation of this lower-dimensional system is of great interest, since understanding the mechanisms governing two-dimensional solid-liquid phase transitions is a long-standing problem. It was shown first that those phases transitions in two-dimensional systems are impossible from the thermodynamical point of view, since the Mermin-Wagner theorem forbids any long-range order in only two dimensions [214]. Later, a topological phase transition for two-dimensional systems was predicted by the Kosterlitz-Thouless-Halperin-Nelson-Young (KTHNY) theory [182, 183, 120, 233, 367] (for a review see e.g. [328]). It describes a continuous dislocation-mediated melting transition with the appearance of a so-called hexatic phase between the solid and the liquid state and predicts a long range behavior of translational and orientational correlation functions. A competing scenario for the solid-liquid transition in two dimensions is the grain-boundary-induced melting [52, 53]. Comprehensive experimental investigations of melting in two-dimensional complex plasmas suggest a grain-boundary-induced melting scenario [235]. Rapid cooling of a two-dimensional complex plasma also showed a scale-free transition from an unordered to an ordered state that differs from the KTHNY theory [175, 174].
The solid-liquid phase transitions is by far not the only phase transition that can be studied on the microcanonical level in complex plasma. Rather, it is amazing how many different, yet fundamental self-organizing processes can be realized and investigated with complex plasma. Besides the demixing, lane- and string formation, which will be discussed in detail below, one can exemplary also mention recent microcanonical studies on (the onset of)

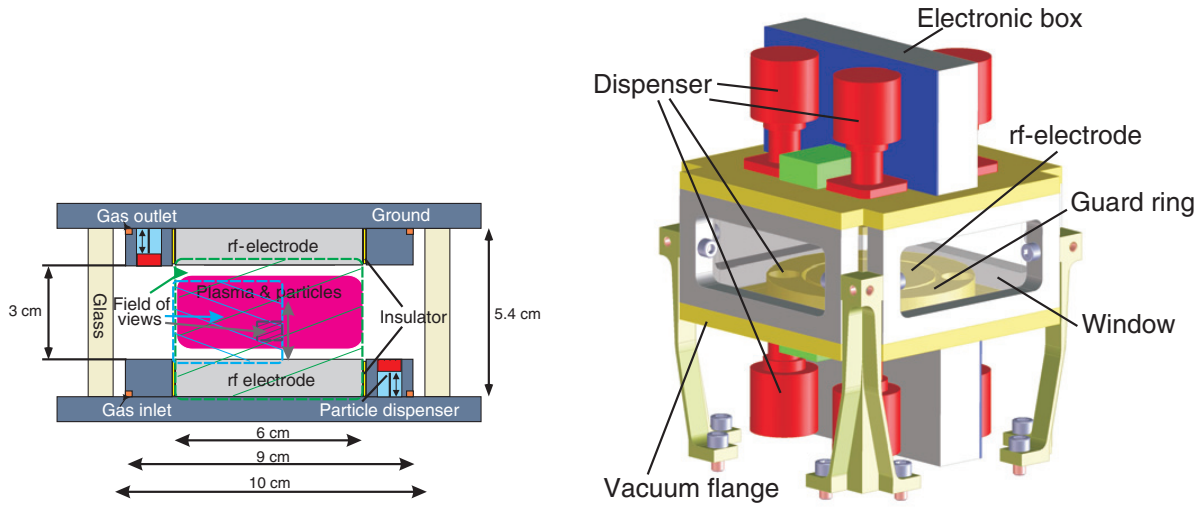

Figure 4.1: Sketches of the 2D (left) and 3D view of the plasma chamber PK-3 Plus (Source: [345]).

turbulence [308, 369] and asymmetric synchronization in two-dimensional plasma crystals [64, 194]. It has also shown that there is the possibility to reach critical point [168, 180]. It might even be possible to test predictions from supersymmetry via the viscosity to entropy density ratio [342].
The general setup for conducting experiments with complex plasmas is comparatively simple. In a small vacuum chamber (few centimeters in diameter) a plasma is generated. Next, monodisperse microparticles – typically melamine formaldehyde (MF) – with diameters ranging between 0.5 and 15 μm are injected by using several dispensers. The microparticles in the plasma become immediately negatively charged and start to interact with each other. The position and motion of the particles is optically detected. The system is illuminated by adjustable laser light. Usually, several CCD-cameras observe the reflected light with different magnifications and fields of view. In addition, the particles can be manipulated, e.g. accelerated or trapped, by an RF field of an external coil, by gas flow, by modulation of the dc power, or by a strong laser beam.

There are a number of different plasma chambers being optimized for the use in (ground-based) laboratories or under microgravity conditions. The results presented in this thesis were all obtained from experiments under microgravity conditions using the laboratories PK-3 Plus [345] and PK4 [341]. PK-3 Plus was the second-generation laboratory for the investigation of complex plasmas on the International Space Station (ISS). It succeeded the PKE-Nefedov experiment [232] and was in operation from 2006 to 2013. The setup consists of a capacitively coupled radio-frequency (rf) chamber and surrounding infrastructure including laser illumination, a gas system, a video recording system, a vacuum system, as well as a control system. The chamber itself has a cubic shape and contains two circular electrodes that are at a distance of 3 cm from each other. Each electrode has a diameter of 6 cm and is surrounded by a grounded guard ring of 1.5 cm width. Each guard

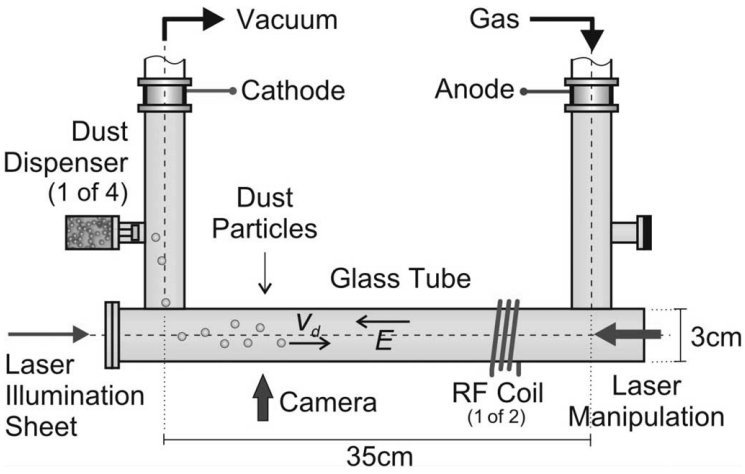

Figure 4.2: Sketch of the PK4 setup (Source:[341]).

ring includes three dispensers, which allow the injection of monodisperse microparticles of different sizes (see Fig. 4.1). The glass walls are made of quartz through which the dynamics of individual particles and the structure of the microparticle cloud can be recorded by three CCD cameras: the "overview (OV) camera" includes the whole area inside the chamber, the "high resolution (HR) camera" focuses on the center of the chamber and a "glow camera" records the plasma discharge with a similar field of view as the OV camera. PK4 is the experiment being designed for investigating complex plasmas in a dc discharge using an elongated glass chamber with a length of 35 *cm* and a diameter of 3 *cm* (see Fig. 4.2). The linear design of PK-4 allows the study of the fluid phase of microparticles inside a complex plasma, produced in the positive column of the DC glow discharge, on the kinetic level of single particles. The glass tube (as opposed to the RF chambers in PKE-Nefedov and PK-3 Plus) also provides a better optical access for observation, diagnostics, and laser manipulation of the particles. The plasma is produced by a voltage of about 1000 V applied to the dc electrodes in a neon or argon gas discharge at pressures between 10 and 200 Pa. The microparticles are injected by using several dispensers. Obtaining a negative charge in the plasma, they drift within the longitudinal electric field from the cathode to the anode. They are illuminated by a vertical laser sheet along the glass tube and observed by cameras perpendicular to the tube. The glass tube also provides a better optical access for observation, diagnostics, and laser manipulation of the particles. PK4 was developed since 2002. In a number of parabolic flight campaigns the apparatus was tested under microgravity conditions and the first scientific experiments were carried out. In October 2014, PK4 was launched and is since then the current plasma crystal experiment on the ISS.

4.2 Fluid demixing

Fluid demixing, i.e. the phase separation in multicomponent mixtures, is a ubiquitous phenomenon occurring in diverse systems such as e.g. molecular fluids [291], colloid suspensions [126], active and Brownian particles [207, 326] and granular media consisting of particles of different masses [283] or different diffusivity [356]. The tendency for particles of different types to mix or demix is basically determined by the relative strengths of their interactions [125]. Demixing is generally preferred when the interaction between the two types of particles is more repulsive than the (geometric mean of) interactions of the particles within one type. This asymmetry in the mutual interactions is often called "interaction nonadditivity". It was shown that in a complex plasma, which consists of a mixture of particles of two different sizes, the interparticle interactions always exhibit a positive nonadditivity, which stimulates the phase separation of the two types of particles. For a standard plasma screening model the spinodal line was calculated and it was found that spinodal decomposition is easily achievable for typical experimental conditions suggesting that binary complex plasmas could be an ideal model system to study fluid phase transitions on the atomistic (individual particle) level [148].
Following these theoretical findings it is demonstrated in

Paper VI. [364]: Kinetics of fluid demixing in complex plasmas: role of two-scale interactions, Phys. Rev. Lett., ***105*** *045001 (2010)*

by using experimental data and combining theory and computer simulations that binary complex plasmas are indeed a particularly well-suited model systems to study the kinetics of fluid-fluid demixing at the atomistic level. The essential parameters of interparticle interactions in complex plasmas, such as the interaction range(s) and degree of nonadditivity, can be varied significantly, which allows systematic investigations of different demixing regimes. The critical role of competition between long-range and short-range interactions at the initial stage of the spinodal decomposition is discussed. For being able to do so an extensive analysis of the temporal development of the (linear) structure factor $S(k,t)$ of simulated binary mixture systems had to be performed.
Very recently Killer et al. showed [171] in a microgravity experiment that phase separation already occurs for binary dust systems with size disparities as low as 3%. These observations were made possible by the use of fluorescent dust particles that allowed to distinguish between particles of slightly different size. Yet, the occurrence of demixing at these low size differences cannot entirely be explained by spinodal decomposition as it is expected only for a relative size disparity of ca. 25% [148].
We ourselves started recently to reanalyze the demixing data from [364] using Minkowski tensors [307]. By analyzing the temporal evolution of Minkowski tensor measures qualitative differences between the case of particle interaction with a single length scale compared to particle interactions with two different length scales (dominating long range interaction) are revealed: In the case of different length scales the slope grows fast until it reaches its maximal value and then decays whereas for a single length scale no decay is observed. After proper scaling the graphs for the two length scale scenario coincide, pointing towards a

universal behavior. These differences are evidenced by distinct demixing behavior: In the long range dominated cases demixing occurs in two stages. At first neighboring particles agglomerate then domains start to merge in cascades. However in the case of only one interaction length scale only agglomeration but no merging of domains can be observed [22]. None of those differential features were observable with the structure factor $S(k,t)$. Thus both, refined experimental techniques e.g. with fluorescent dust particles as well as analyses methods like Minkowski Tensors, which go beyond a linear global description of the emerging demixing patterns will open up new possibilities to study phase separation in strongly coupled Coulomb systems on the kinetic level of individual particles and offers new insight on phase separation in binary systems. Further experimental results are expected to be gained e.g. during the next parabolic flight campaigns with PK4 and with PlasmaLab, a newly developed plasma chamber.

4.3 Lane formation

Equilibrium bulk phase transitions are nowadays well understood [201]. Phase transitions in non-equilibrium systems as characterized by not being closed, i.e., by having an exchange of energy, particles and/or information with their environment, often show a more complex behavior which is sometimes even opposite to the transitions one is used to in equilibrium systems like e.g. the "freezing by heating" transition for a system of particles driven in opposite directions and interacting via a repulsive potential [133]. For non-equilibrium systems there are normally no general results such as the laws of thermodynamics and statistical mechanics for closed systems of gases, fluids or solids in equilibrium. Rather, the competition between e.g. external driving forces and the dissipative friction forces leads to a spatio-temporal redistribution of energy, which produces a great variety of self-organization phenomena. These result from nonlinearities in the equations of motion, which allow small initial perturbations to be enhanced and nonequilibrium patterns to be dynamically stabilized.
Lane formation can be considered as a "classical" non-equilibrium phase transition in a continuous system [63] that develops when dissipative system is externally driven. It is observed in lattices gases [301], colloids [78, 198, 281] but also in pedestrian dynamics [132], [133] (for a review: [134]). Performing experiments in the plasma chamber PK-3 Plus onboard the International Space Station (ISS) under zero gravity conditions, it became possible to conduct laboratory experiments exhibiting lane formation in complex plasmas. In paper

Paper VII. [331]: Dynamics of lane formation in driven binary complex plasmas, Phys. Rev. Lett. ***102****, 085003 (2009)*

it is outlined how for the very first time the ubiquitous phenomenon of lane formation caused by penetration of two particle species has been experimentally investigated on the microcanonical level and compared with particle-resolved Langevin simulations. For the analysis of the lane formation on the single particle level the locally adaptive anisotropic

scaling indices played a major role as it became possible with these local nonlinear structure measures to define a novel nematic order parameter for the quantitative characterization of lane formation. The use of this order parameter became crucial for studying the onset of this nonequilibrium phase transitions. In particular, it appears to be well suited to resolve the principal issue of the order of such phase transitions, to characterize possible universality and to identify dynamical regimes of structural relaxation.
The research on lane formation of moving pedestrians was significantly advanced recently, when it was demonstrated with both computational and analytical results that it is also possible to generate a two-lane ordered state, in which particles (people) always move (walk) on the left-hand side (or right-hand side). This is achieved by solely giving the walls an asymmetric zigzag shape [236]. It is an intriguing idea to confirm these results experimentally with a dusty plasma system, in which two particle species penetrate each other within a confinement with a similar asymmetric zigzag shape.

4.4 String formation in electrorheological plasmas

Electrorheological (ER) fluids are suspensions of dielectric particles in nonconducting or weakly conducting solvents. In moderately large electric fields chainlike and columnar structures form parallel to the field causing dramatic changes in the rheological properties of the suspensions [122, 44]. The apparent viscosities increase by several orders of magnitude at low shear rates. The rheological response is observed to occur in milliseconds and is reversible. This combination of electrical and rheological properties has led to many proposals for applications of ER fluids in such devices as hydraulic valves, clutches, brakes, and in photonic devices. The large variation of the rheology of the fluid can be explained by the polarization of the dielectric particles by by applying the external electric field, which leads to an additional dipole-dipole interaction. The electric field plays the role of a control parameter which allows to tune the range and the anisotropy of the interaction between particles. This makes the phase diagram of ER fluids remarkably diversified [366]. Solving the kinetic equations for the plasma species in complex plasmas allows for a quantitative determination of the interparticle interaction under various conditions [179]. It turned out that complex plasmas can have electrorheological properties, if the external electric field satisfies some conditions. Specifically, it can be shown that for small Mach numbers the interactions in electrorheological plasmas are *equivalent* to dipolar interactions in conventional electrorheological fluids. Those findings opened the door to study processes that govern the dynamics of electrorheological fluids on the microcanonical level. In the paper

Paper VIII. [147]: First observation of electrorheological plasmas, Phys. Rev. Lett. ***100****, 095003 (2008)*

it is for the first time experimentally shown using the PK-3 Plus chamber that dusty plasmas can – under certain conditions – exhibit electrorheological properties. This is the case, when an external alternating electric field is applied to the Due to this additional field the interaction potential between the charged particles is changed and an additional,

anisotropic and attractive component is added. Those electrorheological systems show much more phase transitions than "ordinary" systems with isotropic interaction potentials. In this work the experimentally observed phase transition from "normal" fluids to string fluids was quantitatively analyzed and compared with MD-simulations. The order parameter based on the use of anisotropic scaling indices was newly developed. Our results suggest that the transition from normal fluids to string fluids is a second order phase transition.
The investigations of string formation as an effect of external electric fields were further pursued by conducting dedicated experiments with strongly coupled complex plasmas in external electric fields under microgravity conditions using the PK4 setup. PK4 offers the opportunity to produce a homogeneous uniaxial electric field which can either be an ac field or dc field. While the former leads to reciprocal (Hamiltonian) interactions between the particles, the latter makes the interactions nonreciprocal (non-Hamiltonian), which can lead under proper conditions to an increase of the kinetic energy of the particles. The focus in the paper

Paper IX. [150]: Complex plasmas in external fields: role of non-Hamiltonian interactions, Phys. Rev. Lett. ***106****, 155001 (2011)*

was put on the comparative analysis of the formation of string-like anisotropic structures due to reciprocal and non-reciprocal interactions between microparticles. The experiments complemented by numerical simulations demonstrate that the responses of complex plasmas in these two regimes are drastically different. String formation that is once again quantitatively characterized by anisotropic scaling indices is only observed in the case of Hamiltonian interaction between the microparticles. The observed distinction is a striking manifestation of the intrinsic thermodynamic openness of driven strongly coupled systems. Although these experiments were only performed under conditions of approximate weightlessness during a parabolic flight campaign, they already showed the potential of the PK4 setup for high-precision studies of complex plasmas in external fields. Experiments in the ac mode (polarity switching) provide the path for comprehensive studies of electrorheological systems in liquid and solid states. By varying the duty cycle one can control the strength of the ac mode and thus study phase transition phenomena, i.e. string formation, during the crossover from non-Hamiltonian to Hamiltonian behavior.

A number of further experimental [157, 74, 75, 362] and theoretical [29, 30, 31, 149] work on string formation and phase transitions in dusty plasmas with anisotropic interaction potentials were conducted in the following and refined the knowledge of the self-organizing effect in electro- and magnetorheological complex plasmas.
In October 2014 the experiment PK4 was launched and carried to the International Space Station (ISS). In June 2015 the first PK4 commissioning runs took place. One snapshot of the dust cloud in the ac mode is shown in Fig. 4.3. The (expected) presence of strings is more than obvious. Experiments with varying duty cycle are planned for the campaigns to come so that we expect to study for the first time the nature of the phase transition from liquids to string liquids on the single particle level using experimental PK4 data in the near future. The use of the previously developed order parameter, which is based on

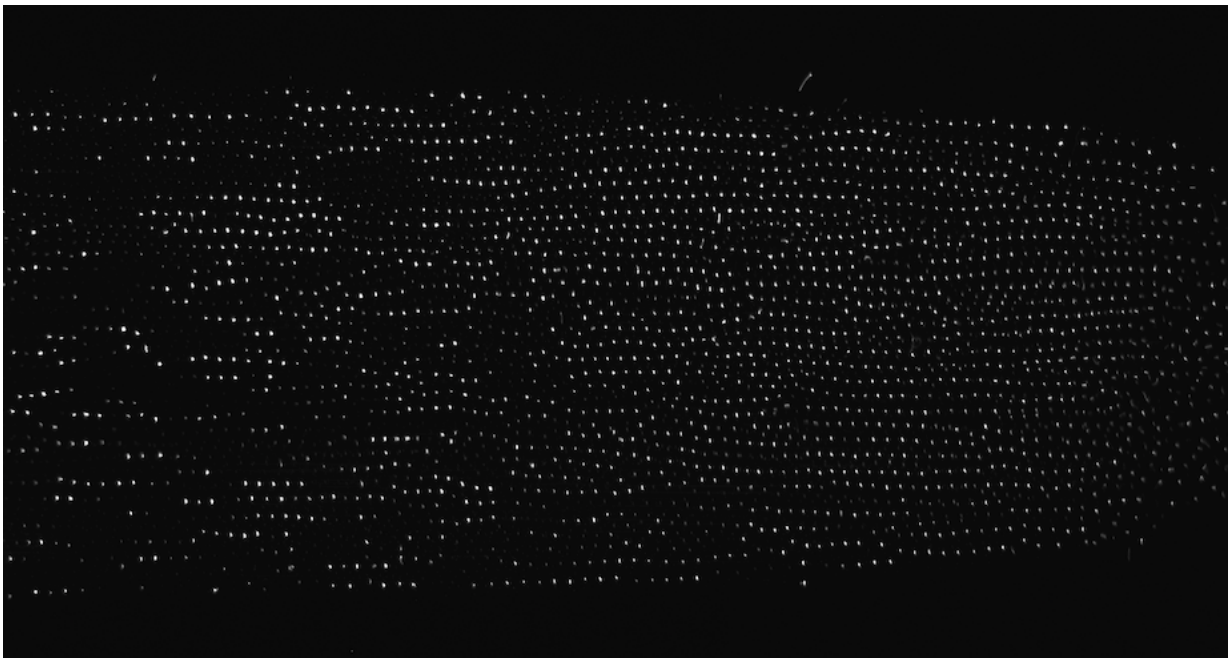

Figure 4.3: Snapshot from PK4 commissioning runs aboard the ISS conducted between 1st and 6th of June 2015.

anisotropic scaling indices, is very likely to become - once again - essential for the data interpretation and for determining the nature of the phase transition.

Chapter 5

Complex patterns in astrophysics

5.1 Sources of information in astrophysics

The bulge of information about typically very distant and thus unreachable astrophysical objects - be it stars, galaxies, galaxy clusters, the interstellar medium (ISM) - is contained in the electromagnetic radiation being emitted or absorbed by these objects. Further information can be gained by cosmic rays and by the direct detection of gravitational waves - as recently demonstrated for the first time [1]. However, most areas of astrophysics mainly rely on the analysis of the electromagnetic radiation with its variations in energy and time to gain knowledge about the constituents of our Universe and their evolution in time.
All energy bands of the electromagnetic spectrum ranging from radio waves to γ-rays contain valuable information about astrophysical processes.
Karl Jansky observed the first astronomical radio source serendipitously in the early 1930s [156]. By comparing his observations with optical astronomical maps he concluded that the radiation was coming from the Milky Way and was strongest in the direction of the constellation of Sagittarius A - the nowadays well-know position of the central black hole of our galaxy. Such radio emissions from active galactic nuclei, which are now known to mostly stem from jets of charged particles which emit synchrotron radiation, were then frequently observed and found to be characteristic for certain classes of AGNs (see below). The radiation in the microwave band, which roughly covers the frequencies from 300 MHz to 300 GHz, yielded decisive measurements for both galactic and extragalactic astrophysics. The 21 cm line emission from neutral hydrogen atoms (HI) first helped to uncover the structure and dynamics of the Milky Way. This 1420 MHz radiation comes from the transition between the two levels of the hydrogen ground state, which is slightly split by the interaction between the electron spin and the nuclear spin. As opposed to optical light, this radiation in the radio band can penetrate dust and show us the galactic center and even the opposite side of the galaxy. The Doppler shift of the frequency of this line allows to measure the velocity of the HI gas clouds. One can then study the differential rotation of the galaxy and estimate distances to gas clouds, and thus map the distribution of matter in the galaxy. This kind of radiation from space was sought after

by J. Oort in the 1940s. In 1945 his student, H.C. van de Hulst, predicted the existence of the 21 cm line in the galactic radio spectrum [142]. Its first detection by H. Ewen and E. Purcell in 1951 [89] marked the beginning of the observational 21 cm astrophysics. Nowadays, observations of redshifted 21 cm radiation from the large scale distribution of neutral hydrogen is one of the most promising probes to study the high redshift Universe and to gain information about the very early structure formation processes in the dark ages before and during the epoch of reionisation. Also in the 1940s a cosmic microwave background (CMB) radiation was predicted as a consequence of the big bang theory of the Universe [97, 6] . Electrons and photons that were in thermal equilibrium in the hot and dense phase of the Universe, decoupled when the temperature became lower that approx. 3000 K and the protons and electrons (re)combined. Thus, the photons were no longer scattered via Thomson scattering at free electrons and the Universe became transparent for them. The photons from the radiation field propagated henceforward freely in space and time and formed a relic radiation filling the whole Universe. But due to the expansion of it, their wavelengths were redshifted to the microwave range. The CMB radiation was discovered in 1964 by Penzias and Wilson [243] (Nobel Prize in 1978) as a highly isotropic excess microwave radiation. It was R. Dicke et al. [71], who immediately interpreted the new signal as the long sought-after cosmic black-body radiation. Since the beginning of the 1990s accurate measurements of the CMB became the cornerstone of precision cosmology, which will be described in some details below.

Infrared radiation (ir) roughly covers the wavelength range from 1 mm to 700 nm and is followed by the visible light, whose wave length range is as small as from 700 nm to 380 nm. Astronomical observations in the visible light were naturally the first to be performed and can be traced back to ancient times. It was William Herschel in 1800 who discovered infrared radiation from the sun by measuring the temperature increase of sunlight that passed through a prism just beyond the red end of the visible spectrum. But only with the development of powerful photodiode detectors and bolometers in the 1950s and 1960s the rise of the infrared astronomy began. As infrared radiation with wavelengths just longer than visible light behaves in a very similar way to visible light, it can be detected using similar solid state detectors. For this reason, the near infrared region of the spectrum is commonly incorporated as part of the optical spectrum, along with the near ultraviolet. Many optical telescopes operate effectively in the near infrared as well as at visible wavelengths. The same is true for the astrophysical objects that are to be observed in the optical and infrared light. Planets, comets and asteroids in the solar system, stars and star forming regions in the milky way and close and distant galaxies in the universe are all key observation targets for optical and infrared astronomy. In cosmology ir-measurements become increasingly important as the visible or uv-light of galaxies in the early universe are observed in the near infrared due to the cosmological redshift. The design of contemporary and future ir telescopes (foremost to mention the James Webb Space Telescope) is largely determined by the requirements for being able to observe these distant galaxies.

Hot regions in the universe emit light with small wavelengths, i.e. X-rays or γ-rays. X-rays have a wavelength ranging from 0.01 to 10 nanometers, corresponding to photon energies in the range from 100 eV to 100 keV. Photons with an energy larger of the somewhat

arbitrarily defined threshold of 100 keV are classified as γ-rays. They can have even much higher energies extending into the TeV. Hot objects are typically compact stars, such as neutron stars or black holes. Material falling into a black hole may emit X-rays, but the black hole itself does not. The energy source for the X-ray emission is gravity. Infalling gas and dust is heated by the strong gravitational fields of these celestial objects. As most, if not all, galaxies have a supermassive black hole at their center, they can accrete material from the dense central region of the galaxy. As the material falls in towards the black hole, angular momentum will cause it to spiral in and form a disk. This disk, called an accretion disk, heats up due to the gravitational and frictional forces at work and can thus become an x-ray source. Those so-called active galactic nuclei (AGNs) will be described in some details below. In addition, the space between galaxies in galaxy clusters is filled with a very hot, but very dilute gas at a temperature between 10 and 100 megakelvins (MK). The total amount of hot gas is five to ten times the total mass in the visible galaxies. It is detected as a broad and fainter signal in x-ray detectors and yields important informations about the physical parameters (foremost to mention the mass) of galaxy clusters, the largest virialized objects in the universe. As tracers of the cosmic large-scale structure they are also important probes for cosmology. Since galaxy clusters are very sensitive tracers of the growth of structures, a census of the cluster population as a function of redshift can be used to test cosmological models. As X-rays are absorbed by the Earth's atmosphere, instruments to detect them must be taken to high altitude by balloons, sounding rockets, and satellites. Consequently, X-ray astronomy is also a new branch of astronomy which could only come into being after the development of sufficiently powerful rockets, which could bring payloads to higher altitudes. The first X-ray source (Scorpius X-1) beyond the solar system was discovered in 1962 with detectors on an Aerobee 150 sounding rocket by R. Giacconi and co-workers [100], for which he received the Nobel prize in 2002 [101]. The discovery came first as a surprise, but the interest in the new field of x-ray astronomy for studying the hot universe grew quickly. Finally, γ-rays in the MeV range are generated in solar flares, but γ-rays in the GeV range do not originate in the Solar System and are important in the study of extrasolar, and especially extra-galactic astronomy. The mechanisms emitting γ-rays are diverse, mostly identical with those emitting X-rays but at higher energies, including electron-positron annihilation, the Inverse Compton Effect, and in some cases also the decay of radioactive material in space reflecting extreme events such as supernovae and hypernovae, and the behavior of matter under extreme conditions, as in pulsars and blazars. As in the case of X-rays most γ-rays coming from space are absorbed by the Earth's atmosphere, so γ-ray astronomy could not develop until it was possible to get detectors above most of the atmosphere using balloons and spacecraft. The first γ-ray telescope, that was carried into orbit in 1961, was mounted on the Explorer 11 satellite. Although it picked up only fewer than 100 cosmic γ-ray photons, this mission opened for the first time the observational window of the most energetic form of electromagnetic radiation.

All observations of astrophysical objects have in common that high quality data are difficult to achieve. For some of the energy bands extraterrestrial experiments are a necessary prerequisite for acquiring data as the atmosphere absorbs most of the radiation of the re-

spective wavelength. Therefore, the data are precious and – as the measurements are often hardly repeatable – there is a strong need to make the most out of the limited data available. Sophisticated, often nonlinear, data analysis techniques are therefore to be employed already for data preprocessing and data reduction for e.g. denoising, filtering, deconvolution, component separation or source detection.
Furthermore, the objects and processes of astrophysical interest are often far from equilibrium. Consequently, a large variety of structure formation processes are observed. Their measurements reflect some complex behavior giving rise to complex patterns in space and/or time. The formation of the large scale structure of the galaxy distribution as shown in the introduction (see Fig. 1.2) shows prototypically the emergence of complex patterns in astrophysics. It is evident that the traditional approach that is based on linear methods such as spectral and correlation analyses is often not sufficient to analyze such data. Rather, it has to be complemented by approaches from nonlinear dynamics.
In the following we will present two examples of nonlinear analyses of astrophysical data. Specifically, we will present studies of temporal variability of galactic black holes (GBH) and active galactic nuclei (AGN) and of the statistical properties of the cosmic microwave background radiation. The two study subjects are quite diverse in several respects. While the former one is based on count rates, i.e. time series, of high energetic x-ray radiation from hot localized objects, the latter one is based on the spatial distribution of low-energetic microwave radiation which is to be considered as a two-dimensional random field. Yet, in both cases fundamental concepts of nonlinear data analysis like assessing scaling properties or the method of surrogates do give new insights into the physics of accretion disks close to the event horizon of black holes and into the physics of the very early universe and its fundamental assumptions.

5.2 Time series analysis of galactic black holes (GBH) and active galactic nuclei (AGN)

The idea of a black hole, which is defined as a volume of space where gravity is so strong that nothing, not even light, can escape from it, can be traced back to the 18th century. It was John Michell, who hypothesized that a star with the same density as the sun but with a diameter that is 500 times larger than the sun's one would create a gravitational potential that is so strong that the escape velocity at its surface would exceed the speed of light [216]. But in the light of Einsteins's theory of general relativity Michell's essentially Newtonian view of gravity and light as corpuscles turns out to be fundamentally incorrect. Nonetheless black holes reappear also in general relativity as solutions to the Einstein field equations, which describe the gravitational field of a point mass and a spherical mass, as it was first found by Karl Schwarzschild [311, 312]. These solutions have a peculiar behavior at the so-called Schwarzschild radius, where they become singular, meaning that some of the terms in the Einstein equations become infinite. The Schwarzschild radius is the radius of a sphere such that, if all the mass of an object were to be compressed within that

sphere, the escape velocity from the surface of the sphere would equal the speed of light. Thus, the surface at the Schwarzschild radius acts as an event horizon. Black holes were first considered to be some mathematical curiosity of general relativity, but then Tolman, Oppenheimer and Volkoff showed that stars with a mass larger than approximately three solar masses can collapse, because there is no law of physics to intervene and to stop them from forming black holes. After a black hole has formed, it can continue to grow by absorbing mass from its surroundings. By absorbing other stars and merging with other black holes, supermassive black holes of millions of solar masses may form. There is, nowadays, general consensus that supermassive black holes exist in the centers of most galaxies.

By their very nature, black holes cannot directly be observed, so the search for them must generally rely on indirect observations. For example, a black hole's existence can sometimes be inferred by observing its gravitational interactions with its surroundings. The proper motions of stars near the center of our own Milky Way provide strong observational evidence that these stars are orbiting a supermassive black hole. Since twenty-five years, the motions of stars orbiting around an invisible object has been tracked, which is coincident with the radio source Sagittarius A^*. By fitting their motions to Keplerian orbits, one could infer that a single-point-like object with approx. 4.28 million solar masses causes the motions of those stars [103, 104]. In September 2015 the LIGO gravitational wave observatory made the first successful observation of gravitational waves [1]. The signal was consistent with theoretical predictions for the gravitational waves produced by the merger of two black holes: one with about 36 solar masses, and the other around 29 solar masses. This observation provides the most concrete evidence for the existence of black holes to date. For instance, the gravitational wave signal suggests that the separation of the two objects prior to the merger was just 350 km (or roughly four times the Schwarzschild radius corresponding to the inferred masses). The objects must therefore have been extremely compact, leaving black holes as the most plausible interpretation.

Matter that falls onto a black hole can form an external accretion disk heated by friction, forming some of the brightest objects in the universe. First systematic studies of such active galactic nuclei (AGN) can be traced back to work by C. Seyfert done in the 1940s [315]. He showed that some galaxies have a nucleus with high surface brightness and characteristic emission lines which cannot be assigned to emission by stars and which show more or less Doppler-broadening. Those observations led to the definition and classification of Seyert 1 and Seyfert 2 galaxies. While the former only have "small" emission lines up to a width of 1000 km/s, the latter also have broad lines up to widths of more than 10.000 km/s.

In 1963 M. Schmidt could identify the redshift of the star-like radio source 3C273 to be $z = 0.158$ [299]. This quasi-stellar object (Quasar) turned out to be the most distant object at that time. Taking the large distant into account the absolute magnitude of this source must be 100 times larger than for normal spiral galaxies. Subsequently, a number of further quasars were identified. With the beginning of x-ray astronomy it also turned out that some of the most prominent active galactic nuclei are bright x-ray sources as well. AGNs are variable on short timescales which means that they themselves are very small, as the largest size they can be is limited by the time taken for light to cross them.

Taking all observational findings together one has to conclude that the only plausible explanation is that those point-like, quasi-stellar objects are powered by accretion onto a supermassive black hole with up to 10^6 to 10^{10} times the solar mass [279]. As the infall of mass onto a black hole can potentially give very efficient conversion of potential and kinetic energy to radiation and as a massive black hole has a high Eddington luminosity, the accretion process can provide the observed high persistent luminosity. When the material falls in towardd the black hole, angular momentum will cause it to spiral in and form a disk. This disk, called an accretion disk, heats up due to the gravitational and frictional forces at work. The light emission of the heated accretion disk and of the jet is what one typically observes as AGN radiation, where different regions of the accretion-jet system emit light of different wavelengths.
The spectral properties of AGNs vary significantly, but their appearances can be brought together in a Unified Model [7, 15]. The central supermassive black hole is surrounded by a gaseous accretion disk of a few light days across. Moving outwards from the center of the AGN fast moving gas clouds exist at a distance of approx. 100 light days. This is the so-called "broad line region", which produce the broad emission lines seen in AGN spectra. Further outwards, at approx. 100 light years in diameter, a molecular torus of colder gas exists. It is optically thick, and if viewed edge on will block out the accretion disk and broad line region from view. At larger distances (approx. 1000 light years) one finds the "narrow line region". It is comprised of small, low density gas clouds moving at lower velocities (than the broad line region). It is believed that these clouds are energized (usually close to the direction of the radio jets) and that they produce the narrow emission lines seen in some AGN spectra. Many AGNs have jets of fast moving particles, that propagate in the direction perpendicular to the plane of the accretion disk. Collimated radio (synchrotron) emission is produced in them and can be as large as several Mpc in size. The appearance of the AGN is mainly determined by the viewing angle as it is sketched in Fig. 5.1.

When the molecular torus is viewed edge-on, the black hole, accretion disk and broad line region are hidden. Thus when spectra are taken we see emission lines from the narrow region only, and some infrared emission from the torus itself. In this case we detect Seyfert 2, (narrow line) radio galaxies and quasars. If the line of sight allows us to view into the central region both broad and narrow lines are visible. In this case we detect Seyfert 1, broad line radio galaxies and quasars. If we can look directly into the torus (if it is tilted at 90 degrees to our line of sight), we look face-on at the nucleus and jets. Radiation from the jet moves close to the speed of light and can be beamed. It can also be variable on periods from hours to days. This emission can dominate any narrow or broad lines and the spectra will appear featureless. In this case blazars are detected.
Studies of the variability of the light emission in the different bands are essential in understanding the physics of the central regions of AGNs [350]. The time scales, the spectral changes, the correlations and delays between variations in different continuum or line components as well as the presence or absence of nonlinearities provide crucial information on the nature and location of the inner components of AGNs and on their interdependencies. In this thesis we complement conventional, linear methods of time series analysis most often applied in AGN research with nonlinear techniques to investigate the x-ray variability

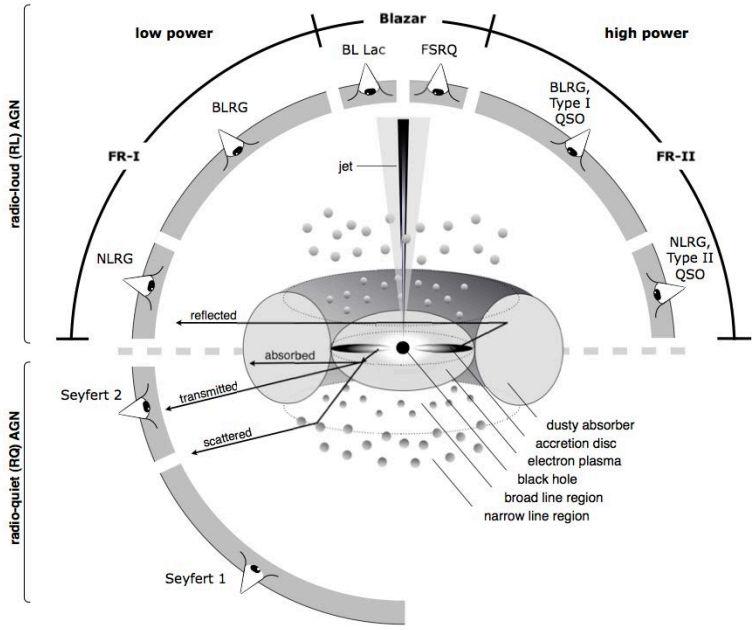

Figure 5.1: Basic scheme of the unified AGN model. The object we see depends on the viewing angle, the presence or absence of a jet and the mass of the central black hole. Note that radio-loud objects are thought to have two symmetric jets (Source: [15]).

of AGNs and the counterparts with lower mass, namely galactic black holes (GBHs). Since x-rays originate from very close to the central black hole, x-ray studies give us a unique view of the processes at work in the very center of the object close to the event horizon of the AGN or GBH. In the paper

Paper X. [105]: On the nature of x-ray variability in Ark 564, Astron. & Astrophys. ***391****, 875-886 (2002)*

we analyze a long observation of Ark 564, the brightest narrow line Seyfert 1 (NLS1) galaxy in the 2-10 keV band with the x-ray satellite ASCA (Advanced Satellite for Cosmology and Astrophysics) taken in 2000. We test for nonlinearities by using surrogates and the nonlinear prediction error and scaling indices as test statistics for nonlinearities. As the source was observed for more than four days, the x-ray emission could not be continuously measures. The time series of Ark 564 rather contains a number of gaps. As outlined in chapter 2 it is not possible to apply Fourier based methods to generate surrogates. Therefore, we used for these data sets simulated annealing techniques for generating surrogates with the same linear properties as the original ones. We found – among other results – signatures of nonlinear correlations in the lightcurve, while the source was in the high state. As a consequence one has to conclude that intrinsically linear models, where the variability is e.g. caused by many independent active regions, as magnetic flares [96] or the traditional shot noise model should be ruled out for Ark 564. Rather, nonlinear models like e.g. a

self-organized criticality model [219] or the emission from the base of a putative x-ray jet, as found in several radio-loud AGN, have to be favored.
This work represents the first publication in a series of articles in which we analyzed the temporal variations of x-ray luminosities of AGNs and GBHs in order to gain more knowledge about the physical processes in the innermost regions of accretion disks and at the edge of the event horizon of a black hole in the centre of an AGN [32, 33, 34, 239, 240, 107, 108, 109].
With the notable exception of the Blazar Mrk 421 [32], we concentrated our studies on narrow line Seyfert 1 galaxies, where we put an emphasis on the analyses of PKS 0558504 partly on the basis of dedicated XMM-Newton observation that have been granted to our research group. This AGN belongs to the rare class of radio loud NLS1 galaxies exhibiting large amplitude x-ray flux variations.
Due to their closeness, brightness and their shorter time scales better observations of galactic black holes are feasible and the physical conditions of GBH are better known than those of supermassive black holes in AGNs. Thorough studies of GBH may thus lead to refined models for the accretion disk physics that can be used in principle to infer information about their scaled-up extragalactic analogs – if the unified picture of AGNs and GBHs is truly valid. Following this line we investigate in the paper

Paper XI. [106]: Characterizing black hole variability with nonlinear methods: the case of the x-ray Nova 4U 1543-47, Astron. & Astrophys. ***512****, A21 (2010)*

the possible nonlinear variability properties of the black hole x-ray nova 4U 1543-47 to complement the temporal studies based on linear techniques, and to search for signs of (deterministic and stochastic) nonlinearity in Galactic black hole light curves. It is found that scaling indices are able to parametrize uniquely the temporal variability properties of GBHs. The search for nonlinear temporal correlations reveals that the variability is linear in all light curves with the notable exception of the very high state (VHS). The detection of nonlinearity in the VHS, that is characterized by the presence of most prominent quasiperiodic orbit (QPO), suggests that intrinsically linear models like e.g. the global disk oscillation model [346], which have been proposed to account for the low frequency QPOs in GBHs are to be ruled out. A shock oscillation model [42] or the accretion-ejection instability model [334] are, on the other hand, still viable solutions for explaining the nonlinear behavior in the VHS.
Let us finalize the section about nonlinear time series analysis of astrophysical objects with some more recent results that are – so far – not published elsewhere. With the first detection of a QPO in an AGN (RE J1034+396) [102] a comparison of states with QPOs in GBHs and AGNs became possible. In Fig. 5.2 the XMM-Newton light curve for this narrowline Seyfert 1 galaxy is shown. We performed the standard test for nonlinearities involving surrogates and nonlinear prediction error, where we used exactly the same settings (e.g. embedding dimension, criterion for optimal delay time, etc.) as for the GBH 4U 1543-47. The result is displayed in Fig. 5.3. It can immediately be seen that the QPO detected in this AGN is not associated with the simultaneous presence of nonlinearities as we found in the GBH 4U 1543-47. This results does not corroborate a unified picture

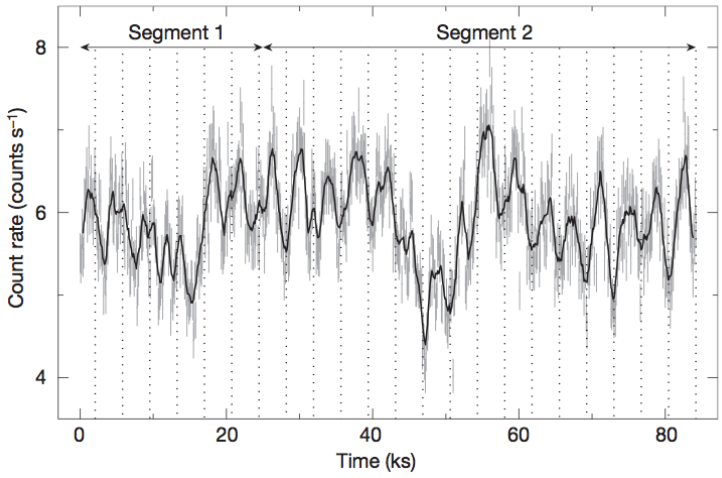

Figure 5.2: XMM-Newton light curve of RE J1034+396. The presence of a periodic time variation is obvious (Source: [102]).

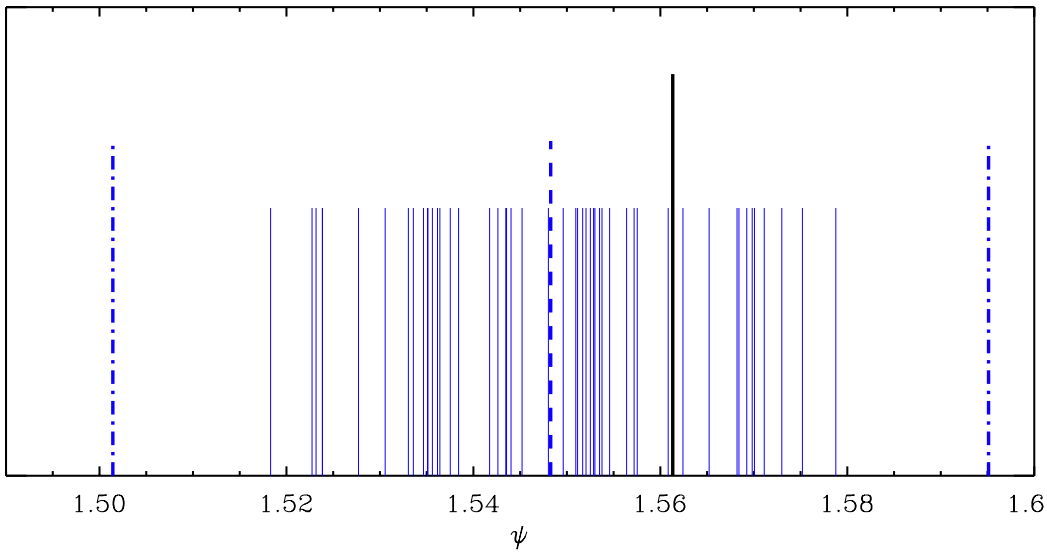

Figure 5.3: Nonlinear prediction error ψ of RE J1034+396 (black long line) and 50 corresponding surrogates (blue short lines). The blue dashed line marks the mean value derived from the surrogates. The blue dash-dotted lines indicate the $3\sigma_{psi}$ confidence interval. This plot is to be contrasted with Fig. 8 in [106].

for GBHs and AGNs, where the latter ones are just upscaled versions of the former with essentially the same accretion physics [211]. The presence/absence of nonlinearities in otherwise similar states rather points towards qualitatively different physical mechanisms playing important roles in the two cases.
Very recently it was also convincingly shown that the repetitive patterns in rapid optical variations in the nearby black-hole binary V404 Cygni is – in contradiction to common belief – not critically determined by the accretion rate, which is far below the Eddington limit in the considered GBH. It is rather argued that the large amplitudes in long period systems are caused by the lack of sustained accretion [172]. These two examples show that there are still many unsolved questions in understanding how black holes accrete surrounding matter and that we are far from having a unified picture of this fundamental phenomenon in astrophysics. Further analyses of past and present observations will help to give new insights into the complex physical processes in accretion disks. Nonlinear time series analysis will help to better show (dis-)similarities of different objects and thus to better categorize them. This will enable a better model selection – especially when nonlinear interactions play an important role. We are currently compiling a large set of x-ray light curves of prominent and well-studied GBHs and AGNs with the aim being to refine models of accretion flows around black holes by using the information about the presence and strength of nonlinearities in the x-ray time series.

5.3 Probing isotropy and statistics of the CMB

The analysis of the cosmic microwave background (CMB) radiation has led to major breakthrough discoveries in Cosmology. The mere discovery of this relic radiation in 1964 by Penzias and Wilson [243] (Nobel Prize in 1978) originating from a hot and dense era of the Universe [71] in the very distant past became one of the first and major proofs for the standard Big Bang cosmological model. The first full-sky observations of the CMB with the COBE satellite [205, 320, 206] in the nineties of the last century (Nobel Prize in 2006) revealed the amazing homogeneity of this radiation – although the shape of detected fluctuations in the temperature (being as small as of the order of $O(10^{-5})$ C) could corroborate the assumption of an inflationary period right after the Big Bang. This period of inflation had to be postulated [117, 200, 5] to find a solution for the flatness and horizon problem. The former refers to the fact that the observed highly accurate flatness of the Universe would require a very fine-tuned value for the critical density, for which an explanation (omitting anthropic arguments) has to be found. The latter states that the same temperature in different regions of the sky as measured with the CMB can only be achieved if they had been close enough to each other for information to be exchanged between them so that they can equilibrate to a common state. Yet, distant regions in the sky are too far away even for light to travel between the regions, they are beyond their (event) horizons and thus causally disconnected. Assuming inflation yields also an explanation for the primordial density fluctuations, which are the seeds for cosmic structure formation. They can be interpreted as quantum fluctuations of the inflaton field, which are stretched

during inflation [322, 228] (for a review see: [229]). A number of inflationary scenarios have been developed, where many predict the presence of significant three- and four-point correlations, i.e. non-Gaussiantities (for a review see e.g. [45]). Alternative models comprise e.g. an ekpyrotic universe [167, 325], where the universe undergoes an endless sequence of cosmic epochs that begin with a "bang" and end in a "crunch". An appealing property of the cyclic universe model is that no initial conditions at the "beginning of time" have to be defined.
Higher precision measurements of the CMB as obtained in the last fifteen years with e.g. the WMAP- [18] and PLANCK-satellite [246] (see Fig. 5.4) have helped to make cosmology a precision science and to constrain scenarios of the very early universe by measuring the power spectrum with unprecedented accuracy up to multipoles of $l = 2500$ and by investigating possible higher order correlations, i.e non-Gaussianities (NGs), in the fields of temperature and polarization fluctuations.

Thorough analyses of the PLANCK temperature and polarization data showed, however, that there are no significant signatures of non-Gaussiantities in the CMB as parametrized by the bispectra with special triangle configurations (local, equilateral and orthogonal) [250, 255]. This has led to the exclusion of a number of the more complicated scenarios such as multi-field inflation, Dirac-Born-Infield (DBI) inflation and others. Rather, the simplest, single field scenario with a plateau-like potential for the inflaton field has to be favored [248, 256]. Although it was first claimed that ekpyrotic scenarios are "under severe pressure" in the light of the PLANCK results, it was a short time later argued that a cyclic universe is still supported by the data [196]. There is an ongoing discussion, whether ekpyrotic of inflationary models are in trouble in view of the data from the PLANCK satellite[143, 118, 144]. The detection of the curl component (B-mode) in the cosmic microwave background (CMB) polarization induced by inflationary gravitational waves will be a decisive criterion to (dis-)favour on of the two scenarios. While inflation predicts the presence of gravitational waves, ekpyrotic models does not and so B-modes should be absent. The quest for B-modes represents thus one of the present and future hot topics in CMB physics and cosmology.
The homogeneity and isotropy of the Universe – also known as the Copernican principle – is a major postulate of modern cosmology and an underlying axiom of the standard cosmological models. Obviously this assumption does not imply exact homogeneity and isotropy, but merely that the observed cosmological inhomogeneities are random fluctuations around a uniform background, extracted from a homogeneous and isotropic statistical ensemble. One may expect that the ever improving observations of CMB fluctuations should lead to the greatest vindication of this principle. Yet, there have been a number of disturbing claims of evidence for deviations from isotropy and even for a preferred direction in the Universe. One of the first anomalies which has been detected in the WMAP first year data release and persisted in further data releases was the alignment of the low-l multipoles [69, 59, 309, 185], which was then often dubbed "the axis of evil".
Another large scale anomaly that was found in the WMAP data was that the modes at low l's show untypical low power. Corresponding to this, the angular two-point correlation function at large scales (angular separation > 60 deg) was found to be approximately zero

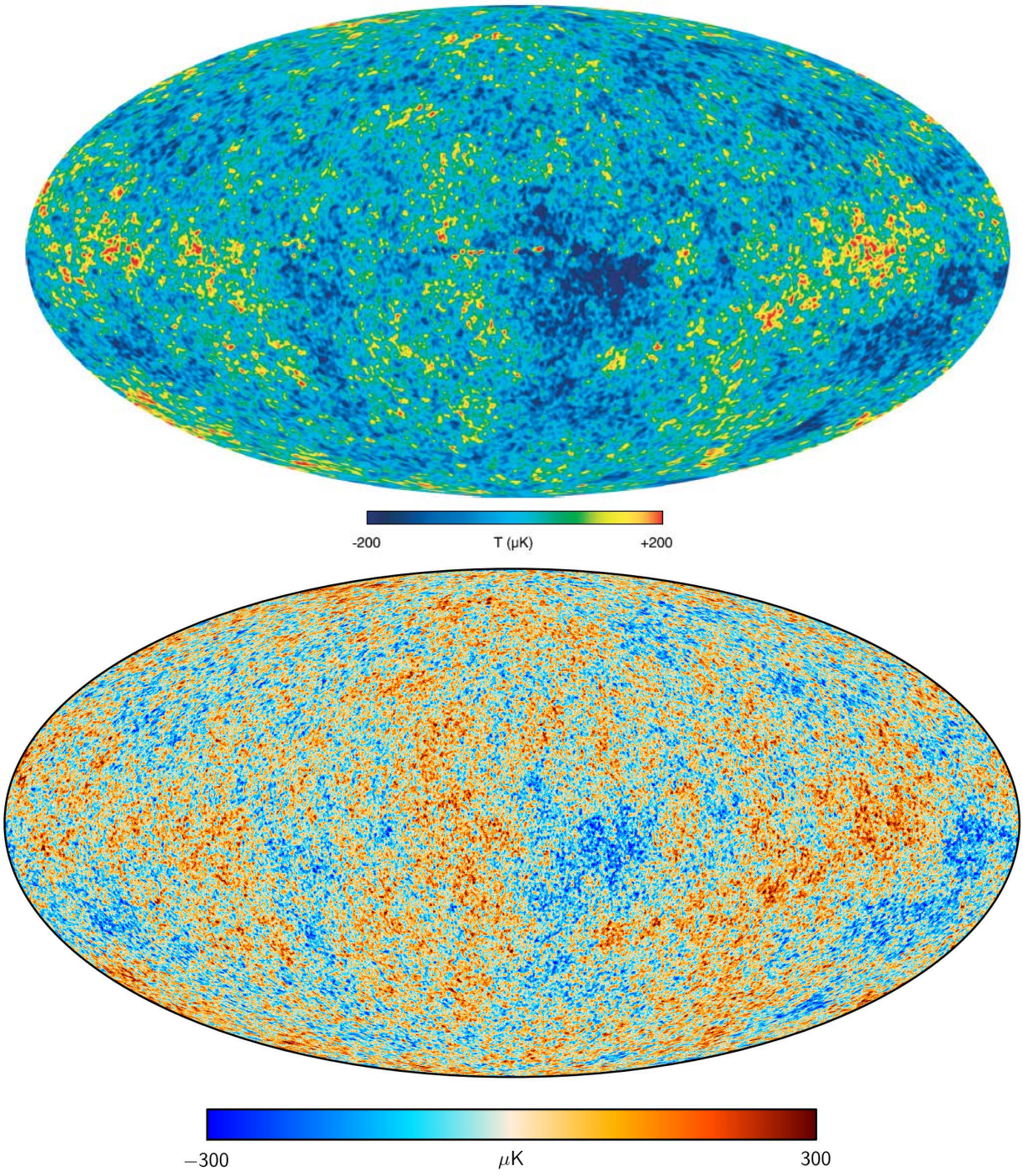

Figure 5.4: Temperature map of the CMB as derived from the full sky survey of the microwave radiation with the WMAP and Planck satellite. Above: WMAP ICL CMB map (source: [18]). Below: Planck SMICA CMB map (source:[246]).

pointing towards an unexpected uncorrelated universe being clearly inconsistent with the standard cosmological ΛCDM model [60].
Hemispherical asymmetries with respect to linear measures (two-point correlation functions and power spectrum) [85], [123] and nonlinear measures (Minkowski functionals) [241], [86] were also quickly identified and confirmed in later releases of WMAP data [87, 138, 124, 11]. It was also assessed, how the differences in the power spectrum influence the determination of the cosmological parameters in a standard ΛCDM cosmology. In particular it was found that for the two opposite hemispheres aligned with the preferred asymmetry axis the spectral index ranged from $n_s = 0.959 \pm 0.022$ to $n_s = 0.989 \pm 0.024$ [11]. This means that in one hemisphere the spectral index is different from one at almost 2σ , whereas in the other it is fully consistent with one. Of course this difference is decisive for the selection of models for inflation.
A localized anomaly that was detected very early in the WMAP data using spherical Mexican hat wavelets (SHMW) [352] as well as directional wavelets [208, 210] and needlets [258] is the so-called cold spot [352]. It is a $\sim 5^\circ$ radius, -150 μK feature in the southern hemisphere which represents a departure arising in only less than 0.2% Gaussian simulations [66]. It has been discussed whether the cold spot is an intrinsic signature of the CMB or an imprint of a supervoid via the Integrated Sachs-Wolfe (ISW) effect. Very recent analyses of galaxy redshift surveys showed, however, that the scale of voids is insufficient to explain the cold spot through the ΛCDM ISW effect [203]. The cold spot may thus have a primordial origin rather than being due to late-time line-of-sight effects.
As it has been outlined in the previous chapters, the use of concepts derived in the realm of nonlinear dynamics may also have the potential to give additional information about the patterns and their complexity in the CMB. Here, we adapt and apply again two key concepts of complex systems theory, namely estimators for local scaling properties and the method of surrogates, for investigating the statistical properties of the CMB. For calculating the scaling indices as estimators for the scaling properties of a CMB map the idea of embedding a data set in a higher-dimensional artificial representation space has been employed. Applying these ideas less formally to image processing tasks allows for the combination of the spatial and intensity (or color) information of the image pixels by representing these physically diverse quantities as points in a common embedding space. The definition of highly sensitive nonlinear local filters relying on the calculation of the local scaling of the point set is thus made possible [263, 264]. They represent a measure for non-Gaussianities similar as wavelets of needlets and can readily be applied to the analysis of CMB data provided a suitable embedding for the spherical symmetric data is found.
Mostly, tests for non-Gaussianities (NG) in cosmology are performed using models for either Gaussian density fluctuations or special types of non-Gaussianity like NGs of the local type, which can be deduced from special shapes of the potential of the inflaton field. To develop complementary and model-independent tests for NGs that are able to investigate *any* deviation from Gaussianity, the method of surrogates was adapted and applied to the case of CMB data analysis. The first application of the idea of phase-randomized surrogates to CMB data (followed by a multifractal analysis) dates back to 1995 [261]. This was only three years after Theiler's seminal paper on surrogates appeared. Yet, in this

work [261] surrogates were only generated for the lines of small simulated patches of the CMB with cosmic string-induces features. Thus the data were treated as a scalar time series and the analysis remained essentially one-dimensional. The methods for generating surrogates had to be extended to higher dimensions and properly validated to make them available for the analysis of CMB maps. Using simulated planar CMB images [266] and LSS simulations [265], it was demonstrated that it is feasible to generate surrogates for two- and three-dimensional data sets using Fourier-based algorithms.
The main contributions to CMB research in this thesis are to adapt, extend and apply two key methods from nonlinear data analysis, namely assessing local scaling properties and the method of surrogates to the analysis of CMB data, in order to test for slight deviations from the standard cosmological ΛCDM model. In the paper

Paper XII. [269] A scaling index analysis of the Wilkinson Microwave Anisotropy Probe three-year data: signatures of non-Gaussianities and asymmetries in the cosmic microwave background, Month. Not. Roy. Astr. Soc. ***380*** *466-478 (2007)*

a dedicated analysis of observations of the CMB with scaling indices using the three-year WMAP data was performed for the first time in order to possibly detect signatures of non-Gaussianities. The embedding of the two-dimensional space and one-dimensional temperature information of the pixelized CMB data in a combined three-dimensional embedding space is performed by transforming the temperature anisotropies to variations in the radial direction around the unit sphere. The calculation of the scaling indices can thus loosely be interpreted as an estimation of the roughness of the last scattering surface. We found highly significant signatures for both global and local anomalies which have to be interpreted as non-Gaussianities. Most of our results are in agreement with other findings. We identified e.g. a pronounced North-South asymmetry as detected previously with e.g. Minkowski functionals and we could redetect the well-known cold spot in the southern hemisphere, yet with a largely increased significance. In a subsequent publication

Paper XIII. [287] Non-Gaussian signatures in the five-year WMAP data as identified with isotropic scaling indices, Month. Not. Roy. Astr. Soc. ***399****, 1921-1933 (2009)*

we repeated and extended the analyses based on scaling indices for the then newly available five-year WMAP data. Again, we found significant signatures for NGs and asymmetries. Here, we put emphasis on the elimination of boundary effects in the calculation of the scaling indices by developing an appropriate mask-filling technique. Furthermore, we performed a thorough band-wise analysis of the WMAP-data. We did not detect any band-dependent changes in the signatures of non-Gaussianity. This result suggests that the anomalies cannot be attributed to yet not understood foreground effects but are rather CMB-intrinsic. In the paper

Paper XIV. [272] Model-Independent Test for Scale-Dependent Non-Gaussianities in the Cosmic Microwave Background, Physical Review Letters ***102*** *131301 (2009)*

we applied the method of surrogate data in such a way that fully model-independent tests for non-Gaussianities in the CMB can deliberately be performed. By introducing a two-

step phase shuffling for an a priori selected range of scales, where first the phases of the modes outside the chosen scales are randomizes and then the phases of the modes insides, dedicated tests for scale-dependent NGs can be devised. Applying these newly developed methods to foreground-cleaned full sky three years and five years WMAP CMB maps we identified significant signatures of non-Gaussianities and asymmetries on large scales (l < 20). These results are in line with a list of previous results, in which anomalies in the CMB at low l's (power asymmetry, axis of evil, lack of two-point correlation function etc.) are reported. The paper

Paper XV. [274] Scale-Dependent non-Gaussianities in the WMAP data as identified by using surrogates and scaling indices, Month. Not. Roy. Astr. Soc. ***415****, 2205 - 2214 (2011)*

extends the analyses using the methodology proposed in [272] to a larger range of scales up to the multipoles of $l = 300$. The signatures for scale-dependent non-Gaussianities at smaller scales are not as pronounced as those found for the largest ones (l <20). Extensive checks on systematics show that the anomalies found at low l (l < 20) must be taken to be cosmological at high significance.

Summarizing the results of the four papers above (for a review see [289]), the analyses of the WMAP CMB data involving scaling indices as test statistics and the method of surrogates as a statistical tool yielded highly significant evidence of anisotropies and non-Gaussianities in the CMB, which are most likely of cosmological origin. As the Galactic plane might contain possible foreground residuals, it is also desirable to be able to use the surrogate approach for a cut sky, where the Galactic region is masked. However, when applying a sky cut, orthonormality of the spherical harmonics no longer holds on this new incomplete sky - making a naive phase shuffling impossible. On the other hand, one can transform the spherical harmonics into a new set of harmonics, which forms an orthonormal basis on the incomplete sky, where phase manipulation can then take place again. We also pursued this approach in the work by Rossmanith et al. [288, 290] to perform a further check on systematics. There, the transformation of the spherical harmonics into a new set of harmonics was combined with the idea of phase shuffling, thus enabling investigations by means of surrogates on an incomplete sky. The feasibility of this approach was once again first demonstrated for the case of phase correlations on large scales, which also allows for a direct comparison of the full sky and cut sky results. A scaling index analysis showed again signatures for non-Gaussianities and pronounced asymmetries, which are consistent with the full sky results and persist even when removing larger parts of the sky. This result confirms that the influence of the Galactic plane is not responsible for the detected deviations from Gaussianity and isotropy. In the absence of an explanation in terms of Galactic foregrounds or known systematic artefacts, the signatures in the WMAP data must so far be taken to be cosmological at high significance. These findings disagree with predictions of isotropic cosmologies with single field slow roll inflation and might point to a violation of the Cosmological principle.

Given the far-reaching consequences of the results described above on fundamental aspects of our current cosmological model, further confirmations of the detected anomalies are

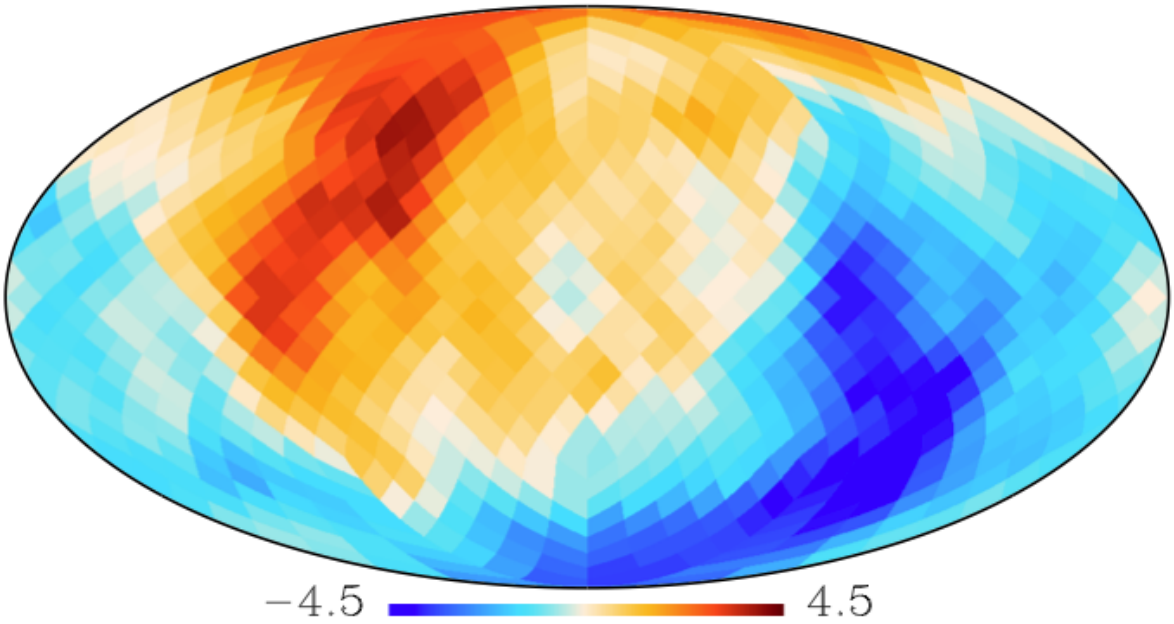

Figure 5.5: Deviations of the rotated hemispheres derived from the mean of the scaling indices determined from the Planck `SMICA` map (Source: [249]). This map is to be compared with Fig. 2 in Paper XIV. ([272]) in this thesis.

desirable. Therefore, additional, independent tests were performed

- by using a new, much more accurate CMB data set, namely the CMB-maps derived from microwave measurements of the Planck satellite [246] and
- by taking a different test statistics, namely the Minkowski functionals.

As it was shown in [272, 274], the main signature for phase correlations was found at the largest scales ($l < 20$). Therefore, the analyses of the Planck temperature data by means of surrogates and scaling indices were concentrated on these scales. The papers of the Planck consortium on cosmological results that were released in 2013 together with the first set of CMB maps based on the nominal mission data includes one contribution, which is solely dedicated to the investigation of isotropy and statistics of the CMB [249]. It contains a number of model-independent test of the statistical properties of the CMB including most of those methods, which led to the detection of anomalies in the WMAP data. Repeating the analyses of [272] for the Planck data led to the results shown in Figs. 5.5 and 5.6.

A comparison of the results obtained for WMAP and Planck data immediately shows that the signature of hemispherical asymmetry is persistent and remains on the same level of significance for the much more precise Planck data. It is further worth noting that the results remain practically unchanged (see Table 24 in [249]) when using four different and complementary component separation methods (SMICA, Commander-Ruler, NILC

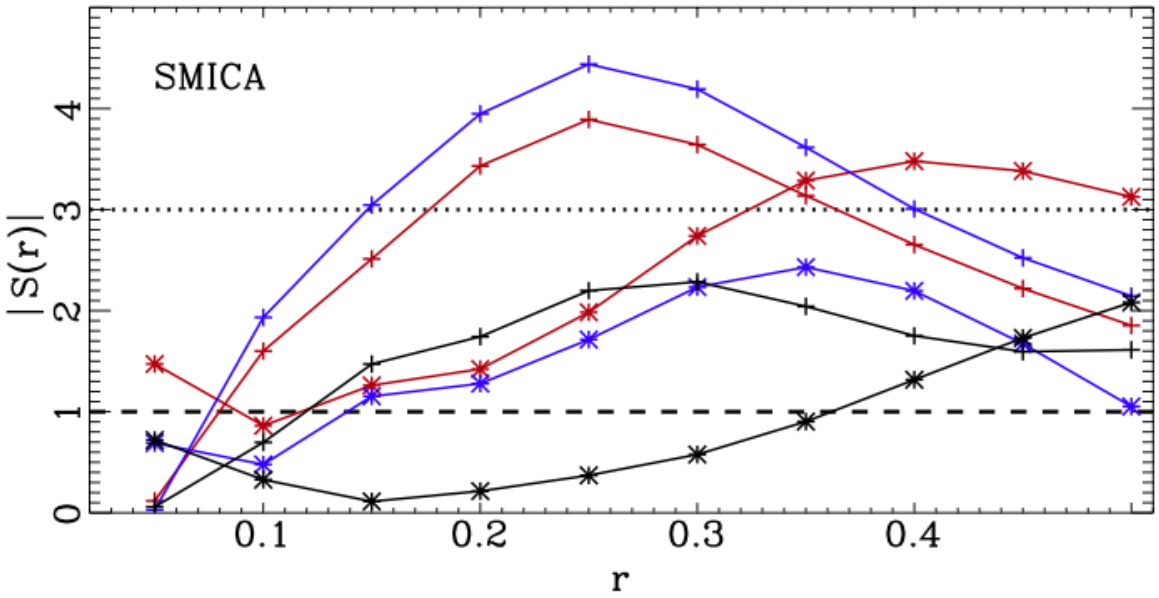

Figure 5.6: Deviations $|S(r)|$ for the PLANCK `SMICA` map as a function of the scale parameter r for the full sky (black) and positive (red) and negative (blue) rotated hemisphere. The plus signs denote the results for the mean $\langle\alpha\rangle$, the star-signs represent the standard deviation σ_α. The dashed (dotted) line indicates the 1 (3) σ significance level. (Source: [249]). This plot is to be compared with Fig. 4 in Paper XIV. ([272]) in this thesis.

and SEVEM [247]) that were selected among twelve competing methods. Other anomalies that were searched for by the Planck collaboration like the multipole alignment, power asymmetry, cold spot etc. were also found to be persistent. Copi et al. confirmed the lack of power in the angular two-point correlation function [61, 62]. Many tests on isotropy and statistics were again performed for the full mission data [254, 26] and the results, where they overlap, are consistent with the Planck 2013 analyses based on the nominal mission data.

Further confirmation of signatures for hemispherical asymmetries induced by large scale phase correlations can be obtained by using another test statistics. We thus repeated the analysis by using Minkowski functionals as scale free and purely morphological estimators for higher order correlations [221, 222, 223] and applied them to WMAP and Planck maps. The results for two different component separation methods (ILC and NILC) and two different surrogate generation techniques (phase shuffling and phase replacement) based on seven year WMAP data are shown in Fig. 5.7. It becomes obvious that the anomalies detected with scaling indices are consistently redetected with all three Minkowski functionals. Thus, all results obtained so far with surrogates and the scaling indices and Minkowski functionals as higher order statistics for both the WMAP and Planck CMB temperature data yield significant signatures of ecliptic hemispherical asymmetries. Due to the use of the surrogate approach, where all but parts of the phase information of the random field

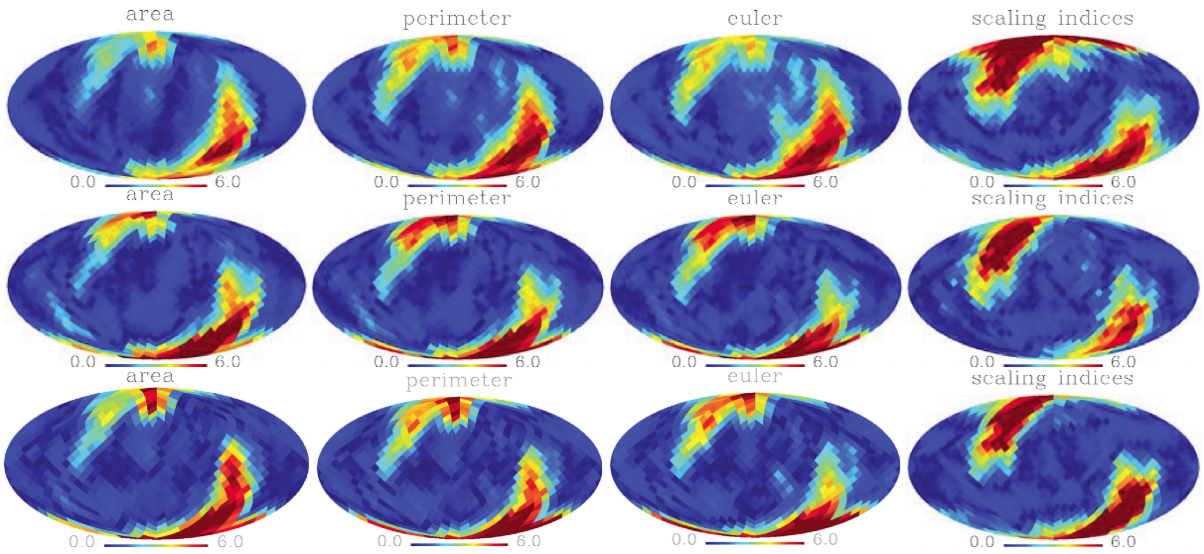

Figure 5.7: Deviations of the rotated hemispheres derived from a χ^2-statistics for the area (first column), perimeter (second column), Euler characteristic (third column) and scaling indices (fourth column, for comparison) for phase shuffled ILC-surrogates, phase-shuffled NILC surrogates and phase-replaced NILC surrogates. (Source: [221])

is left unchanged one has to infer that the anomalies can solely be induced by the presence of phase correlations in the original (CMB-)data. The signal varies only marginally for the data sets stemming from the two different satellites. Furthermore, we analyzed in the course of our investigations CMB maps, which were generated by applying in total six different, partly quite complementary, component separation methods. This consistency of our results makes it very unlikely that detected signal is to be interpreted as an observational or post-processing artefact. One has rather conclude that the phase correlations are of primordial origin questioning the cosmological standard model. Or as it was phrased in the summary of the Planck overview paper of products and scientific results [246]: *These results highlight the maturity and high precision being achieved in our understanding of the Universe, and at the same time herald a new era in which we can no longer ignore tiny but significant deviations at low l's from our current standard model.*

A number of attempts have already been made to explain the observed anomalies by cosmological models reaching beyond the standard single field inflation ΛCDM model. One first has to notice that the Friedmann-Robertson-Walker (FRW) metric is a special case of more general solutions to the Einstein field equations. Relaxing the requirement of isotropy leads to more complicated solutions which contain the FRW metric as a special case. The Bianchi models VII_h, VII_0, and IX are the most general solutions for a homogeneous but anisotropic universe which contain the open, flat, or closed FRW metric as a special case [58, 13, 35, 177]. Correcting the WMAP data with a best-fit Bianchi VII_h template greatly reduced the significance of the large-scale power asymmetry, resolved several anomalies detected on large angular scales (i.e. the low quadrupole amplitude and quadrupole/octupole

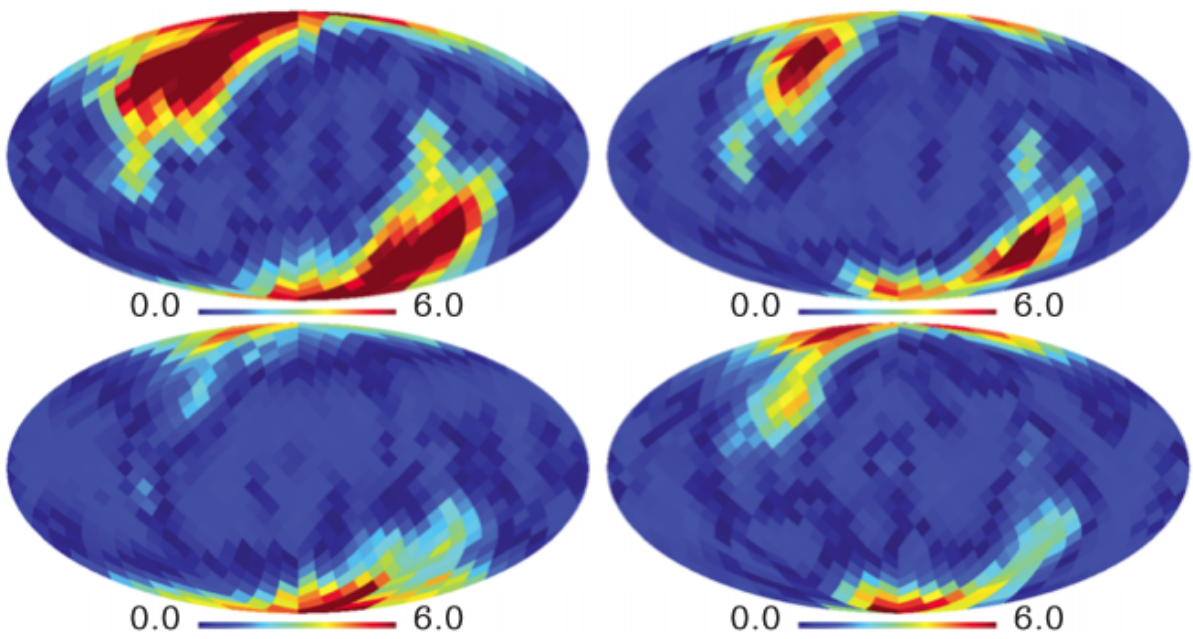

Figure 5.8: Deviations of the rotated hemispheres derived from a χ^2-statistics for the the scaling indices for the Planck SMICA map. The Bianchi template is subtracted with a factor of $f = 0.0, 0.3, 0.7$ and 1.0 (upper left to lower right), respectively (Source: [222]).

planarity and alignment) [151, 152, 153] and reduced the signatures of localized anomalies like the cold spot that were detected with wavelets [209]. We also studied, whether subtracting Bianchi templates can reduce the large scale phase correlations and the effects they have on higher order statistics like scaling indices and Minkowski functionals [222]. The results based on the Planck data are displayed in Figs. 5.8 and 5.9.

It becomes obvious the signature of hemispherical asymmetry is gradually diminished when Bianchi templates with different strength are subtracted. We also found that the phase correlations as measured with the Kuiper statistics monotonically decrease with increasing strength of the Bianchi template. Thus, Bianchi templates offer a viable correction for both the linear and nonlinear anomalies. However, it was also shown by the Planck collaboration that the cosmological parameters that generate the best fit Bianchi pattern are in strong disagreement with those found from CMB anisotropy data alone [251]. Given the lack of consistency of the physical parameters of the model with the Planck cosmological model, the results obtained using Bianchi-subtracted input maps might thus be considered moot. Yet, the morphology of the maps may provide insight into the type of underlying structures associated with the anomalies.

Further theoretical studies propose a number of other physical explanations for the (linear) power asymmetries. One class of models demonstrate that the linear low-l anomalies can also be induced within the framework of inflation. A variety of possibilities leading power asymmetry have already been discussed (see e.g. [68]). Erickcek et al. showed as one

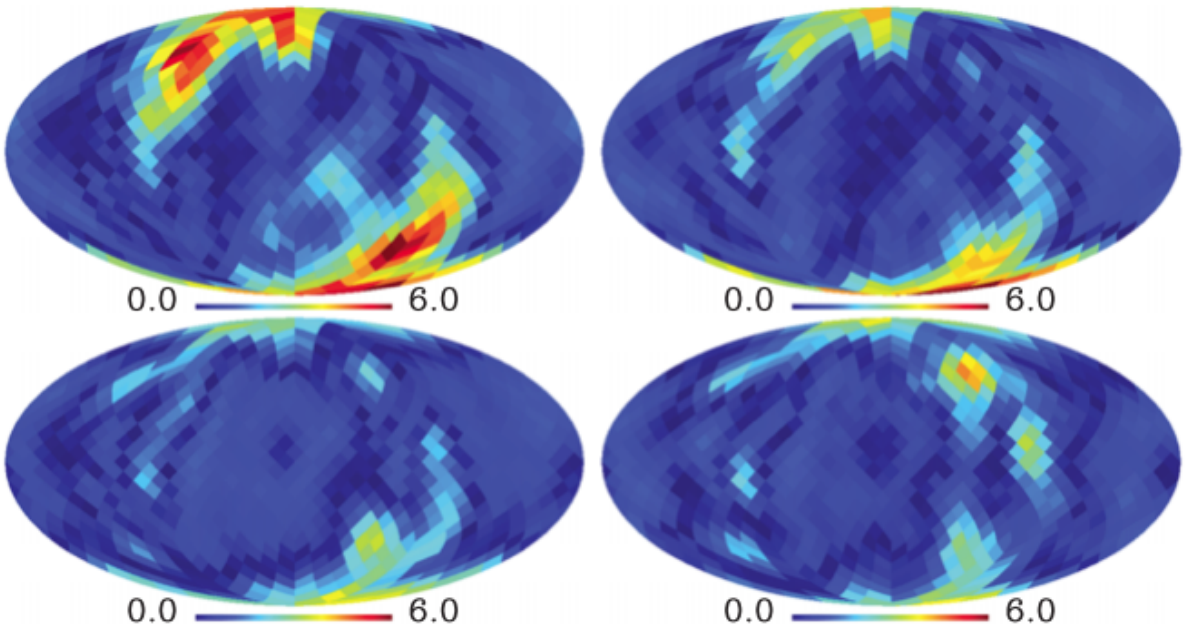

Figure 5.9: Same as Fig. 5.8 but for the Euler characteristic (Source: [222]).

of the first [84] that the power asymmetry can be induced by inflation, if the two-point function at a certain scale k is modulated by perturbations of much larger wavelength. A superhorizon fluctuation in a subdominant scalar field, namely a curvaton perturbation, is a viable multi-field inflation scenario. Yet, such a model entails the presence of non-Gaussianities, namely of a bispectrum with nonempty squeezed limit and there have been concerns that a bispectrum of this type may already be ruled out by observation. Very recently, though, Byrnes et al. demonstrated [38, 39] that it is possible to generate the observed power asymmetry as parametrized by a scale-dependent asymmetry factor [3] by a scale-dependent bispectrum while respecting observational constraints on the *wavelength-averaged* bispectrum, i.e. $|f_{nl}^{local}| \sim |f_{nl}^{ortho}| \sim |f_{nl}^{equi}| \leq 1$, and on the low-l multipoles.
It was also shown recently that cosmic strings formed during inflation (and not before) can mimic a dipole modulation at large angular scales while being negligible at small angles. Interestingly, such a scenario generically produces even one cold spot from the thawing of a cosmic string loop [282].
And even a modification of Einstein General Relativity by adding non-dynamical scalar fields to account simultaneously for both dark matter and dark energy may account for the CMB anomalies. If dark energy (and dark matter) is assumed to be inhomogenously distributed, some of the multipole anomalies in the temperature fluctuations of the CMB spectrum can possibly be removed [43]. It remains to be investigated if and to which extent those models can also account for the large scale phase correlations. From an observational point of view the validity of the observed anomaly has to be tested with alternative cos-

mological probes. First of all one has to test whether a similar signal is found in the CMB polarization data. Planck has measured also the polarized CMB radiation for the full sky. The component separation, i.e. the separation between foreground and CMB signal, of the polarization data is by far more difficult than for the CMB temperature maps. It was actually an underestimation of the dust contribution, which led to the false [20] claim [19] of the detection of B-modes and thus gravitational waves, which kept cosmologists and physicist during 2014 in suspense. The Planck-collaboration learned from this experience and did so far not publish the final polarization maps. Specifically, the latest polarization maps that were made publicly available in 2015 are high-pass filtered, because systematics are still non-negligible compared to the expected cosmological signal on angular scales greater than 10^o, corresponding to $l \leq 20$. All information at scales larger than $l < 20$ was removed by setting the respective spherical harmonic coefficients of the maps to zero [252, 253]. As the phase correlations on which we reported above were identified at these large scales it is so far impossible to search for similar primordial signatures in the polarization maps which would corroborate the existence of deviations from isotropy in the CMB.
Other forthcoming cosmological probes besides the CMB will include large galaxy surveys e.g. with the EUCLID [192] satellite. But these surveys only observe a limited sky area ($15.000 deg^2$) making them less suited for isotropy studies. The X-ray mission eROSITA [262, 213] will perform a full sky survey and is supposed to detect $O(10^6)$ galaxy clusters. Their spatial statistics will give new insights on the isotropy of the structures in the universe. However, galaxies and galaxy clusters are already the result of (nonlinear) structure formation processes making it difficult to disentangle late-time effects from primordial ones. Thus, the most promising cosmological probe seems to be the observation of the brightness-temperature fluctuations in the 21 cm radio emission line during the dark ages ($z \sim 30 - 100$) on a large sky area as it will be performed e.g. with SKA [70]. Theoretical calculations have already shown the enormous potential of this cosmological probe for both estimating parametrized non-Gaussianities [230] and studies of isotropy and statistics [310].
To summarize, it is a tantalizing possibility that the anomalies described in this thesis will take us beyond the standard model of cosmology. It is thus certainly worth spending further effort in probing the validity of one of the fundamental axioms in science, namely the Copernican principle, with both future cosmological probes and even more refined nonlinear statistics. A short outlook on the latter one will be given in chapter 7 of this thesis.

Chapter 6

Synthesizing complex structures

As already mentioned in the introduction and outlined throughout the previous chapters the Fourier phase information is crucial for understanding of complex systems and their presumably nonlinear behavior. This insight marked e.g. the starting point for the development of the Fourier-based method for generating surrogates. Yet, one has only tested with surrogates whether there are correlations among the Fourier phases of a given data set or not. A closer investigation, which effects identified phase correlations have on complex systems and how they are reflected in the higher order statistics in real space, has so far hardly been performed. There are only a few examples, where the phase information is attributed to system properties. It has e.g. been shown in the work by Ivanov et al. [146] that measuring a decline in a multifractal measure of an electrocardiogram can indicate life-threatening heart conditions. It has further uncovered by means of surrogates that the *nonlinear properties of the healthy heart rate are encoded in the Fourier phases.* But it was not studied how and where this information is coded.
Here, we undertake first steps in this direction by synthesizing and analyzing data sets with predefined Fourier phase properties. We use as starting point comparably simple data sets, namely one-dimensional time series. As it was already shown in chapter 1 (Fig. 1.3) financial time series exhibit correlations among the Fourier phases that are clearly visible in phase maps with the naked eye. A similar type of phase correlations is induced by the (I)AAFT surrogate generating algorithms (see chapter 2). In both cases one can see stripe-like patterns that must be associated with linear correlations among Fourier phases. Those correlations can easily be modeled as it is outlined in

Paper XVI. [277]: Time series with tailored nonlinearities, Phys. Rev. E ***92****, 040902(R) (2015).*

In this paper the concept of surrogate data is extended by demonstrating how to generate time series with tailored nonlinearities. This is achieved by inducing well-defined constraints on the otherwise random Fourier phases. The effects of linear correlations among adjacent phases as usually induced by (I)AAFT algorithms on time series are studied. Correlations between the phase information and static (networks) and dynamic (nonlinear prediction error) measures of nonlinearities are established and their origin is explained.

By applying a set of linear constraints on the phases of an originally linear and uncorrelated Gaussian time series, the observed scaling behavior of the intensity distribution of empirical time series can be well reproduced. The power law character of these leptokurtic intensity distributions being typical for intermittent signals as observed in turbulence and in financial data can thus be explained in terms of phase correlations.
These first results may be a starting point for future research also on turbulence. Intermittency is still the main obstacle hampering theoretical, numerical, and phenomenological advancements in understanding and controlling the energy transfer process in turbulent flows. Further studies with tailored nonlinear time series and well-studied model systems, where the occurrence of strong bursts is tunable [257, 190, 37], will most likely shed new light on the nature of intermittency by analyzing and parametrizing the phase information of systems with leptokurtic probability distributions.

Chapter 7

Summary and outlook

In this work we presented further developments of techniques for the quantitative characterization of complex structures and outlined applications of them in the fields of medical physics, plasma physics and astrophysics. The main results of the studies presented in this work can be summarized as following:

- A reassessment of the most popular methods for generating surrogates revealed that they do not always yield fully linear surrogate data. The further use of these methods for generating surrogates has thus to be discouraged.

- In the context of the quantitative characterization of the inner bone structure on the basis of high resolution magnetic resonance imaging three different classes of texture measures, spherical Mexican hat wavelets, scaling indices and Minkowski functionals, were tested with respect to their sensitivity on higher order spatial correlations in this class of images. By means of surrogates it is shown that scaling indices and Minkowski functionals were highly sensitive to the nonlinear information content of these images, while the spherical Mexican hat wavelets only showed poor performance. These results were decisive for selecting proper texture measure in future biomedical studies of this class of images.

- Structural complexity measures assessing the local scaling properties or measuring the morphology of image structures yield refined insights on the changes of bone structures in the context of osteoporosis. This leads to a better diagnostic performance in discriminating osteoporotic and healthy patients. Furthermore, scaling relations between the trabecular bone volume fraction and the trabecular microstructure at different skeletal sites could be established. It was found that they show a rather universal behavior indicating that the relation does not depend on the exposure of the bone to external mechanical forces.

- The kinetics of fluid demixing in a complex plasma was systematically studied using the linear structure factor $S(k,t)$. The role of the nonlinear two-scale Yukawa interactions is clarified. Specifically it is shown that the demixing dynamics depends crucially on the interaction range of the potential.

- The dynamics of lane formation in driven binary complex plasmas was studied as a prototypical non-equilibrium phase transition applying anisotropic scaling indices. The use of this nonlinear structural complexity measure lead to a universal order parameter for driven systems. The observed time-resolved lane-formation process was found to be in good agreement with computer simulations of a binary Yukawa model with Langevin dynamics.

- For the first time the transition from normal fluids to string fluids in electrorheological plasmas was experimentally observed with the PK-3 Plus plasma chamber and subsequently analyzed with anisotropic scaling indices. A comparison with MD-simulations suggested that the phase transition is a second order phase transition. It is further shown in a second set of experiments using the PK4 plasma chamber as well as MD simulations that string formation only appears – as theoretically predicted – in Hamiltonian systems.

- Signatures of nonlinearities could be identified in the x-ray light curve of the brightest narrow line Seyfert 1 galaxy Ark 564 by means of surrogate data. The surrogates had to be generated with techniques involving simulated annealing as the time series showed many gaps. The presence of nonlinearities leads to the exclusion of linear models like e.g. the traditional shot noise model for explaining the variability of this AGN.

- The analysis of x-ray light curves of the galactic black hole 4U 1543-47 revealed that states where QPOs are observed go along with significant signatures of nonlinearities. Again, intrinsically linear models like e.g. the global disk oscillation model are to be ruled out.

- The method of surrogates has been extended to two-dimensional data (on the unit sphere) such that model independent tests for scale-dependent non-Gaussianities were made possible. Using surrogates as well as simulations and scaling indices as test statistics we found significant signatures for large scale phase correlations and for anisotropies in the maps of the CMB as measured with the WMAP and Planck satellite. It is a tantalizing possibility that the detected anomalies will take us beyond the standard model of cosmology, which is based on the Copernican principle, i.e. on isotropy and homogeneity of the universe.

- We further extend the method of surrogates and demonstrate how to generate time series with tailored nonlinearities. It is found that the power law character of leptokurtic probability distributions being typical for intermittent signals found in turbulence and financial data can thus be explained in terms of linear phase correlations.

As outlined in the respective chapters, a number of open questions in the different fields of research are currently under investigation like longitudinal studies in bone research, experimental observations of phase transitions in complex plasmas, categorizing AGNs by means of nonlinear measures and refining the nature of anomalies in the CMB and finding

models for them.
From a more general point of view the eminent importance of the Fourier phases for a better understanding of complex structures becomes obvious. It is surprising that the study of the Fourier phases has so far attracted only little attention, since the clearest, yet most general definition of nonlinearity in data sets is given in the Fourier representation of the data, because solely the nonlinear (non-Gaussian) information of a data set is fully contained in the phases.
Deciphering the meaning of the phase information represents thus the most direct way to study the nonlinear information content in data sets. It is thus likely that major breakthroughs in the physics of complex systems can be achieved by conducting further research on Fourier phases, which will enable investigations of the pure nonlinear information content of a large range of complex systems in a systematic manner. First steps in this direction were already outlined in chapter 6. Furthermore, first results on establishing correlations of Fourier phase correlations as measured with the Kuiper statistics with the strength of higher order statistics on the basis of CMB data could also already be established [222].
Systematic studies by means of surrogates capable to also preserve specific nonlinearities and refined phase statistics may eventually lead to heuristical and subsequently hopefully analytical extension of the (Einstein-)Wiener-Khintchine theorem to the nonlinear case. A good starting point for these studies are data sets on the unit sphere simply because they are closed. Therefore, they represent an ideal test bed to find and establish new phase statistics, because one need not worry about boundary effects and their influence on the higher order (phase-)statistics. Besides the enormous impact, which these studies may have on cosmology, further applications in statistical physics like phase separation [25] and motion of active particles [319] on the sphere have only recently also become of growing interest. For these two examples it is very interesting to study, if and to which extent the demixing or collective motion differs from the results observed in flat space, especially when one considers and quantifies the higher order spatial correlations.

Bibliography

[1] B. Abbott et al. (LIGO Scientific Collaboration and Virgo Collaboration), Observation of Gravitational Waves from a Binary Black Hole Merger, Phys. Rev. Lett. **116**, 061102 (2016) 5.1, 5.2

[2] R. Adler, The geometry of random fields, Wiley, Chichester (1981) 1.2.2

[3] S. Aiola, B. Wang, A. Kosowsky, T. Kahniashvili, and H. Firouzjahi, Microwave background correlations from dipole anisotropy modulation, Phys. Rev. D **92**, 063008 (2015) 5.3

[4] R. Albert and A.-L. Barabasi, Statistical mechanics of complex networks, Rev. Mod. Phys. **74**, 47-97 (2002) 1.2

[5] A. Albrecht and P. Steinhard, Cosmology for grand unified theories with radiatively induced symmetry breaking, Phys. Rev. Lett. **48**, 1220-1223 (1982) 5.3

[6] R. Alpher and R. Herman, Evolution of the Universe, Nature **162**, 774 (1948) 5.1

[7] , R. Antonucci, Unified models for active galactic nuclei and quasars, Annual Rev. Astron. Astrophys. **31**, 473-521 (1993) 5.2

[8] E. Appleton and M. Barnett, Local reflection of wireless waves from the upper atmosphere, Nature **115**, 333-334 (1925) 4.1

[9] J. Argyris et al., An exploration of dynamical systems and chaos, Springer, Berlin Heidelberg (2015) 1.1

[10] H. Atmanspacher, C. Räth and G. Wiedenmann, Statistics and meta-statistics in the concept of complexity, Physica A **234**, 819-829 (1997) 1.2

[11] M. Axelsson, Y. Fantaye, F. Hansen, A. Banday, H. Eriksen and K. Gorski, Directional dependence of ΛCDM cosmological parameters, Astrophysical Journal Letters **773**, L3 (2004) 5.3

[12] R. Aymar, P. Barabaschi and Y. Shimomura, The ITER design, Plasma Physics and Controlled Fusion **44**, 519-565 (2002) 4.1

[13] J. Barrow, R. Juszkiewicz and D. Sonoda, Universal rotation - How large can it be?, Mon. Not. R. Astron. Soc. **213**, 917-943 (1985) 5.3

[14] W. Baumjohann and R. Treumann, Basic space plasma physics, World Scientific Publishing, Singapore (1996) 4.1

[15] V. Beckmann and C. Shrader, Active Galactic Nuclei, Wiley-VCH Verlag, Weinheim (2012) 5.2, 5.1

[16] R. Behrisch, R. Blewer, H. Kukral, B. Scherzer, H. Schmidl, P. Staib and G. Staudenmaier, Spatial distribution of limiter material and impurities on the first wall of TFR 400, Journal of Nuclear Materials **76-77**, 437-444 (1978) 4.1

[17] H. Bénard, Les tourbillons cellulaires dans une nappe liquide. Revue Générale des Sciences **11**, 1261-1271, 1309-1328 (1900) 1.1

[18] C. Bennett et al., First-Year Wilkinson Microwave Anisotropy Probe (WMAP) observations: preliminary maps and basic results, Astrophysical Journal Supplement Series **148**, 1-27 (2003) 5.3, 5.4

[19] BICEP2 Collaboration, Detection of B-Mode Polarization at Degree Angular Scales by BICEP2, Phys. Rev. Lett. **112**, 241101 (2014) 5.3

[20] BICEP2/Keck and Planck Collaborations, Joint Analysis of BICEP2/Keck Array and Planck Data, Phys. Rev. Lett. **114**, 101301 (2015) 5.3

[21] F. Bleibler, A. Konnopka, P. Benzinger, K. Rapp and H.-H. König, The health burden and costs of incident fractures attributable to osteoporosis from 2010 to 2050 in Germany - a demographic simulation model, Osteoporosis International **24**, 835-847 (2013) 3.2

[22] A. Böbel and C. Räth, Kinetics of Fluid Demixing in Complex Plasmas: Domain Growth Analysis using Minkowski Tensors, Phys. Rev. E **94**, 013201 (2016) 4.2

[23] L. Bonewald, The amazing osteocyte, J. Bone Miner. Res. **26**, 229-238 (2011) 3.1

[24] M. Bonitz, C. Henning and D. Block, Complex plasmas: a laboratory for strong correlations, Rep. Prog. Phys. **73**, 066501 (2010) 4.1

[25] M. Bott and J. Brader, Phase separation on the sphere: Patchy particles and self-assembly, Phys. Rev. E **94**, 012603 (2016) 7

[26] F. Bouchet, Planck 2015 results and inflation, C. R. Physique, **16**, 891-913 (2015) 5.3

[27] L. Boufendi, A. Bouchoule, R. Porteous, J. Blondeau, A. Plain and C. Laure, Particle-particle interactions in dusty plasmas, J. Appl. Phys. **73**, 2160-2162 (1993) 4.1

[28] G. Box, G. Jenkins and G. Reinsel, Time series analysis, forecasting and control (fourth edition), John Wiley & Sons, Hoboken (2008) 2.1

[29] P. Brandt, A. Ivlev and G. Morfill, Solid phases in electro- and magnetorheological systems, J. Chem. Phys. **130**, 204513 (2009) 4.4

[30] P. Brandt, Phasenübergänge in komplexen Systemen mit anisotropischen Potenzialen, Dissertation, Ludwig Maximilian Universität, München (2010) 4.4

[31] P. Brandt, A. Ivlev and G Morfill, String-fluid transition in systems with aligned anisotropic interactions, J. Chem. Phys. **132**, 234709 (2010) 4.4

[32] W. Brinkmann, I. Papadakis, C. Räth, P. Mimica and F. Haberl, XMM-Newton timing mode observations of Mrk 421, Astron. & Astrophys. **443**, 397-411 (2005) 5.2

[33] W. Brinkmann, T. Wang, D. Grupe and C. Räth, PG 0844+349 revisited - is there any outflow?, Astron. & Astrophys. **450**, 925-931 (2006) 5.2

[34] W. Brinkmann, I. Papadakis and C. Räth, Spectral variability analysis of an XMM-Newton observation of Ark 564, Astron. & Astrophys. **465**, 107-118 (2007) 5.2

[35] E. Bunn, P. Ferreira, and J. Silk, How Anisotropic is Our Universe?, Phys. Rev. Lett. **77**, 2883-2886 (1996) 5.3

[36] R. Burge, B. Dawson-Hughes, D. Solomon, J. Wong, A. King and A. Tosteson, Incidence and economic burden of osteoporosis-related fractures in the United States, 2005-2025, J. Bone Miner. Res. **22**, 465 - 475 (2007) 3.2

[37] M. Buzzicotti, L. Biferale, U. Frisch and S. Ray, Intermittency in fractal Fourier hydrodynamics: Lessons from the Burgers equation, Phys. Rev. E **93**, 033109 (2016) 6

[38] C. Byrnes, D. Regan, D. Seery and E. Tarrant, The hemispherical asymmetry from a scale-dependent inflationary bispectrum, Journal of Cosmology and Astroparticle Physics **6**, 25 (2016) 5.3

[39] C. Byrnes, D. Regan, D. Seery and E. Tarrant, Implications of the CMB power asymmetry for the early universe, Phys. Rev. D **93**, 123003 (2016) 5.3

[40] G. Chaitin, On the length of programs for computing finite binary sequences, Journal of the ACM **13**, 145-159 (1966) 1.2

[41] G. Chaitin, Algorithmic information theory, IBM Journal of Research and Development **21**, 350-359 (1977) 1.2

[42] S. Chakrabati and S. Manickam, Correlation among Quasi-Periodic Oscillation Frequencies and Quiescent-State Duration in Black Hole Candidate GRS 1915+105, Astrophysical Journal, **531**, L41-L44 (2000) 5.2

[43] A. Chamseddine and V. Mukhanov, Inhomogeneous Dark Energy, Journal of Cosmology and Astroparticle Physics **2**, 040 (2016) 5.3

[44] T. Chen, R. Zitter and R. Tao, Laser diffraction determination of the crystalline structure of an electrorheological fluid, Phys. Rev. Lett. **68**, 2555-2558 (1992) 4.4

[45] X. Chen, Primordial Non-Gaussianities from inflation models, Advances in Astronomy **2010**, 638979 (2010) 5.3

[46] L.-Y. Chiang and P. Coles, Phase information and the evolution of cosmological density perturbations, Mon. Not. R. Astron. Soc. **311**, 809-824 (2000) 1.2.3

[47] L.-Y. Chiang, P. Coles and P. Naselsky, Return mapping of phases and the analysis of the gravitational clustering hierarchy, Mon. Not. R. Astron. Soc. **337**, 488-494 (2002) 1.2.3

[48] L.-Y. Chiang, P. Naselsky. O. Verkhodanov and M. Way, Non-Gaussianity of the derived maps from the first-year Wilkinson Microwave Anisotropy Probe data, Astrophysical Journal **590**, L65 - L68 (2003) 1.2.3

[49] L.-Y. Chiang, P. Naselsky and P. Coles,The robustness of phase mapping as a non-Gaussianity test, Astrophysical Journal **602**, L1 - L4 (2004) 1.2.3

[50] L.-Y. Chiang, P. Naselsky, and P. Coles, Departure from Gaussianity of the cosmic microwave background temperature anisotropies in the three-year WMAP data, Astrophysical Journal **664**, 8-13 (2007) 1.2.3

[51] J. Chu and L. I, Direct observation of Coulomb crystals and liquids in strongly coupled rf dusty plasmas, Phys. Rev. Lett. **72**, 4009 - 4012 (1994) 4.1

[52] S. Chui, Grain-boundary theory of melting in two dimensions, Phys. Rev. Lett. **48**, 933-935 (1982) 4.1

[53] S. Chui, Grain-boundary theory of melting in two dimensions, Phys. Rev. B **28**, 178-194 (1983) 4.1

[54] P. Coles and J. Barrow, Non-Gaussian statistics and the microwave background radiation, Mon. Not. R. Astron. Soc. **228**, 407-426 (1987) 1.2.2

[55] P. Coles, Statistical geometry and the microwave background radiation, Mon. Not. R. Astron. Soc. **234**, 509-531 (1988) 1.2.2

[56] P. Coles and L.-Y. Chiang, Characterizing the nonlinear growth of large-scale structure in the Universe, Nature **406**, 376-378 (2000) 1.2, 1.2.3

[57] P. Coles, P. Dineen, J. Earl and D. Wright, Phase correlations in cosmic microwave background temperature maps, Mon. Not. R. Astron. Soc. **350**, 989-1004 (2000) 1.2.3

[58] C. Collins and S. Hawking, The rotation and distortion of the Universe, Mon. Not. R. Astron. Soc. **162**, 307-320 (1973) 5.3

[59] C. Copi, D. Huterer and G. Starkman, Multipole vectors: A new representation of the CMB sky and evidence for statistical anisotropy or non-Gaussianity at $2 \leq l \leq 8$, Phys. Rev. D **70**, 043515 (2004) 5.3

[60] C. Copi, D. Huterer, D. Schwarz and G. Starkman, Uncorrelated universe: statistical anisotropy and the vanishing angular correlation function in WMAP years 1-3, Phys. Rev. D, **75**, 023507 (2007) 5.3

[61] C. Copi, D. Huterer, D. Schwarz and G. Starkman, Large-scale alignments from WMAP and Planck, Month. Not. Roy. Astr. Soc. **449** 3458-3470 (2015) 5.3

[62] C. Copi, D. Huterer, D. Schwarz and G. Starkman, Lack of large-angle TT correlations persists in WMAP and Planck , Month. Not. Roy. Astr. Soc. **451** 2978-2985 (2015) 5.3

[63] L. Corté, P. Chaikin, J. Gollub and D. Pine, Random organization in periodically driven systems, Nat. Phys., 4, 420-424 (2008) 4.3

[64] L. Couedel, S. Zhdanov, V. Nosenko, A. Ivlev, H. Thomas and G. Morfill, Synchronization of particle motion induced by mode coupling in a two-dimensional plasma crystal, Phys. Rev. E, **89**, 053108 (2014) 4.1

[65] J. Crutchfield and K. Young, Inferring statistical complexity, Phys. Rev. Lett. **63**, 105-109 (1989) 1.2

[66] M. Cruz, E. Martinez-Gonzalez, P. Vielva and L. Cayon, Detection of a non-Gaussian spot in WMAP, Mon. Not. R. Astron. Soc. **356**, 29-40 (2005) 5.3

[67] S. Cummings, J. San Martin, M. McClung et al., Denosumab for prevention of fractures in postmenopausal women with osteoporosis, New England Journal of Medicine, **361**, 756-765 (2009) 3.2

[68] L. Dai, D. Jeong, M. Kamionkowski, and J. Chluba, The pesky power asymmetry, Phys.Rev. D **87**, 123005 (2013) 5.3

[69] A. De Oliveira-Costa, M. Tegmark, M. Zaldarriaga and A. Hamilton, Significance of the largest scale CMB fluctuations in WMAP, Phys. Rev. D **69**, 063516 (2004) 5.3

[70] P. Dewdney, P. Hall, R. Schilizzi and J. Lazio, The Square Kilometre Array, Proceedings of the IEEE **97**, 1482-1496 (2009) 5.3

[71] R. Dicke, P. Peebles, P. Roll and D. Wilkinson, Cosmic black-body radiation, Astrophysical Journal **142**, 414-419 (1965) 5.1, 5.3

[72] R. Donner, Y. Zou, J. Donges, N. Marwan and J. Kurths, Recurrence networks - a novel paradigm for nonlinear time series analysis, New J. Phys. **12**, 033025 (2010) 1.2.1

[73] J. Doyne Farmer and J. Sidorowich, Predicting chaotic time series, Phys. Rev. Lett. **59**, 845-848 (1987) 1.2.1

[74] C.-R. Du, K. Sütterlin, K. Jiang, C. Räth, A.Ivlev, S. Khrapak, M. Schwabe, H. Thomas, V. Fortov, A. Lipaev, V. Molotkov, O. Petrov, Y. Malentschenko, F. Yurtschichin, Y. Lonchakov and G. Morfill, Experimental investigation on lane formation in complex plasmas under microgravity conditions, New J. Phys. **14**, 073058 (2012) 4.4

[75] C.-R. Du, K. Sütterlin, A.Ivlev, H. Thomas and G. Morfill, Model experiment for studying lane formation in binary complex plasmas, Europhys. Lett. **99**, 45001 (2012) 4.4

[76] P. Ducy, T. Schinke and G. Karsenty, The osteoblast: a sophisticated fibroblast under central surveillance, Science **289**, 1501-1504 (2000) 3.1

[77] G. Duffing, Erzwungene Schwingungen bei veranderlicher Eigenfrequenz und ihre technische Bedeutung, F. Vieweg & Sohn, Braunschweig (1918) 1.1

[78] J. Dzubiella, G. Hofmann and H. Löwen, Lane formation in colloidal mixtures driven by an external field, Phys. Rev. E **65**, 021402 (2002) 4.3

[79] J.-P. Eckmann and D. Ruell, Ergodic theory of chaos and strange attractors, Rev. Mod. Phys. **57**, 617 - 656 (1985) 1.2.3

[80] A. Eddington, The deviation of stellar material from a perfect gas, Mon. Not. R. Astron. Soc. **88**, 352 - 369 (1928) 4.1

[81] B. Efron and R. Tibshirani, An Introduction to the bootstrap, Chapman and Hall, New York (1993) 2.1

[82] E. Eggl, A. Malecki, F. Schaff, G. Potdevin, P. Noel, J. Bauer, O. Gordijenko, E. Garcia, R. Burgkart, E. Rummeny, T. Baum and F. Pfeiffer, Prediction of vertebral failure load by using x-ray vector radiographic imaging, Radiology **275**, 553-561 (2015) 3.3

[83] A. Einstein, Method for determination of the statistical values of observations concerning quantities subject to irregular fluctuations, Arch. Sci. Phys. et Nat. **37**, 254-256 (1914) 1.2

[84] A. Erickcek, M. Kamionkowski, and S. Carroll, A hemispherical power asymmetry from inflation, Phys. Rev. D **78**, 123520 (2008) 5.3

[85] H. Eriksen, F. Hansen, A. Banday, K. Gorski and P. Lilje, Asymmetries in the cosmic microwave background anisotropy field, Astrophysical Journal **605**, 14-20 (2004) 5.3

[86] H. Eriksen, D. I. Novikov, P. Lilje, A. Banday and K. Gorski, Testing for non-Gaussianity in the Wilkinson Microwave Anisotropy Probe data: Minkowski functionals and the length of the skeleton, Astrophysical Journal **612**, 64-80 (2004) 5.3

[87] H. Eriksen, A. Banday, K. Gorski, F. Hansen and P. Lilje, Hemispherical power asymmetry in the third-year Wilkinson Microwave Anisotropy Probe sky maps, Astrophysical Journal **660**, L81-L84 (2007) 5.3

[88] B. Ettinger, D. Black, B. Mitlak et al., Reduction of vertebral fracture risk in postmenopausal women with osteoporosis treated with raloxifene - results from a 3-year randomized clinical trial , JAMA **282**, 637-645 (1999) 3.2

[89] H. Ewen and E. Purcell, Observation of a line in the galactic radio spectrum: radiation from galactic hydrogen at 1,420 Mc./sec., Nature **168**, 356 (1951) 5.1

[90] H. Faulkner and J. Rodenburg, Movable aperture lensless transmission microscopy: a novel phase retrieval algorithm, Phys. Rev. Lett. **93**, 023903 (2004) 2.2

[91] J. Faure et al., A laser-plasma accelerator producing monoenergetic electron beams, Nature **431**, 541-544 (2004) 4.1

[92] V. Fortov, A. Ivlev, S. Khrapak, A. Khrapak and G. Morfill, Complex (dusty) plasmas: current status, open issues, perspectives, Physics Reports **421**, 1-103 (2005) 4.1

[93] J. Fineup, Reconstruction of an object from the modulus of its Fourier transform, Optics Letters **3**, 27-29 (1978) 2.2

[94] J. Fineup, Phase retrieval algorithms: a comparison, Applied Optics **21**, 2758-2769 (1982) 2.2, 2.3

[95] A. Fraser and H. Swinney, Independent coordinates for strange attractors from mutual information. Physical Review A **33**, 1134-1140 (1986) 1.2.1

[96] A. Galeev, R. Rosner and G. Vaiana, Structured coronae of accretion disks, Astrophysical Journal **229**, 318-326 (1979) 5.2

[97] G. Gamow, Expanding Universe and the origin of elements, Phys. Rev. **70**, 572 (1946) 5.1

[98] C. Geddes et al., High-quality electron beams from a laser wakefield accelerator using plasma-channel guiding, Nature **431**, 538-541 (2004) 4.1

[99] R. Gerchberg and W. Saxton, A practical algorithm for the determination of the phase from image and diffraction plane pictures, Optik **35**, 237 (1972) 2.2

[100] R. Giacconi, H. Gursky, F. Paolino and B. Rossi, Evidence for x-rays from sources outside the solar system, Phys. Rev. Lett. **9**, 439-443 (2008) 5.1

[101] R. Giacconi, Nobel Lecture: The dawn of x-ray astronomy, Reviews of Modern Physics **75**, 995-1010 (2003) 5.1

[102] M. Gierlinski, M. Middleton, M. Ward and C. Done, A periodicity of sim1 hour in x-ray emission from the active galaxy RE J10341396, Nature **455**, 369-371 (2008) 5.2, 5.2

[103] S. Gillessen, F. Eisenhauer, S. Trippe, T. Alexander, R. Genzel, F. Martins and T. Ott, Monitoring Stellar Orbits Around the Massive Black Hole in the Galactic Center, Astrophysical Journal **692**, 1075-1109 (2009) 5.2

[104] S. Gillessen, P. Plewa, F. Eisenhauer, R. Sari, I. Waisberg, M. Habibi, O. Pfuhl, E. George, J. Dexter, S. von Fellenberg, T. Ott and R. Genzel, An Update on Monitoring Stellar Orbits in the Galactic Center, Astrophysical Journal **837**, 30 (2017) 5.2

[105] M. Gliozzi, W. Brinkmann, C. Räth, I. Papadakis, H. Negoro and H. Scheingraber, On the nature of X-ray variability in Ark 564, Astron. & Astrophys. **391**, 875-886 (2002) 5.2

[106] M. Gliozzi, C. Räth, I. Papadakis and P. Reig, Characterizing black hole variability with nonlinear methods: the case of the x-ray nova 4U 1543-47, Astron. & Astrophys. **512**, A21 (2010) 5.2, 5.3

[107] M. Gliozzi, I. Papadakis, D. Grupe, W. Brinkmann, C. Räth and L. Kedziora-Chudczer, A panchromatic view of PKS 0558-504: an ideal laboratory to study the disk-jet link, Astrophysical Journal **717**, 1243-1252 (2010) 5.2

[108] M. Gliozzi, I. Papadakis, D. Grupe, W. Brinkmann and C. Räth, Long-term monitoring of PKS0558-504 with Swift: the disk-corona link, Mon. Not. R. Astron. Soc. **433**, 1709-1717 (2013) 5.2

[109] M. Gliozzi, I. Papadakis, D. Grupe, W. Brinkmann and C. Räth, Long-term monitoring of Ark 120 with Swift, Mon. Not. R. Astron. Soc. **464**, 3955-3964 (2017) 5.2

[110] D. Goodall, High speed, cine film studies of plasma behaviour and plasma surface interactions in tokamaks, Journal of Nuclear Materials **111-112**, 11-22 (1982) 4.1

[111] A. Golestani and R. Grass, Can we predict the unpredictable?, Sci. Rep. **4**, 6834 (2014) 2.1

[112] J. Gott, D. Weinberg, A. Melott, A quantitative approach to the topology of large-scale structure, Astrophysical Journal **319**, 1-8 (1987) 1.2.2

[113] P. Grassberger and I. Procaccia, Characterization of strange attractors, Phys. Rev. Lett. **50**, 346-349 (1983) 1.2.1

[114] P. Grassberger and I. Procaccia, Measuring the strangeness of strange attractors, Physica D **9**, 189-208 (1983) 1.2.1

[115] P.Grassberger, Toward a quantitative theory of self-generated complexity, Int. J. Theor. Phys. **25**, 907-928 (1986) 1.1, 1.2

[116] P. Grassberger, Problems in quantifying self-generated complexity, Helv. Phys. Acta **62**, 489-511 (1989) 1.2

[117] A. Guth, Inflationary Universe: a possible solution to the horizon and flatness problems, Phys. Rev. D **23**, 347-356 (1981) 5.3

[118] A. Guth, D. Kaiser and Y. Nomura, Inflationary paradigm after Planck 2013, Physics Letters B **733**, 112-119 (2013) 5.3

[119] H. Hadwiger, Vorlesungen über Inhalt, Oberfläche und Isoperimetrie, Springer Verlag, Berlin (1957) 1.2.2, 1.2.2

[120] B. Halperin and D. Nelson, Theory of two-dimensional melting, Phys. Rev. Lett. **41**, 121-124 (1978) 4.1

[121] T. Halsey, M. Jensen, L. Kadanoff, I. Procaccia, and B. Shraiman, Fractal measures and their singularities: the characterization of strange sets, Phys. Rev. A **33**, 1141-1151 (1986) 1.2.1

[122] T. Halsey and W. Toor, Structure of electrorheological fluids, Phys. Rev. Lett. **65**, 2820-2823 (1990) 4.4

[123] F. Hansen, A. Banday and K. Gorski, Testing the cosmological principle of isotropy: local power-spectrum estimates of the WMAP data, Mon. Not. R. Astron. Soc. **354**, 641-665 (2004) 5.3

[124] F. Hansen, A. Banday, K. Gorski, H. Eriksen and P. Lilje, Power asymmetry in cosmic microwave background fluctuations from full sky to sub-degree scales: is the Universe isotropic?, Astrophysical Journal **704**, 1448-1458 (2009) 5.3

[125] J.-P. Hansen and I. McDonald, Theory of Simple Liquids, Academic, New York (1986) 4.2

[126] J.-P. Hansen and H. Löwen, Effective interactions between electric double layers, Annu. Rev. Phys. Chem. **51** 209-242 (2000) 4.2

[127] S. Harris, N. Watts, H. Genant et al., Effects of risedronate treatment on vertebral and nonvertebral fractures in women with postmenopausal - a randomized controlled trial, JAMA **282**, 1344-1352 (1999) 3.2

[128] A. Hartmann, diskrimination of different crystal types in many-particle systems using anisotropic scaling indices, Masterarbeit, Ludwig-Maximilians-Universität München (2015) 4.1

[129] A. Hartmann and C. Räth, Detection and assessment of crystalline structures using anisotropic scaling indices, New J. of Physics (in preparation) 4.1

[130] H. Hauptman, The phase problem of x-ray crystallography, Rep. Prog. Phys. **54** 1427-1454 (1991 2.2

[131] Y. Hayashi and K. Tachibana, Observation of Coulomb-crystal formation from carbon particles grown in a methane plasma, Jap. Journ. Appl. Phys. **33**, L804-L806 (1994) 4.1

[132] D. Helbing and P. Molnár, Social force model for pedestrian dynamics, Phys. Rev. E **51**, 4282-4286 (1995) 4.3

[133] D. Helbing, I. Farkas and T. Vicsek, Freezing by heating in a driven mesoscopic system, Phys. Rev. Lett. **84**, 1240-1243 (2000) 4.3

[134] D. Helbing, Traffic and related self-driven many-particle systems, Rev. Mod. Phys. **73**, 1067-1141 (2001) 4.3

[135] W. Hendrickson, Determination of macromolecular structures from anomalous diffraction of synchrotron radiation, Science **254**, 51-58 (1991) 2.2

[136] H. Hentschel and I. Procaccia, The infinite number of generalized dimensions of fractals and strange attractors, Physica D **8**, 435-444 (1983) 1.2.1

[137] T. Hildebrand, A. Laib, R. Müller, J. Dequeker and P. Rüegsegger, Direct three-dimensional morphometric analysis of human cancellous bone: microstructural data from spine, femur, iliac crest, and calcaneus, J. Bone Miner. Res. **14**, 1167-1174 (1999) 3.3

[138] J. Hoftuft, H. Eriksen, A. Banday, K. Gorski, F. Hansen and P. Lilje, Increasing evidence for hemispherical power asymmetry in the five-year WMAP data, Astrophysical Journal **699**, 985-989 (2009) 5.3

[139] M. Horanyi, G. Morfill and E. Grün, Mechanism for the acceleration and ejection of dust grains from Jupiter's magnetosphere, Nature, **363**, 144-146 (1993) 4.1

[140] M. Horanyi, Charged dust dynamics in the solar system, Annual Review of Astronomy and Astrophysics, **34**, 383-418 (1996) 4.1

[141] R. Huiskes, R. Ruimerman, G. van Lenthe, J. Janssen, Effects of mechanical forces on maintenance and adaptation of form in trabecular bone, Nature **405**, 704-706 (2000) 3.1

[142] H. van de Hulst, Radio waves from space: origin of radiowaves, Ned. tijd. natuurkunde **11**, 210-221 (1945) 5.1

[143] A. Ijjas, P. Steinhardt and A. Loeb, Inflationary paradigm in trouble after Planck2013, Physics Letters B **723**, 261-266 (2013) 5.3

[144] A. Ijjas, P. Steinhardt and A. Loeb, Inflationary schism, Physics Letters B **736**, 142-146 (2014) 5.3

[145] H. Ikezi, Coulomb solid of small particles in plasmas, Physics of Fluids **29**, 1764-1766 (1986) 4.1

[146] P. Ivanov, L. Amaral, A. Goldberger, S. Havlin, M. Rosenblum, Z. Struzikk and E. Stanley, Multifractality in human heartbeat dynamics, Nature **399**, 461-465 (1999) 6

[147] A. Ivlev, G. Morfill, H. Thomas, C. Räth, G. Joyce, P. Huber, R. Kompaneets, V. Fortov, A. Lipaev, V. Molotkov, T. Reiter, M. Turin and P. Vinogradov, First observation of electrorheological plasmas, Phys. Rev. Lett. **100**, 095003 (2008) 4.4

[148] A. Ivlev, S. Zhdanov, H. Thomas and G. Morfill, Fluid phase separation in binary complex plasmas, EPL **85**, 45001 (2009) 4.2

[149] A. Ivlev, P. Brandt, G. Morfill, C. Räth, H. Thomas, G. Joyce, V. Fortov, A. Lipaev, V. Molotkov, and O. Petrov, Electrorheological complex plasmas, IEEE Transactions on Plasma Science **38**, 733 (2010) 4.4

[150] A. Ivlev, M. Thoma, C. Räth, G. Joyce and G. E. Morfill, Complex plasmas in external fields: role of non-Hamiltonian interactions, Phys. Rev. Lett. **106**, 155001 (2011) 4.4

[151] T. Jaffe, A. Banday, H. Eriksen, K. Gorski and F. Hansen, Evidence of vorticity and shear at large angular scales in the WMAP data: a violation of cosmological isotropy?, Astrophysical Journal **629**, L1-L4 (2005) 5.3

[152] T. Jaffe, A. Banday, H. Eriksen, K. Gorski and F. Hansen, Fast and efficient template fitting of deterministic anisotropic cosmological models applied to WMAP data, Astrophysical Journal **643**, 616-629 (2006) 5.3

[153] T. Jaffe, A. Banday, H. Eriksen, K. Gorski and F. Hansen, Bianchi type VIIh models and the WMAP 3-year data, Astronomy and Astrophysics **460**, 393-396 (2006) 5.3

[154] A. Jain and F. Farrokhnia, Unsupervised texture segmentation using Gabor filters, Pattern Recognition **24**, 1167-1186 (1991) 2.1

[155] I. Jang, I. Kim, Computational study of Wolff's law with trabecular architecture in the human proximal femur using topology optimization, J. Biomech. **41**, 2353-2361(2008) 3.1

[156] K. Jansky, Electrical disturbances apparently of extraterrestrial origin, Proceedings of the Institute of Radio Engineers **21**, 1387-1398 (1933) 5.1

[157] K. Jiang, C.-R. Du, K. Sütterlin, A. Ivlev and G. Morfill, Lane formation in binary complex plasmas: role of non-additive interactions and initial configurations, Europhys. Lett. **92**, 65002 (2010) 4.4

[158] C. Joshi and T. Katsouleas, Plasma accelerators at the energy frontier and on tabletops, Physics Today **56**, 47-53 (2003) 4.1

[159] G. Joyce, C. Räth, P. Huber, H. Thomas, G. Morfill, V. Molotkov and V. Fortov, Addendum: structural properties of 3D complex plasmas under microgravity conditions, Europhys. Lett. **93**, 29901 (2011) 4.1

[160] B. Julesz, Textons, the elements of texture perception, and their interactions, Nature **920**, 91-97 (1981) 2.1

[161] B. Julesz, Early vision and focal attention, Rev. Mod. Phys. **63**, 735 - 772 (1991) 2.1, 2.1

[162] J. Karle and H. Hauptman, The phases and magnitudes of the structure Factors, Acta Cryst. **3**, 181-187 (1950) 2.2

[163] J. Karle and H. Hauptman, A theory of phase determination for the four types of non-centrosymmetric space groups $1P222$, $2P22$, $3P_12$, $3P_22$, Acta Cryst. **9**, 635-651 (1956) 2.2

[164] L. Keller, L. Oren, R. Taylor, F. Schwirzke, R. Bunash and C. Wagner, Structure of Metallic Coatings for Impurity Control in Macrotor, Journal of Nuclear Materials **111-112**, 493-497 (1982) 4.1

[165] M. Kennell and H. Abarbanel, False neighbors and false strands: A reliable minimum embedding dimension algorithm, Phys. Rev. E **66**, 026209 (2002) 1.2.1

[166] A. Khintchine, Korrelationstheorie der stationären stochastischen Prozesse, Math. Ann. **109**, 604-615 (1934) 1.2

[167] J. Khoury, B. Ovrut, P. Steinhardt and N. Turok, Ekpyrotic universe: Colliding branes and the origin of the hot big bang, Phys. Rev. D **64**, 123522 (2001) 5.3

[168] S. Khrapak, G. Morfill, A. Ivlev, H. Thomas, D. Beysens, B. Zappoli, V. Fortov, A. Lipaev, and V. Molotkov, Critical point in complex plasmas, Phys. Rev. Lett. **96**, 015001 (2006) 4.1

[169] S. Khrapak, B. Klumov, P. Huber, V. Molotkov, A. Lipaev, V. Naumkin, H. Thomas, A. Ivlev, G. Morfill, O. Petrov, V. Fortov, Y. Malentschenko and S. Volkov, Freezing and melting of 3D complex plasma structures under microgravity conditions driven by neutral gas pressure manipulation, Phys. Rev. Lett. **106**, 205001 (2011) 4.1

[170] S. Khrapak, B. Klumov, P. Huber, V. Molotkov, A. Lipaev, V. Naumkin, A. Ivlev, H. Thomas, M. Schwabe, G. Morfill, O. Petrov, V. Fortov, Y. Malentschenko and S. Volkov, Fluid-solid phase transitions in three-dimensional complex plasmas under microgravity conditions, Phys. Rev. E **85**, 066407 (2012) 4.1

[171] C. Killer, T. Bockwoldt, S. Schütt, M. Himpel, A. Melzer and A. Piel, Phase separation of binary charged particle systems with small size disparities using a dusty plasma, Phys. Rev. Lett. **116**, 115002 (2016) 4.2

[172] M. Kimura et al., Repetitive patterns in rapid optical variations in the nearby black-hole binary V404 Cygni, Nature **529**, 54-58 (2016) 5.2

[173] S. Kirkpatrick, C. Gelatt and M. Vecchi, Optimization by simulated annealing, Science **220**, 671-680 (1983) 2.2

[174] C. Knapek, C. Durniak, D. Samsonov and G. Morfill, Scale-free behavior of a 2D complex plasma during rapid cooling, Phys. Rev. Lett. **110**, 035001 (2013) 4.1

[175] C. Knapek, D. Samsonov, S. Zhdanov, U. Konopka and G. Morfill, Recrystallization of a 2D plasma crystal, Phys. Rev. Lett. **98**, 015004 (2007) 4.1

[176] B. Klumov, G. Joyce, C. Räth, P. Huber, H. Thomas, G. Morfill, V. Molotkov and V. Fortov, Structural properties of 3D complex plasmas under microgravity conditions, Europhys. Lett. **92** 15003 (2010) 4.1

[177] A. Kogut, G. Hinshaw, and A. J. Banday, Limits to global rotation and shear from the COBE DMR four-year sky maps, Phys. Rev. D **55**, 1901 (1997) 5.3

[178] A. Kolmogorov, Three approaches to the quantitative definition of complexity, Problems of Information Transmission **1**, 3-11 (1966) 1.2

[179] R. Kompaneets, Complex plasmas: Interaction potentials and non-Hamiltonian dynamics, Dissertation, Ludwig Maximilian Universität, München (2007) 4.4

[180] R. Kompaneets, G.Morfill and A.Ivlev, Design of new binary interaction classes in complex plasmas, Physics of Plasmas **16**, 043705 (2009) 4.1

[181] M. Kong, G. Kroesen, G. Morfill, T. Nosenko, T. Shimizu, J. van Dijk and J. Zimmermann, Plasma medicine: an introductory review, New J. Phys. **11**, 115012 (2009) 4.1

[182] J. Kosterlitz and D. Thouless, Long range order and metastability in two-dimensional solids and superfluids, J. Phys. C **5**, L124-L126 (1972) 4.1

[183] J. Kosterlitz and D. Thouless, Ordering, metastability and phase transitions in two-dimensional systems, J. Phys. C **6**, 1181-1203 (1973) 4.1

[184] N. Kuiper, Tests concerning random points on a circle, Proceedings of the Koninklijke Nederlandse Akademie van Wetenschappen Series A **63** 38-47 (1960) 1.2.3

[185] K. Land and J. Magueijo, Examination of evidence for a preferred axis in the cosmic radiation anisotropy, Phys. Rev. Lett. **95**, 071301 (2005) 5.3

[186] A. La Porta, G. Voth, A. Crawford, J. Alexander and E. Bodenschatz, Fluid particle accelerations in fully developed turbulence, Nature **409**, 1017-1019 (2001) 4.1

[187] I. Laut and C. Räth, Surrogate-assisted network analysis of nonlinear time series, Chaos **26**, 103108 (2016) 1.2.1, 2.3

[188] S. Krasheninnikov, R. Smirnov and D. Rudakov, Dust in magnetic fusion devices, Plasma Phys. Control. Fusion **53**, 083001 (2011) 4.1

[189] I. Langmuir, Oscillations in ionized gases, PNAS **14**, 627 - 637 (1928) 4.1

[190] A. Lanotte, R. Benzi, S. Malapaka, F.Toschi and L. Biferale, Turbulence on a fractal Fourier set, Phys. Rev. Lett. **115**, 264502 (2015) 6

[191] M. Laroussi, M. Kong, G. Morfill and W. Stolz (eds), Plasma medicine: applications of low-temperature gas plasmas in medicine and biology, Cambridge University Press, Cambridge (2012) 4.1

[192] R. Laureijs et al., Euclid definition study report, arXiv:1110.3193 (2011) 5.3

[193] I. Laut, Network analyses of nonlinear time series and complex spatial structures, Masterarbeit, Ludwig Maximilian Universität, München (2014) 1.2.1

[194] I. Laut, C. Räth, S. Zhdanov, V. Nosenko, L. Couedel and H. Thomas, Synchronization of particle motion in compressed two-dimensional plasma crystals, Europhys. Lett. **110**, 65001 (2015) 4.1

[195] I. Laut and C. Räth, Surrogate-assisted network analysis of nonlinear time series, Chaos **26**, 103108 (2016) 1.2.1, 2.3

[196] J.-L. Lehners and P. Steinhardt, Planck 2013 results support the cyclic universe, Phys. Rev. D **87**, 123533 (2013) 5.3

[197] R. Levien and S. Tan, Double pendulum: an experiment in chaos, Am. J. Phys. **61**, 1038-1044 (1993) 1.1

[198] M. Leunissen, C. Christova, A.-P. Hynninen, C. Patrick Royall, A. Campbell, A. Imhof, M. Dijkstra, R. van Roij and A. van Blaaderen, Ionic colloidal crystals of oppositely charged particles, Nature **437**, 235-240 (2005) 4.3

[199] U. Liberman, S. Weiss, J. Broll et al., Effect of oral alendronate on bone-mineral density and the incidence of fractures in postmenopausal osteoporosis, New England Journal of Medicine, **333**, 1437-1443 (1995) 3.2

[200] A. Linde, A new inflationary universe scenario: a possible solution of the horizon, flatness, homogeneity, isotropy and primordial monopole problems, Physics Letters B **108**, 389-393 (1982) 5.3

[201] H. Löwen, Melting, freezing and colloidal suspensions, Physics Reports **237**, 249-324 (1994) 4.3

[202] E. Lorenz, Deterministic nonperiodic flow, J. Atmos. Sci. **20**, 130-141 (1963) 1.1

[203] R. Mackenzie, T. Shanks, M. Bremer, Y.-C. Cai, M. Gunawardhana, A. Kovacs, P. Norberg and I. Szapudi, Evidence against a supervoid causing the CMB cold spot, arXiv:1704.03814 (2017) 5.3

[204] Mangles et al., Monoenergetic beams of relativistic electrons from intense laser-plasma interactions, Nature **431**, 535-538 (2004) 4.1

[205] J. Mather et al., A preliminary measurement of the cosmic microwave background spectrum by the Cosmic Background Explorer (COBE) satellite, Astrophysical Journal **354**, L37-L40 (1990) 5.3

[206] J. Mather et al., Measurement of the cosmic microwave background spectrum by the COBE FIRAS instrument, Astrophysical Journal **420**, 439-444 (1994) 5.3

[207] S. McCandlish, A. Baskaran and M. Hagan, Spontaneous segregation of self-propelled particles with different motilities, Soft Matter **8**, 2527-2534 (2012) 4.2

[208] J. McEwen, M. Hobson, A. Lasenby and D. Mortlock, A high-significance detection of non-Gaussianity in the Wilkinson Microwave Anisotropy Probe 1-yr data using directional spherical wavelets, Mon. Not. R. Astron. Soc. **359**, 1583-1596 (2005) 5.3

[209] J. McEwen, M. Hobson, A. Lasenby and D. Mortlock, Non-Gaussianity detections in the Bianchi VIIh corrected WMAP one-year data made with directional spherical wavelets, Mon. Not. R. Astron. Soc. **369**, 1858-1868 (2006) 5.3

[210] J. McEwen, M. Hobson, A. Lasenby and D. Mortlock, A high-significance detection of non-Gaussianity in the WMAP 5-yr data using directional spherical wavelets, Mon. Not. R. Astron. Soc. **388**, 659-662 (2008) 5.3

[211] I. McHardy, E. Koerding, C. Knigge, P. Uttley and R. Fender, Active galactic nuclei as scaled-up Galactic black holes, Nature **444**, 730-732 (2006) 5.2

[212] K. Mecke, T. Buchert and H. Wagner, Robust morphological measures for large-scale structure in the Universe, Astronomy and Astrophysics **288**, 697-704 (1994) 1.2.2

[213] A. Merloni et al., eROSITA science book: mapping the structure of the energetic Universe, arXiv:1209.3114 (2012) 5.3

[214] N. Mermin and H. Wagner, Absence of ferromagnetism or antiferromagnetism in one- or two-dimensional isotropic Heisenberg models, Phys. Rev. Lett. **17**, 1133-1136 (1966) 4.1

[215] N. Metropolis, A. Rosenbluth, M. Rosenbluth, A. Teller, and E. Teller, Equation of state calculations by fast computing machines, J. Chem. Phys. **21**, 1087-1092 (1953) 2.2

[216] J. Michell, On the means of diskovering the distance, magnitude etc. of the fixed stars, in consequence of the diminution of the velocity of their light, in case such a diminution should be found to take place in any of them, and such other data should be procured from observations, as would be farther necessary for that purpose, Phil. Trans. R. Soc. Lond. **74**, 35-57 (1784) 5.2

[217] K. Michielsen, H. de Raedt, Integral-geometry morphological image analysis, Physics Reports **347**, 461-538 (2001) 1.2.2

[218] R. Millane, Phase retrieval in crystallography and optics, J. Opt. Soc. Am. A **7**, 394-411 (1990) 2.2

[219] S. Mineshige, M. Takeuchi and H. Nishimori, Is a Black Hole Accretion Disk in a Self-organized Critical State?, Astrophysical Journal Letters **435**, L125-L128 (1994) 5.2

[220] H. Minkowski, Volumen und Oberfläche, Mathematische Annalen **57**, 447-495 (1903) 1.2.2

[221] H. Modest, C. Räth, A. J. Banday, G. Rossmanith, K. Sütterlin, S. Basak, J. Delabrouille, K. M. Gorski and G. Morfill, Scale dependent non-Gaussianities in the CMB data identified with Minkowski functionals and scaling indices, Month. Not. Roy. Astr. Soc. **428** 551-562 (2013) 5.3, 5.7

[222] H. Modest, C. Räth, A. Banday, K. Gorski and G. Morfill, Correlating Fourier phase information with real-space higher order statistics, Phys. Rev. D **89** 123004 (2014) 1.2.3, 5.3, 5.8, 5.3, 5.9, 7

[223] H. Modest, Nonlinear data analysis of the CMB: cosmological principles put to test, Dissertation, Ludwig Maximilian Universität, München (2015) 5.3

[224] G. Morfill, H. Thomas, U. Konopka, H. Rothermel, M. Zuzic, A. Ivlev, and J. Goree, Condensed plasmas under microgravity, Phys. Rev. Lett. **83**, 1598-1601 (1999) 4.1

[225] G. Morfill, A. Ivlev, Complex plasmas: an interdiskiplinary research field, Rev. Mod. Phys. **81** 1353-1404 (2009) 4.1

[226] G. Morfill, C. Räth, Y.-F. Li, J. S. Hu, B. Ling, X. Gao and M. Horanyi, Dust capture experiment in HT-7, New J. of Physics **11**, 113041 (2009) 4.1

[227] D. Müller, T. Link, R. Monetti, J. Bauer, H. Böhm, V. Seifert-Klauss, E. Rummeny, G. Morfill and C. Räth, The 3D-based scaling index algorithm- a new structure measure to analyze trabecular bone architecture in high-resolution MR images in vivo, Osteoporosis International **17**,1483-1493 (2006) 3.3

[228] V. Mukhanov and G. Chibisov, Quantum fluctuations and a nonsingular universe, JETP Lett. **33**, 532-535 (1981) 5.3

[229] V. Mukhanov, H. Feldmann and R. Brandenberger, Theory of cosmological perturbations, Physics Reports **215**, 203-333 (1992) 5.3

[230] J. Munoz, Y. Ali-Haimoud and M. Kamionkowski, Primordial non-Gaussianity from the bispectrum of 21-cm fluctuations in the dark ages, Phys. Rev. D **92**, 083508 (2015) 5.3

[231] R. Neer, C. Arnaud, J. Zanchetta et al., Effect of parathyroid hormone (1-34) on fractures and bone mineral density in postmenopausal women with osteoporosis, New England Journal of Medicine **344**, 1434-1441 (2001) 3.2

[232] A. Nefedov, G. Morfill, V. Fortov et al., PKE-Nefedov: plasma crystal experiments on the International Space Station, New J. Phys. **5**, 33.1-33.10 (2003) 4.1

[233] D. Nelson and B. Halperin, Dislocation-mediated melting in two dimensions, Phys. Rev. B **19**, 2457-2484 (1979) 4.1

[234] T. Negishi-Koga and H. Takayanagi, Bone cell communication factors and Semaphorins, BoneKEy Reports **1**, 183 (2012) 3.1

[235] V. Nosenko, S. Zhdanov, A. Ivlev, C. Knapek and G. Morfill, 2D melting of plasma crystals: equilibrium and nonequilibrium regimes, Phys. Rev. Lett. **103**, 015001 (2009) 4.1

[236] C. Oliveira, A. Vieira, D. Helbing, J. Andrade and H. Herrman, Keep-left behavior induced by asymmetrically profiled walls, Phys. Rev. X **6**, 011003 (2016) 4.3

[237] E. Ott, C. Grebogi and J. Yorke, Controlling chaos, Phys. Rev. Lett. **64**, 1106 (1990) 1.2.1

[238] N. Packard, J. Crutchfield, D. Farmer and R. Shaw, Geometry from a time series, Phys. Rev. Lett. **45**, 712-716 (1980) 1.2.1

[239] I. Papadakis, W. Brinkmann, M. Gliozzi, C. Räth, F. Nicastro and M. L. Conciatore, XMM-Newton long-look observation of the narrow line Seyfert 1 galaxy PKS 0558-504. I. Spectral analysis, Astron. & Astrophys. **510**, A65 (2010) 5.2

[240] I. Papadakis, W. Brinkmann, M. Gliozzi, C. Räth, XMM-Newton long-look observation of the narrow-line Seyfert 1 galaxy PKS 0558-504. II. Timing analysis, Astron. & Astrophys. **518**, A28 (2010) 5.2

[241] C.-G. Park, Non-Gaussian signatures in the temperature fluctuation observed by the Wilkinson Microwave Anisotropy Probe, Mon. Not. R. Astron. Soc. **349**, 313-320 (2004) 5.3

[242] A. Parfitt, M. Drezner, F. Glorieux, J. Kanis, H. Malluche, P. Meunier, S. Ott, R. Recker, Bone Histomorphometry: Standardization of Nomenclature, Symbols, and Units, Journ. Bone Miner. Res. **2**, 595-610 (1987) 3.3

[243] A. Penzias and R. Wilson, A measurement of excess antenna temperature at 4080 Mc/s, Astrophysical Journal **142**, 419-421 (1965) 5.1, 5.3

[244] F. Pfeiffer, T. Weitkamp, O. Bunk and C. David, Phase retrieval and differential phase-contrast imaging with low-brilliance x-ray sources, Nature Physics **2**, 258-261 (2006) 3.3

[245] A. Pikovsky, M. Rosenblum and J. Kurths, Synchronization: A universal concept in nonlinear sciences, Cambridge University Press, Cambridge (2001) 1.1

[246] Planck Collaboration: P. Ade et al., Planck 2013 results. I. Overview of products and scientific results, Astron. & Astrophys. **571**, A1 (2014) 5.3, 5.4, 5.3, 5.3

[247] Planck Collaboration: P. Ade et al., Planck 2013 results. XII. Diffuse component separation, Astron. & Astrophys. **571**, A12 (2014) 5.3

[248] Planck Collaboration: P. Ade et al., Planck 2013 results. XXII. Constraints on inflation, Astron. & Astrophys. **571**, A22 (2014) 5.3

[249] Planck Collaboration: P. Ade et al., Planck 2013 results. XXIII. Isotropy and statistics of the CMB, Astron. & Astrophys. **571**, A23 (2014) 5.5, 5.3, 5.3, 5.6

[250] Planck Collaboration: P. Ade et al., Planck 2013 Results. XXIV. Constraints on primordial non-Gaussianity, Astron. & Astrophys. **571**, A24 (2014) 5.3

[251] Planck Collaboration: P. Ade et al., Planck 2013 results. XXVI. Background geometry and topology of the Universe, Astron. & Astrophys. **571**, A26 (2014) 5.3

[252] Planck Collaboration: P. Ade et al., Planck 2015 results. I. Overview of products and scientific results, Astron. & Astrophys. **594**, A1 (2016) 5.3

[253] Planck Collaboration: P. Ade et al., Planck 2015 results. IX. Diffuse component separation: CMB maps, Astron. & Astrophys. **594**, A9 (2016) 5.3

[254] Planck Collaboration: P. Ade et al., Planck 2015 results. XVI. Isotropy and statistics of the CMB, Astron. & Astrophys. **594**, A16 (2016) 5.3

[255] Planck Collaboration: P. Ade et al., Planck 2015 results. XVII. Primordial non-Gaussianity, Astron. & Astrophys. **594**, A17 (2016) 5.3

[256] Planck Collaboration: P. Ade et al., Planck 2015 results. XX. Constraints on inflation, Astron. & Astrophys. **594**, A20 (2016) 5.3

[257] N. Platt, E. Spiegel and C. Tresser, On-Off intermittency: A mechanism for bursting, Phys. Rev. Lett. **70**, 279-282 (1993) 6

[258] D. Pietrobon, A. Amblard, A. Balbi, P. Cabella, A. Cooray and D. Marinucci, Needlet detection of features in the WMAP CMB sky and the impact on anisotropies and hemispherical asymmetries, Phys. Rev. D **78**, 103504 (2008) 5.3

[259] H. Poincaré, Sur le problème des trois corps et les équation de la dynamique, Act. Math. **13**, 1-270 (1890) 1.1

[260] P. Proff and P. Römer, The molecular mechanism behind bone remodelling: a review, Clin. Oral Invest. **13**,355-362 (2009) 3.1

[261] M. Pompilio, F. Bouchet, G. Murante and A. Provenzale, Multifractal analysis of string-induced cosmic microwave background radiation anisotropies, Astrophysical Journal **449**, 1-8 (1995) 5.3

[262] P. Predehl et al., eROSITA on SRG, Proc. of SPIE **7732**, 77320U (2010) 5.3

[263] C. Räth, G. Morfill, Texture detection and texture diskrimination with anisotropic scaling indices, Journal of the Optical Society of America A **14**, 3208-3215 (1997) 5.3

[264] C. Räth, Analyse statischer Strukturen mit strukturellen Komplexitätsmaßen erster und zweiter Stufe, Dissertation, Ludwig Maximilian Universität, München (1998) 1.2, 5.3

[265] C. Räth, W. Bunk, M. Huber, G. Morfill, J. Retzlaff and P.Schuecker, Analysing large-scale structure - I. weighted scaling indices and constrained randomization, Mon. Not. R. Astron. Soc. **337**, 413-421 (2002) 1.2.1, 5.3

[266] C. Räth, P. Schuecker, Analysing large-scale structure - II. testing for primordial non-Gaussianity in CMB maps using surrogates, Mon. Not. R. Astron. Soc. **344**, 115-128 (2003) 5.3

[267] C. Räth, R. Monetti, D. Müller, H. Böhm, E. Rummeny and T. Link, Comparing nonlinear texture measures for quantifying trabecular bone structures using surrogates, Proc. of SPIE **5370**, 207-214 (2004) 2.2

[268] C. Räth, D. Müller, H. Böhm , E. Rummeny , T. Link and R. Monetti, Improving the textural characterization of trabecular bone structure to quantify its changes: the locally adapted scaling vector method, Proc. of SPIE **5747**, 240-248 (2005) 3.1

[269] C. Räth, P. Schuecker and A. Banday, A scaling index analysis of the Wilkinson Microwave Anisotropy Probe three-year data: signatures of non-Gaussianities and asymmetries in the cosmic microwave background, Month. Not. Roy. Astr. Soc. **380** 466-478 (2007) 5.3

[270] C. Räth, R. Monetti, J. Bauer, I. Sidorenko, D. Müller, M. Matsuura, E.-M. Lochmüller, P. Zysset and F. Eckstein, Strength through structure: visualization and local assessment of the trabecular bone structure, New J. of Physics **10**, 125010 (2008) 3.3

[271] C. Räth, J. Bauer, D. Müller, I. Sidorenko, T. Link and R. Monetti, Comparing the sensitivity of wavelets, Minkowski functionals and scaling indices to higher order correlations in MR images of the trabecular bone using surrogates, Proc. of SPIE **7259**, 72590D (2009) 2.3

[272] C. Räth, G. Morfill, G. Rossmanith, A. Banday and K. Gorski, Model-independent test for scale-dependent non-Gaussianities in the cosmic microwave background, Phys. Rev. Lett. **102**, 131301 (2009) 5.3, 5.5, 5.6

[273] C. Räth, D. Müller, I. Sidorenko, R. Monetti and J. Bauer, Assessing texture measures with respect to their sensitivity to scale-dependent higher order correlations in medical images using surrogates, Proc SPIE **7623**, 762354 (2010) 2.3

[274] C. Räth, A. Banday, G. Rossmanith, H. Modest, K. Sütterlin, K. Gorski, J. Delabrouille and G. Morfill, Scale-dependent non-Gaussianities in the WMAP data as identified by using surrogates and scaling indices, Month. Not. Roy. Astr. Soc. **415**, 2205-2214 (2011) 5.3

[275] C. Räth, M. Gliozzi, I. Papadakis and W. Brinkmann, Revisiting algorithms for generating surrogate time series, Phys. Rev. Lett. **109**, 144101, (2012) 2.2

[276] C. Räth, T. Baum, R. Monetti, I. Sidorenko, P. Wolf, F. Eckstein, M. Matsuura, E.-M. Lochmüller, P. Zysset, E. Rummeny, T. Link and J. Bauer, Scaling relations between trabecular bone volume fraction and microstructure at different skeletal sites, Bone **57**, 377-383 (2013) 3.3

[277] C. Räth, I. Laut, Time series with tailored nonlinearities, Phys. Rev. E **92**, 040902(R) (2015) 6

[278] Lord Rayleigh, On convection currents in a horizontal layer of fluid, when the higher temperature is on the under side, Phil. Mag., Ser.6, **32**, 529 - 546 (1916) 1.1

[279] M. Rees, Black hole models for active galactic nuclei, Ann. Rev. Astron. Astrophys. **22**, 471-506 (1984) 5.2

[280] P. Refregier and B. Javidi, Optical image encryption based on input plane and Fourier plane random encoding, Opt. Lett. **20**, 767-769 (1995) 2.2

[281] C. Reichhardt and C. Olson Reichhardt, Cooperative behavior and pattern formation in mixtures of driven and nondriven colloidal assemblies, Phys. Rev. E **74**, 011403 (2006) 4.3

[282] C. Ringeval, D. Yamauchi, J. Yokoyama and F. Bouchet, Large scale CMB anomalies from thawing cosmic strings, Journal of Cosmology and Astroparticle Physics **2**, 033 (2016) 5.3

[283] N. Rivas, S. Ponce, B. Gallet, D. Risso, R. Soto, P. Cordero and N. Mujica, Sudden Chain Energy Transfer Events in Vibrated Granular Media, Phys. Rev. Lett. **106**, 088001 (2011) 4.2

[284] O. Rössler, An equation for continuous chaos, Phys. Lett. A, **57**, 397-398 (1976) 1.1

[285] J. Rodenburg, A. Hurst, A. Cullis, B. Dobson, F. Pfeiffer, O. Bunk, C. David, K. Jefimovs and I. Johnson, Hard x-ray lensless imaging of extended objects, Phys. Rev. Lett. **98**, 034801 (2007) 2.2

[286] A. Rosenfeld and A. Kak, Digital picture processing, Computer Science and Applied Mathematics, Springer, Berlin (1976) 1.2.2

[287] G. Rossmanith, C. Räth, A. Banday and G. Morfill, Non-Gaussian signatures in the five-year WMAP data as identified with isotropic scaling indices, Mon. Not. Roy. Astron. Soc. **399**, 1921-1933 (2009) 5.3

[288] G. Rossmanith, Concepts of non-linear data analysis applied to the search of non-Gaussianities in the CMB, Dissertation, Ludwig Maximilian Universität, München (2011) 2.2, 5.3

[289] G. Rossmanith, H. Modest, C. Räth, A. Banday, K. Gorski and G. Morfill, Search for non-Gaussianities in the WMAP data with the scaling index method, Advances in Astronomy **2011**, 174873 (2011) 5.3

[290] G. Rossmanith, H. Modest, C. Räth, A. Banday, K. Gorski and G. Morfill, Probing non-Gaussianities in the cosmic microwave background on an incomplete sky using surrogates, Phys. Rev. D, **86**, 083005 (2012) 2.2, 5.3

[291] J. Rowlinson and F. Swinton, Liquids and Liquid Mixtures, Butterworths, London (1982) 4.2

[292] M. Rubin-Zuzic, G. Morfill, A. Ivlev, R. Pompl, B. Klumov, W. Bunk, H. Thomas, H. Rothermel, O. Havnes and A. Fouquét, Kinetic development of crystallization fronts in complex plasmas, Nature Physics **2**, 181-185 (2006) 4.1

[293] N. Rucci, Molecular biology of bone remodelling, Clinical Cases in Mineral and Bone Metabolism **5**, 49-56 (2008) 3.1

[294] R. Ruimerman, P. Hilbers, R. van Rietbergen and R. Huiskes, A theoretical framework for strain-related trabecular bone maintenance and adaptation, J. Biomech. **38**, 931 (2005) 3.1

[295] L. Santaló, Integral geometry and geometric probability, Addison-Wesley, Reading (1976) 1.2.2

[296] T. Sauer, J. Yorke and M. Casdagli, Embedology, Journal of Statistical Physics **65**, 579-616 (1991) 1.2.1

[297] F. Schaff, A. Malecki, G. Potdevin, E. Eggl, P. Noel, T. Baum, E. Garcia, J. Bauer and F. Pfeiffer, Correlation of x-ray vector radiography to bone micro-architecture, Scientific Reports **4**, 3695 (2014) 3.3

[298] J. Schmalzing and K. Gorski, Minkowski functionals used in the morphological analysis of cosmic microwave background anisotropy maps, Mon. Not. R. Astron. Soc. **297**, 355-365 (1998) 1.2.2

[299] M. Schmidt, 3C 273 : A Star-Like Object with Large Red-Shift, Nature **197**s, 1040 (1963) 5.2

[300] A. Schmitz and T. Schreiber, Testing for nonlinearity in unevenly sampled time series, Phys. Rev. E, **59**, 4044-4047 (1999) 2.2

[301] B. Schmittmann and R. Zia, Driven diffusive systems. An introduction and recent developments, Phys. Rep. **301**, 45-64 (1998) 4.3

[302] K. Schreiber, Phase walk analysis for leptokurtic time series, Masterarbeit, Ludwig Maximilian Universität, München (2015) 1.2.3

[303] T. Schreiber and A. Schmitz, Improved surrogate data for nonlinearity tests, Phys. Rev. Lett. **77**, 635-638 (1996) 2.2

[304] T. Schreiber, diskrimination power of measures for nonlinearity in a time series, Phys. Rev. E **55**, 5443-5447 (1997) 1.2.1, 2.3

[305] T. Schreiber, Constrained randomization of time series data, Phys. Rev. Lett. **80**, 2105-2108 (1998) 2.2

[306] T. Schreiber and A. Schmitz, Surrogate time series, Physica D **142**, 346-382 (2000) 2.1

[307] G. Schröder-Turk, W. Mickel, S. Kapfer, F. Schaller, B. Breidenbach, D. Hug and K. Mecke, Minkowski tensors of anisotropic spatial structure, New J. of Physics **15**, 083028 (2008) 1.2.2, 4.2

[308] M. Schwabe, S. Zhdanov, C. Räth, D. Graves, H. Thomas and G. Morfill, Collective effects in vortex movements in complex plasmas, Phys. Rev. Lett. **112**, 115002 (2014) 4.1

[309] D. Schwarz, G. Starkman, D. Huterer and C. Copi, Is the low-l microwave background cosmic?, Phys. Rev. Lett. **93**, 221301 (2004) 5.3

[310] D. Schwarz, D. Bacon, S. Chen, C. Clarkson, D. Huterer, M. Kunz, R. Maartens, A. Raccanelli, M. Rubart and J.-L. Starck, Testing foundations of modern cosmology with SKA all-sky surveys, arxiv:1501.03820 (2015) 5.3

[311] K. Schwarzschild, Über das Gravitationsfeld eines Massenpunktes nach der Einsteinschen Theorie, Sitzungsberichte der Königlich Preussischen Akademie der Wissenschaften **7**, 189196 (1916) 5.2

[312] K. Schwarzschild, Über das Gravitationsfeld einer Kugel aus inkompressibler Flüssigkeit nach der Einsteinschen Theorie, Sitzungsberichte der Königlich Preussischen Akademie der Wissenschaften **18**, 424434 (1916) 5.2

[313] G. Selwyn, J. Heidenreich and K. Haller, Particle trapping phenomena in radio frequency plasmas, Appl. Phys. Lett. **57**, 1876 (1990) 4.1

[314] J. Serra, Image analysis and mathematical morphology, Academic Press, London (1982) 1.2.2

[315] C. Seyfert, Nuclear Emission in Spiral Nebulae, Astrophysical Journal, **97**, 28 (1943) 5.2

[316] T. Shinbrot, C. Grebogy, J. Wisdom and J. Yorke, Chaos in a double pendulum, Am. J. Phys. **60**, 491- 499 (1992) 1.1

[317] P. Shukla and A. Mamun, Introduction to dusty plasma physics, Institute of Physics Publishing, Bristol and Philadelphia (2002) 4.1

[318] P. Shukla and B. Eliasson, Colloquium: fundamentals of dust-plasma interactions, Rev. Mod. Phys. **81**, 25-44 (2009) 4.1

[319] R. Sknepnek and S. Henkes, Active swarms on a sphere, Phys. Rev. E **91**, 022306 (2015) 7

[320] G. Smoot et al., Structure in the COBE differential microwave radiometer first-year maps, Astrophysical Journal **396**, L1-L5 (1992) 5.3

[321] J. Sprott, Chaos and time series analysis, Oxford University Press, Oxford (2003) 1.1

[322] A. Starobinsky, A new type of isotropic cosmological models without singularity, Physics Letters B **91**, 99-102 (1980) 5.3

[323] P. Steinhardt, D. Nelson and M. Ronchetti, Icosahedral bond orientational order in supercooled liquids, Phys. Rev. Lett. **47**, 1297-1300 (1981) 4.1

[324] P. Steinhardt, D. Nelson and M. Ronchetti, Bond-orientational order in liquids and glasses, Phys. Rev. B **28**, 784-805 (1983) 4.1

[325] P. Steinhardt and N. Turok, A cyclic model of the universe, Science **296**, 1436-1439 (2002) 5.3

[326] J. Stenhammar, R. Wittkowski, D. Marenduzzo and M. Cates, Activity-induced phase separation and self-assembly in mixtures of active and passive particles, Phys. Rev. Lett. **114**, 018301 (2015) 4.2

[327] D. Stoyan, W. Kendall and J. Mecke, Stochastic geometry and its applications, Wiley, Chichester (1995) 1.2.2

[328] K. Strandburg, Two-dimensional melting, Rev. Mod. Phys. **60**, 161-207 (1988) 4.1

[329] S. Strogatz, Exploring complex networks, Nature **410**, 268-276 (2001) 1.2

[330] I. Sidorenko et al., Assessing methods for characterising local and global structural and biomechanical properties of the trabecular bone network, Curr. Med. Chem. **18**, 3402 (2011) 3.3

[331] K. Sütterlin, A. Wysocki, A. Ivlev, C. Räth, H. M. Thomas, M. Rubin-Zuzic, W. Goedheer, V. Fortov, A. Lipaev, V. Molotkov, O. Petrov, G. Morfill, and H. Löwen, Dynamics of lane formation in driven binary complex plasmas, Phys. Rev. Lett. **102**, 085003 (2009) 4.3

[332] G. Sugihara and R. May, Nonlinear forecasting as a way of distinguishing chaos from measurement error in time series, Nature **344**, 734-741(1990) 1.2.1

[333] X. Sun, M. Small, Y. Zhao, and X. Xue, Characterizing system dynamics with a weighted and directed network constructed from time series data, Chaos **24**, 024402 (2014) 1.2.1

[334] M. Tagger and R. Pellat, An accretion-ejection instability in magnetized disks, Astron. Astrophys. **349**, 10031016 (1999) 5.2

[335] F. Takens, Detecting strange attractors in turbulence, in D. Rand and L.-S. Young (eds.). Dynamical systems and turbulence, Lecture Notes in Mathematics, **898**, 366-381, Springer-Verlag (1981) 1.2.1

[336] T. Tajima and J. Dawson, Laser electron accelerator, Phys. Rev. Lett. **143**, 267-270 (1979) 4.1

[337] S. Teitelbaum, Bone Resorption by osteoclasts, Science **289**, 1504-1508 (2000) 3.1

[338] N. Terrell, Shot-noise character of Cygnus X-1 pulsations, Astrophysical Journal **174**, L35 (1972)

[339] J. Theiler, S. Eubank, A. Longtin, B. Galdrikian, J. Doyne Farmer, Testing for nonlinearity in time series: the method of surrogate data, Physica D **58**, 77-94 (1992) 2.1, 2.2

[340] P. Thibault, M. Dierolf, A. Menzel, O. Bunk, C. David, F. Pfeiffer, High-resolution scanning x-ray diffraction microscopy, Science **321**, 379- 382 (2008) 3.3

[341] M. Thoma, M. Fink, H. Höfner, M. Kretschmer, S. Khrapak, S. Ratynskaia, V. Yaroshenko, G. Morfill, O. Petrov, A. Usachev, A. Zobnin, and V. Fortov, PK-4: complex plasmas in space - the next generation, IEEE Trans. on Plasma Science **35**, 255-259 (2007) 4.1, 4.2

[342] M. Thoma and G. Morfill, Ratio of viscosity to entropy density in a strongly coupled one-component plasma, EPL **82**, 65001(2008) 4.1

[343] H. Thomas, G. Morfill, V. Demmel, J. Goree, B. Feuerbacher and D. Möhlmann, Plasma crystal: Coulomb crystallization in a dusty plasma, Phys. Rev. Lett., **73**, 652-655 (1994) 4.1

[344] H. Thomas and G. E. Morfill, Melting dynamics of a plasma crystal, Nature **379**, 806-809 (1996) 4.1

[345] H. Thomas, G. Morfill, V. Fortov, A. Ivlev, V. Molotkov, A. Lipaev, T. Hagl, H. Rothermel, S. Khrapak, K. Suetterlin, M. Rubin-Zuzic, O. Petrov, V. Tokarev, and S. Krikalev, Complex plasma laboratory PK-3 Plus on the international space station, New J. of Phys. **10**, 033036 (2008) 4.1, 4.1

[346] L. Titarchuk and V. Osherovich, The Global Normal Disk Oscillations and the Persistent Low-Frequency Quasi-periodic Oscillations in X-Ray Binaries, Astrophysical Journal, **542**, L111-L114 (2000) 5.2

[347] K. Tsubota, T. Adachi and Y. Tomita, Functional adaptation of cancellous bone in human proximal femur predicted by trabecular surface remodeling simulation toward uniform stress state, J. Biomech., **35**, 1541-1551 (2002) 3.1

[348] K. Tsubota, Y. Suzuki, T. Yamada, M. Hojo, A. Makinouchi and T. Adachi, Computer simulation of trabecular remodeling in human proximal femur using large-scale voxel FE models: approach to understanding Wolff's law, J. Biomech., **42**, 1088-1094 (2009) 3.1

[349] Y. Ueda, Explosion of strange attractors exhibited by Duffing's equation, Annals of the New York Academy of Sciences, **357**, 422-434 (1980) 1.1

[350] M.-H. Ulrich, l. Maraschi and C. Megan Urry, Variability of galactic nuclei, Ann. Rev. Astron. Astrophys. **35**, 445-502 (1997) 5.2

[351] A. Vesterby, Li. Mosekilde, H. Gundersen, F. Melsen, L. Mosekilde, K. Holme and S. Sorensen, Biologically Meaningful Determinants of the in Vitro Strength of Lumbar Vertebrae, Bone **12**, 219-224 (1991) 3.3

[352] P. Vielva, E. Martinez-Gonzalez, R. Barreiro, J. Sanz, and L. Cayon, Detection of Non-Gaussianity in the Wilkinson Microwave Anisotropy Probe First-Year Data Using Spherical Wavelets, Astrophysical Journal **609**, 22-34 (2004) 5.3

[353] S. Vladimirov, K. Ostrikov, and A. Samarian, Physics and applications of complex plasmas, Imperial College Press, London (2005) 4.1

[354] R. Wackerbauer, A. Witt, H. Atmanspacher, J. Kurths and H. Scheingraber, A comparative classification of complexity measures, Chaos, Solitons & Fractals **4**, 133-173 (1994) 1.2

[355] S. Wallach, J. Feinblatt, J. Carstens and L. Avioli, The bone "quality" problem, Calcif. Tissue Int. **51**, 169-172 (1992) 3.3

[356] S. Weber, C. Weber and E. Frey, Binary mixtures of particles with different diffusivities demix, Phys. Rev. Lett. **116**, 058301 (2016) 4.2

[357] D. Weinberg, J. Gott, A. Melott, The topology of large-scale structure. I-topology and the random phase hypothesis, Astrophysical Journal **321**, 2-27 (1987) 1.2.2

[358] T. Weitkamp, A. Diaz, C. David, F. Pfeiffer, M. Stampanoni, P. Cloetens and E. Ziegler, X-ray phase imaging with a grating interferometer, Optics Express **13**, 6296 (2005) 3.3

[359] L. Wegener, Status of Wendelstein 7-X construction, Fusion Engineering and Design **84**, 106-112 (2009) 4.1

[360] H. Whitney, Differentiable manifolds, Ann. Math. **37**, 645-680 (1936) 1.2.1

[361] N. Wiener, Generalized harmonic analysis, Acta Math. **55**, 117-258 (1930) 1.2

[362] L. Wörner, C. Räth, V. Nosenko, S. K. Zhdanov, H. Thomas, G. Morfill, J. Schablinski and D. Block, String structures in driven 3D complex-plasma clusters, Europhys. Lett. **100**, 35001 (2012) 4.4

[363] J. Wolff, Das Gesetz der Transformation der Knochen, Hirschwald Verlag, Berlin (1892) 3.1

[364] A. Wysocki, C. Räth, A. Ivlev, K. Sütterlin, H. Thomas, S. Khrapak, S. Zhadanov, V. Fortov, A. Lipaev, V. Molotkov, O. Petrov, H. Löwen and G. Morfill, Kinetics of fluid demixing in complex plasmas: role of two-scale interactions, Phys. Rev. Lett., **105** 045001 (2010) 4.2

[365] H. Xu, N. Ouellette and E. Bodenschatz, Multifractal Dimension of Lagrangian Turbulence, Phys. Rev. Lett. **96** 114503 (2006) 4.1

[366] A. Yethiraj and A. van Blaaderen, A colloidal model system with an interaction tunable from hard sphere to soft and dipolar, Nature **421** 513-517 (2003) 4.4

[367] A. Young, Melting and the vector Coulomb gas in two dimensions, Phys. Rev. B **19**, 1855-1866 (1979) 4.1

[368] M. Zaidi, Skeletal remodeling in health and disease, Nature Medicine, **13**, 791-801 (2007) 3.1

[369] S. Zhdanov, M. Schwabe, C. Räth, H. Thomas and G. Morfill, Wave turbulence observed in an auto-oscillating complex (dusty) plasma, Europhys. Lett. **110**, 35001 (2015) 4.1

[370] M. Zuzic, A. Ivlev, J. Goree, G. Morfill, H. Thomas, H. Rothermel, U. Konopka, K. Sütterlin and D. Goldbeck, Three-dimensional strongly coupled plasma crystal under gravity conditions, Phys. Rev. Lett. **85**, 4064-4067 (2000) 4.1

Acknowledgements

As the work for this cumulative habilitation thesis was performed during a number of years and as I investigated a number of different topics in distinct research fields, I collaborated with a large number of scientists, who all gave input to my work and many of them inspired me and my thinking. It is impossible to mention all of them and I apologize to all who I forgot to include in my acknowledgements. First of all, I thank Prof. Dr. Dr. h.c. Gregor Morfill not only for his continuous encouragement and support through all the years but also and especially for letting me pursuing my ideas that covered quite diverse fields of research over the years. Greg also managed to built up a working group, which can truly be called unique in the sense that a large number of excellent and original researches gathered there and performed scientific research in an interdisciplinary manner. I always considered it as a privilege to work in such an environment.

I want to continue with thanking the late PD Dr. Peter Schuecker, with whom I started my engagement in Cosmology. Peter died far too early so that he has only seen the results of paper XII. in this thesis. I really would have liked to share and discuss with him the results presented in the following (CMB-)papers. Thanks to my "Cosmology-PhD-students" Dr. Heike Modest and Dr. Gregor Rossmanith with whom I could continue to have a very deep, nonlinear look at CMB-data. We not only performed excellent science together but also spent great time while e.g. hiking in the Alps or skiing in Aspen. I also want to thank Dr. Anthony Banday, Prof. Dr. Krzysztof Gorski and Prof. Dr. Francois Bouchet for their interest in my nonlinear studies of CMB data and for making me become a member of the Planck Core Team. It was a unique and unforgettable experience to be among the first to see and to analyze the Planck data.

Dr. Wolfgang Brinkmann, Dr. Mario Gliozzi and Prof. Dr. Ioannis Papadakis are thanked for their now very long-lasting and productive collaboration in the study of AGNs and GBHs. It was and is always a pleasure to work with you – be it in Munich or in a warmer environment on Crete.

I thank Prof. Dr. Thomas Link for drawing my attention to the complex inner structure of bones. Thomas and I initiated together the so-called TANDEM-project on improving the assessment of osteoporosis, which marked the beginning of very productive and still ongoing interdisciplinary research projects on bone research. Thanks also to Prof. Dr. Ernst Rummeny, who always supported our efforts and to PD Dr. Jan Kirschke (born Bauer) and PD Dr. Thomas Baum, who continued the research on osteoporosis at the Klinikum rechts der Isar of the Technical University of Munich (TUM) , when Thomas

Link left to UCSF.
The studies of self-organizing processes in complex plasmas wouldn't have been possible without being embedded in the PK-3 Plus and PK4 team. Thanks to all researchers and engineers, who worked on these two experiments. Let me mention on behalf of dozens of people Dr. Hubertus Thomas and Prof. Dr. Markus Thoma as the project scientist for PK-3 Plus and PK4, PD Dr. Alexei Ivlev and Prof. Dr. Hartmut Löwen as the theoreticians for the studies I was involved in and the late Dr. Glenn Joyce and Dr. Adam Wysocki for their work on simulations.
Special thanks go to Dr. Hubertus Thomas, Prof. Dr. Andreas Meyer and Prof. Dr. Hans-Jörg Dittus for encouraging me to continue my interdisciplinary research after the research group moved from the Max-Planck Society (MPG) to the German Aerospace Center (DLR) and for giving me the time and resources to finalize my habilitation thesis.
Heartfelt thanks go to my wife Katrin, who supported me all the time, gave me advices, bore a considerable number of my business trips to beautiful locations at home and outlined more than once to me the advantages of being a scientist. Finally, I want to thank my children Benedict and Korbinian first of all for being around with their joy of living, for grounding me and for showing me a number of new facets of life, which are at least as important as physics.

Original Publications

Paper I.:

C. Räth, M. Gliozzi, I. E. Papadakis and W. Brinkmann,
Revisiting algorithms for generating surrogate time series,
Phys. Rev. Lett. ***106****, 155001 (2012)*

Paper II.:

C. Räth, J. Bauer, D. Müller, I. Sidorenko, T. Link and R. Monetti,
Comparing the sensitivity of wavelets, Minkowski functionals and scaling indices to higher order correlations in MR images of the trabecular bone using surrogates,
Proc. of SPIE ***7259****, 72590D (2009)*

The content of this paper was also presented as highlight talk at the SPIE conference on medical imaging in Orlando, Florida in 2009.

Paper III.:

D. Müller, T. Link, R. Monetti, J. Bauer, H. Böhm, V. Seifert-Klauss, E.J. Rummeny, G.E. Morfill and C. Räth,
The 3D-Based Scaling Index Algorithm - A New Structure Measure to Analyze Trabecular Bone Architecture in High-Resolution MR Images In Vivo,
Osteoporosis International, ***17****,1483-1493 (2006)*

Paper IV.:

C. Räth, R. Monetti, J. Bauer, I. Sidorenko, D. Müller, M. Matsuura, E.M. Lochmüller, P. Zysset and F. Eckstein,
Strength through structure: visualization and local assessment of the trabecular bone structure,
New Journal of Physics, ***10****, 125010 (2008)*

This paper was an invited contribution for the Focus Issue "Visualization in Physics", which was compiled and published on the occasion of the 10th anniversary of the New Journal of Physics.
This publication was featured (among others) in in the article "A Feast of Visualization" in Physics World in December 2008.

Paper V.:

C. Räth, T. Baum, R. Monetti, I. Sidorenko, P. Wolf, F. Eckstein, M. Matsuura, E.-M. Lochmüller, P. Zysset, E. Rummeny, T. Link and J. Bauer,
Scaling relations between trabecular bone volume fraction and microstructure at different skeletal sites, Bone ***57****, 377-383 (2013)*

Paper VI.:

A. Wysocki, C. Räth, A. V. Ivlev, K. R. Sütterlin, H. M. Thomas, S. Khrapak, S. Zhadanov, V. E. Fortov, A. M. Lipaev, V. I. Molotkov, O. F. Petrov, H. Löwen and G. Morfill, Kinetics of fluid demixing in complex plasmas: Role of two-scale interactions, Phys. Rev. Lett., ***105*** *045001 (2010)*

Paper VII.:

K. Sütterlin, A. Wysocki, A. V. Ivlev, C. Räth, H. Thomas, M. Rubin-Zuzic, W. Goedheer, V. Fortov, A. Lipaev, V. Molotkov, O. Petrov, G. Morfill, and H. Löwen,
Dynamics of Lane Formation in Driven Binary Complex Plasmas,
Phys. Rev. Lett. ***102****, 085003 (2009)*

The paper was accepted as submitted.
PRL Editors' Suggestion.
This publication was discussed in the article "Linienbildung bei Gegenverkehr" in Physik Journal in June 2009.

Paper VIII.:

A. Ivlev, G. Morfill, H. Thomas, C. Räth, G. Joyce, P. Huber, R. Kompaneets, V. Fortov, A. Lipaev, V. Molotkov, T. Reiter, M. Turin and P. Vinogradov,
First Observation of Electrorheological Plasmas,
Phys. Rev. Lett. ***100****, 095003 (2008)*

Paper IX.:

A. Ivlev, M. Thoma, C. Räth, G. Joyce and G. Morfill,
Complex plasmas in external fields: Role of non-Hamiltonian interactions,
Phys. Rev. Lett. ***106****, 155001 (2011)*

Paper X.:

M. Gliozzi, W. Brinkmann, C. Räth, I. Papadakis, H. Negoro and H. Scheingraber,
On the nature of x-ray variability in Ark 564,
Astronomy & Astrophysics ***391****, 875-886 (2002)*

Paper XI.:

M. Gliozzi, C. Räth, I. Papadakis and P. Reig,
Characterizing black hole variability with nonlinear methods: the case of the x-ray nova 4U 1543-47,
Astronomy & Astrophysics ***512****, A21 (2010)*

Paper XII.:

C. Räth, P. Schuecker, A. J. Banday,
A scaling index analysis of the Wilkinson Microwave Anisotropy Probe three-year data: signatures of non-Gaussianities and asymmetries in the cosmic microwave background,
Month. Not. Roy. Astr. Soc. ***380*** *466-478 (2007)*

Paper XIII.:

G. Rossmanith, C. Räth, A. Banday, G. Morfill,
Non-Gaussian signatures in the five-year WMAP data as identified with isotropic scaling indices,
Month. Not. Roy. Astr. Soc. ***399****, 1921-1933 (2009)*

Paper XIV.:

C. Räth, G. Morfill, G. Rossmanith, A. Banday and K. Gorski,
Model-independent test for scale-dependent non-Gaussianities in the cosmic microwave background,
Physical Review Letters ***102****, 131301 (2009)*

The article was discussed (among others) in a News Feature in Nature (April 2009) entitled "The Test of Inflation", which appeared shortly before the launch of the PLANCK satellite.

Paper XV.:

C. Räth, A. Banday, G. Rossmanith, H. Modest, R. Sütterlin, K.Gorski, J. Delabrouille and G. Morfill,
Scale-dependent non-Gaussianities in the WMAP data as identified by using surrogates and scaling indices,
Month. Not. Roy. Astr. Soc. ***415****, 2205 - 2214 (2011)*

Paper XVI.:

C. Räth and I. Laut,
Time series with tailored nonlinearities,
Phys. Rev. E ***92****, 040902(R) (2015)*